CARBONACEOUS ADSORBENTS AS HETEROGENEOUS CATALYST SUPPORTS: APPLICATIONS AND CHARACTERIZATION

By

TODD JAMES LAFRENZ

A DISSERTATION PRESENTED TO THE GRADUATE SCHOOL
OF THE UNIVERSITY OF FLORIDA IN PARTIAL FULFILLMENT
OF THE REQUIREMENTS FOR THE DEGREE OF
DOCTOR OF PHILOSOPHY

UNIVERSITY OF FLORIDA

1995

ACKNOWLEDGMENTS

My journey through graduate school has been long and arduous, as I am oft inclined to take the more difficult path to the mountain top. However, I am also leaving a much wealthier person in terms of knowledge and fond memories. During this time I have learned much about myself, my friends, human kind, and in no way the least--chemistry. I have realized who and what family and friends truly are, and it is to them I express my sincerest thanks and gratitude. When one looks around and tries to understand the diversity and complexity of the world in which we live, it is only through the love and support of family and friends that we can continue to strive for a better world, and cope with our failures and disappointments along the way. It is also with these same people that we share our joys and accomplishments. There are too many to list by name, and I do not wish to leave anyone out, but I would like to acknowledge one person specifically who has had the greatest impact on my life. This recognition goes to one of the most important women in my life--my mother, Joan Barnett. It has been through her constant support and by her own example that I have been successful in what I have undertaken. I feel very fortunate to have the large number of wonderful friends and family that I do, so let me just say thank you once again to everyone.

Then where would my chemistry career be without the instructors and advisors who had their impact? It is these people who have shared with me the how's and why's of scientific research. First there was Dr. Sandra Etheridge at Gulf Coast Community College, who got me started in chemistry. Next, Dr.

R.K. Birdwhistle at the University of West Florida, who never allowed me to submit or accept a "bullshit" solution to any chemical problem. And finally, there is Professor Russell Drago, my research advisor. Through his patience and his never-ending excitement for chemistry, he has taught me much about how to be a chemist. I can only hope that when I am his age, I will still have that same intensity and interest for research and living (I also wouldn't mind having his hookshot and sharp elbows for 2-on-2 basketball).

Finally, let me acknowledge a few of the people who made my stay in Gainesville so enjoyable. First I must thank the University of Florida and its Chemistry Department. Beyond their financial support, the opportunities and treatment I received while there could not be matched anywhere. I must also thank the faculty, especially my committee members, for their support and input. It was through many conversations with them that my education and research progressed. I cannot forget the support, advice and friendship I received from the Chemistry Departments support staff, especially the guys in the electronics, glass blowing and machine shops. Individual thanks are extended here to Vernon Cook and Rudy Strohschein. Also included in this list are the people at Micromeritics, especially Tommy Hill, J.R. Berrett and Tony Thorton--it was through many visits and discussions with them that I was introduced to much of what I know of gas adsorption theory. Lastly, I would like to acknowledge the Rohm and Haas Company for their financial support during a large portion of my research.

I cannot forget the daily "behind the scenes" help of our secretaries, Maribel Lisk and Diana Williamson. And a sincere "Thank you!" is extended to Ruth Drago for welcoming me as a part of the ever-growing "extended" Drago family, and the fantastic meals. Included in this extended family are all the graduate students that I have had the chance to meet and work with. By far

this has been the most diverse group of people, as far as interests and beliefs, that I've had the pleasure to work with. I truly believe that every one of them helped teach me something while I was at U.F. (although I still haven't figured out what it was for a couple of individuals). I feel especially lucky to have had the opportunity to meet and work with the many postdoctoral researchers that came through our lab. People like Drs. Robert Beer, Krzysztof Jurczyk, Phil Kaufman, David Singh, Garth Dahlen and Doug Burns greatly aided my research, as well as became friends. Finally, I must thank the Florida Men's Rugby Club, for the great times, sportsmanship and camaraderie. It was with this group, and the friends I found within, that some of my fondest memories from graduate school lie.

> It is not the critic who counts; not the man who points out how the strong man stumbles . . . The credit belongs to the man who is actually in the arena, whose face is marred by dust and sweat and blood; who strives valiantly . . . who knows the great enthusiasms, the great devotions; who spends himself in a worthy cause; who at the best knows in the end of triumph of high achievement, and who at the worst, if he fails, at least fails while daring greatly, so that his place shall never be with those cold and timid souls who know neither victory nor defeat.
>
> -Theodore Roosevelt

TABLE OF CONTENTS

LIST OF TABLES

LIST OF FIGURES

Abstract of Dissertation Presented to the Graduate School
of the University of Florida in Partial Fulfillment of the
Requirements for the Degree of Doctor of Philosophy

CARBONACEOUS ADSORBENTS AS HETEROGENEOUS CATALYST SUPPORTS: APPLICATIONS AND CHARACTERIZATION

By

Todd James Lafrenz

December, 1995

Chairman: Dr. Russell S. Drago
Major Department: Chemistry

Porous materials have long been the subject for chemical research in applications as adsorbents and as heterogeneous catalyst supports. Many of the traditional instrumental methods for analyzing the chemical behavior and functionality of compounds do not readily lend themselves to the analysis of carbonaceous adsorbents. This is due in part to carbon's opaqueness and general amorphous nature. Methods do exist to help probe these materials; the most common and widely used of these is the determination and interpretation of gas adsorption isotherms. Several theories exist to help interpret standard adsorption isotherms. From these analyses, surface areas and porosity characteristics can be calculated.

Nine commercially available carbonaceous adsorbents were analyzed using a variety of physical methods in order to further characterize these types of materials. Methods included elemental analysis, thermal behavior, and surface area and porosity determination from gas adsorption/desorption

isotherms. A greater understanding of the physical properties that affect the adsorption behavior of these types of materials was gained.

A detailed and critical analysis of the application and interpretation of the standard BET equation was undertaken. From this analysis, a model complementary to the existing theories was proposed. Derived from a multiple-site Langmuir process, this proposed equation and its solution allow for a more direct comparison of various adsorbents with a variety of gaseous probes. Values for both the capacities and adsorption equilibrium constants for three distinct adsorption processes were derived using this model. The measurement of adsorption isotherms at a variety of temperatures allowed for the calculation of the thermodynamic parameters associated with these adsorption processes.

The understanding gained from the analysis of these carbonaceous adsorbents has assisted in the characterization of a heterogeneous Wacker-type oxidation catalyst. Salts of Pd(II) and Cu(II) were pore-filled onto a porous carbon, Ambersorb® 572, and an active heterogeneous gas flow reactor system for the oxidation of ethylene to acetaldehyde was developed. The employment of the porous carbon as a support was found to provide synergistic benefits for this type of catalysis, arising from the oxidative capability of the carbon itself and its high adsorption capacity and affinity for various substrates.

CHAPTER I
AN INTRODUCTION TO HETEROGENEOUS CATALYSIS

From the days of the alchemists, ideas of catalysis permeated scientific thinking and research. The alchemists' greatest endeavor was the pursuit of the "philosopher's stone," a material which would be able to transform base metals into gold and promote good health and long life. Its conception was catalytic in nature, as it was considered that one needed only a small amount of this material to effect large changes. Ever since these ancient times, the roles and understanding of catalysis in chemical research and industry, as well as the tremendous biological importance of catalysis, have continued to be studied. A greater understanding has been gained, but the concept of the philosopher's stone has changed many times since.

The traditional definition of a catalyst is a compound that facilitates the attainment of equilibrium in any chemical process much more rapidly than in its absence. Most often this is accomplished by the lowering of the activation energy for a reaction. The amount of catalyst required to do this is usually very small in comparison to the molar amounts of reagents and products present, so the catalytically active species itself is used over and over again. A catalyst cannot affect the position of the thermodynamic equilibrium; however, it may change the mechanism of a reaction significantly. Due to the inherent reactivity of many catalyst systems, one must be careful in investigating new catalytic applications. It may be observed that an active catalyst will continue reacting with desired products to yield unwanted by-products. This type of

reactivity problem in catalysis exemplifies that, in addition to present efforts in tailoring the reactivity of systems for specific applications, there already exists a large amount of research in the catalyst systems presently being used.

There are numerous examples in which catalytic processes have affected the consumer market. Included in these are hydrocarbon cracking and reformulation catalysts used in petroleum refining, polymerization catalysts in plastic production, hydrogenation of fats and edible oils for food-stuffs, catalytic converters in automobiles, industrial catalysts for NH_3 and SO_3 syntheses, and the medicinal value of understanding enzymatic catalysis occurring in both plant and animal tissues. Of the many types of catalytic processes that exist, all fall under the general classification of either homogeneous or heterogeneous catalysis. Homogeneous catalyst systems are characterized by the existence of reactants, products and catalyst all in the same phase. Heterogeneous catalyst systems exist in two or more phases. The most common examples of heterogeneous systems are gas phase reactions occurring over the surface of a solid catalyst material. Other types include two-phase liquid mixtures (i.e., organic and aqueous phases), and liquid-solid batch reactor systems.

Heightened interest has been given to the heterogenizing of typical homogeneous catalyst systems since the early 1970's.[1] Advantages of employing heterogeneous catalysts include ease of separation of products from the catalyst, recovery of used catalyst, and the synergistic benefits in cases where supports are used. The immobilization of a catalyst also inhibits its incorporation into the product composition. Synergistic benefits may include size and shape selectivities imparted due to constraints of internal pore volumes and channel dimensions in a support (e.g., molecular sieves), the existence of strong Lewis acid sites (e.g., aluminas, zeolites) or Brønsted-Lowry

acid sites (e.g., silicas, heteropolyacids), and concentration effects due to adsorbent-adsorbate interactions and capillary condensation (e.g., carbonaceous adsorbents). It has also been observed that the electro-chemical behavior of metal species is affected by doping the metal on solid supports, which may have advantages in sensors and electrocatalytic processes.[2,3,4]

There exist some inherent disadvantages to employing heterogeneous catalyst systems. In a homogenous environment almost every active catalyst species is capable of coming in contact with the reactant and, therefore, likely to participate in the reaction process. In a heterogeneous system the only catalytic sites available are those on the surface of the solid or at the interface between two layers. In a heterogeneous system, therefore, it is most desirable to suspend the catalyst in a thin film, as in a membrane type system, or disperse the active catalyst species on a high surface area material. In doing this, the chemical behavior of the support must now be considered. This chemical behavior would ideally be a synergistic benefit by design, but this is not always the case. When employing a solid in a catalytic process, one must also consider its mechanical strength. This may be a solid support, as when employing zeolites, silicas or carbons, or a solid constructed of the catalytic species itself, as in the case of various metal oxides or nickel/platinum hydrogenation catalysts. There are obvious concerns if the solid decomposes mechanically or chemically under the desired reaction conditions.

Despite these apparent disadvantages, heterogeneous catalyst systems have proven to be very useful and applicable to many commercialized processes. A large amount of research continues in all areas of heterogeneous catalysis, and new application and process patents appear regularly. One of the difficulties in doing basic chemical research on these types of systems is that most common experimental methods are most applicable to solution or

gas phase chemistry. Analyses of the chemical structures of carbonaceous solids and macroreticular polymers are further complicated by their opaqueness, and their highly cross-linked network structures which render them insoluble in most traditional solvent systems. Methods do exist that help characterize solid materials, including solid state nuclear magnetic resonance (NMR), X-ray powder diffraction, X-ray photoelectron spectroscopy (XPS), magic angle spinning NMR, diffuse reflectance infra-red fourier transform (DRIFT), photoacoustic infra-red spectroscopy, electron paramagnetic resonance (EPR), low energy electron diffraction spectroscopy (LEEDS), high resolution electron energy loss spectroscopy (HREELS), scanning electron microscopy (SEM), scanning tunneling microscopy (STM), atomic force microscopy (AFM), and extended X-ray absorption fine structure (EXAFS).[5] However, many of these techniques only provide qualitative information, or are limited to probing the surface or only a few molecular diameters beyond the surface. The introduction of ^{129}Xe-NMR experiments[6,7] and the combination of calorimetric and spectroscopic data[8,9] on solids have been helpful in elucidating internal structural and surface information, but these techniques are also limited in their applications. It remains difficult to characterize and understand the intricate chemistry that occurs within the internal porosity of solids employed in catalysis.

The ease with which gaseous or liquid reactant molecules can achieve access to the internal surfaces and pores of a solid is often of crucial importance in the development of a catalyst suitable for industrial applications. If one is to be able to understand, and then further predict catalytic behavior, a reliable methodology must be used to characterize the internal pore structure of the catalyst and the facility of transport of reactants and products through the catalytic material. The interpretation of gas and liquid adsorption

isotherms continues to be an elucidating method to probe the internal porosity of these materials. Various theories have been developed to help interpret gas adsorption isotherms to yield surface area and pore size information of porous solids.[10,11] It is well accepted in the literature, however, that many of these interpretations are derived while making several assumptions, some of which are considered to not be truly representative of the surface being probed. Yet qualitative discussions and direct comparisons of data under the same conditions are considered valid.

Carbon containing polymeric adsorbents and their derivatives are quickly expanding as the newest areas of interest for heterogeneous catalysis. However, because most carbonaceous materials are opaque and amorphous, they do not lend themselves readily to many of the characterization methods previously mentioned. Because of growing interest in the application and characterization of carbonaceous solids as adsorbents and in catalytic applications, it is of great interest to further quantify their chemical and physical behavior. Therefore, an understanding of the interactions involved in the physical and chemical adsorption of gases by solids is of fundamental importance to many of the applications of these types of materials.

In this series of studies, numerous high surface area carbonaceous adsorbents have been characterized. Comparisons of their surface areas and pore distributions, as well as their physical composition, have been made. A model is presented to help interpret gas adsorption isotherm data in attempts of obtaining more quantitative measurements for comparing these types of materials for adsorption and catalytic applications. One of the goals of this research was to avoid many of the assumptions that are made in current interpretations of adsorption isotherms. Ideally, this information could be used

to assist in the choice of an appropriate solid for whatever application is envisioned.

Finally, the understanding gained in characterizing carbonaceous solids has been applied in the development of a viable, heterogeneous catalyst system. This system involves a heterogeneous Wacker process, specifically looking at the oxidation of ethylene to acetaldehyde. Many factors have been found to affect the activity of these types of catalysts, including the surface and pore characteristics of the support, dopant levels, temperature and flow rates of gaseous reactants, and the components of the active catalyst species itself. All of these parameters were considered in detail in the development of this system.

CHAPTER II
CHARACTERIZATION OF CARBONACEOUS MATERIALS

Background

There exist a large variety of carbonaceous materials derived from both natural and synthetic polymeric materials. Natural sources include wood fiber, coconut husks, peat moss, petroleum pitch and coal tar residues. Synthetic precursors include polymers of styrene, acrylonitrile, vinyl and furfuryl alcohols, and phenolic resins. Applications of the carbonized derivatives of these materials include adsorbents for purification of gaseous and liquid streams, pressure-swing applications for gas separations, chromatographic stationary phases, heterogeneous catalyst supports, prosthetic devices in medicine, and composite and electrode materials.[12]

Pyrolysis of many of these polymers produces carbons that can be tailored for specific physical characteristics. These characteristics are determined by the original polymer structure, as well as the pyrolysis conditions and pretreatments. Typical carbonization conditions involve heating the materials under an inert atmosphere (e.g., N_2, Ar) from temperatures of 300°C to 3000°C. The porosity and extent to which these materials graphitise (at temperatures >2000°C) is largely dependent on the properties of the original polymer and the carbonization conditions.[13] Elimination of various volatile by-products during pyrolysis produces additional porosity in the remaining solid.[14] Finally, temperature control during pyrolysis is found to be very important to the resultant adsorbent properties of the carbons.[15]

Various treatments of these polymers are employed prior to pyrolysis to increase their thermal stability, therefore increasing carbon yields. For naturally occurring polymers, this may include chemical treatments with agents such as $ZnCl_2$, carbonates, alkali, sulfates, and sulfuric or phosphoric acids. This results in dehydration and further cross-linking of the polymers, which produce higher carbon yields unaccompanied by tarry residues from pyrolysis.[16] Synthetic polymers are made as macroreticular polymers to impart high thermal stability. Macroreticular polymers are characterized as being highly cross-linked, exhibiting little or no swelling upon wetting with a solvent, and have an open, rigid macroporous structure. Advantages of synthetic polymer precursors include greater control over the homogeneity of the starting material, and greater reproducibility from batch to batch. Synthetic polymers may also be imbibed or treated with chemical agents as in the case of natural polymers. The resultant benefits of a highly cross-linked polymer system, as well as the carbon-fixing agents previously mentioned, are to allow the carbon to char without fusing, therefore retaining its original pore structure. The process referred to as activation may also be employed during or after pyrolysis to impart various functionalities to the surface or increase porosity. This includes treatment with gases such as steam, air, NH_3, HCl, Cl_2, or CO_2, at temperatures that typically range from 300°C to 1000°C.

The resultant materials are generally amorphous in nature and best described as consisting of twisted networks of defective carbon layers bridged together with other similar layers. Although they do not possess uniform pore sizes as in the case of zeolites, they are found to contain unique pore shapes and uniform pore size distributions. From the previous discussion it can be envisioned that through the variation of a large number of parameters, a carbonaceous solid can be designed which will have both a specific pore

structure and surface functionality.[17] With this capability, carbon has advantages as an adsorbent or support over other traditional materials like zeolites or silica. Advantages may include the absence of strong Lewis acid sites as seen with aluminum in zeolites. Additional advantages may include solution and mechanical stability, carbon's general stability in many corrosive environments, and high adsorption capacities for various organic substrates. The very nature of carbon will lead to supported catalyst systems that behave differently than other types of supports currently used.

Carbons Under Study

Ambersorb® carbonaceous adsorbents, made by the Rohm and Haas Company, are among the materials that have been studied. Derived from macroreticular, sulfonated polystyrene, the pyrolyzed product has shown interesting behavior as both an adsorbent and catalytic support. The original polymer is made through a suspension polymerization method, with divinylbenzene as a cross-linking agent. The resultant polymer is in a bead form, which is retained during pyrolysis and mechanically very strong. Two types of Ambersorb® carbons were examined - Ambersorb® 563, lot# 91/3298 (A-563) and Ambersorb® 572, lot# 2125 (A-572). Together with differences in pore distribution and surface area, A-563 is reported to be more hydrophobic than A-572. More information on the physical properties, adsorption characteristics and syntheses of these materials can be found in the text by Neely and Isacoff,[18] and in the patent literature.[16,19]

Pyrolyzed polyacrylonitrile (PPAN) was also investigated. This material, a proprietary, high surface area carbon in bead form, was supplied courtesy of the Rohm and Haas Company. PPAN has been the topic of much research over

the past several years because of its unique mechanical strength, catalytic behavior and electronic properties.[20,21,22] However, there is a concern in developing any large scale synthesis because of HCN production during pyrolysis.

Two different carbons were obtained from the Calgon Carbon Corporation. Calgon BPL® granular carbons are derived from bituminous coal. Their production involves a steam activation treatment, resulting in a high surface area, highly porous material, suitable for vapor phase adsorption and as a heterogeneous catalyst support. For example, these carbons are used in the acetylene process for the production of vinyl chloride and vinyl acetate. Filtrasorb® 300, also made from coal, has been tailored to be an active adsorbent in water purification. Calgon BPL® 4x10 (BPL) and Filtrasorb® 300 8x30 (F-300) were the specific materials examined in these experiments.

A powdered carbon, AX21, was obtained from the Anderson Development Company. This material is made from a patented process involving direct chemical activation of petroleum coke with large amounts of KOH at elevated temperatures.[23] Further details on the preparation and properties of this material are reported elsewhere.[24,25] AX21 has also been previously studied in this research group as a catalytic support.[26]

Another powdered material examined was NORIT™ 211 from Kodak (N-211). Labeled as a decolorizing carbon, it is derived from pyrolyzed peat moss. This is further treated with a steam activation step to increase porosity, followed by an acid wash to leach out impurities. The original manufacturer was Norit N.V., and the NORIT™ line is now being distributed by Fisher Scientific.

A developmental product derived from macroreticular polystyrene was obtained from the Dow Chemical Company, courtesy of Jim Stahlbush. A

spherical bead like the Ambersorb® and PPAN materials, XUS-43493.01 (DOW 493) is designed for the concentration of organics from both air and water. It is reported to possess a unique pore structure and high surface area, with good physical strength and a hydrophobic surface. These materials are reported as having very little catalytic activity themselves due to extremely low ash content. This is in contrast to some activated carbons which contain residual metal salts from their processing or original sources. An advantage of low ash content would be the minimization of adsorbate decomposition, which is not desirable in some applications.

The final carbon considered in these experiments was Kureha BAC-SP. This is a spherical, activated carbon made by Kureha Chemical Industry Co., Ltd. in Japan. These "bead activated carbons" are spherical and reported as having a fairly uniform diameter of 0.7 mm. They are reported to have a low ash content and very high resistance to attrition on repeated usage.

The nine carbonaceous solids described above were chosen in order to examine a broad range of carbon materials. Most are commercially available, and are derived from a variety of both natural and synthetic precursors. The wide range of composition, pore size distributions, surface areas, and functionalities made these ideal materials for the focus of these investigations.

Experimental

Characterization of Supports

All carbons were used as received without further purification or treatment, and were dried/degassed at 200°C under a vacuum of $<10^{-3}$ torr for a minimum of 8 hours before any adsorption isotherms were obtained. All

gases employed in adsorption studies were purchased from the Matheson Gas Company with a minimum 99.99% purity, and were used without any further purification. Surface area and pore information were obtained on a Micromeritics® ASAP 2000 instrument. Elemental analyses (carbon, hydrogen and nitrogen) were performed by the University of Florida elemental analysis laboratory.

Surface areas were determined using a five point Brunauer-Emmett-Teller (BET) type analysis[27] of the N_2 isotherm obtained at 77K. For this entire range of materials, the best fit line for the BET transformation plot was found to be at $0.01 < P/P_0 < 0.07$ (see Results and Discussion for further details). Micropore volumes were calculated using the Harkins-Jura (HJ) model[28] with a t-plot statistical analysis.[29] The statistical thickness parameters used for the best fit line were from 5.5-9.0Å. An algorithm employing the Barret-Joyner-Halenda[30] (BJH) model was used to determine mesopore and macropore volumes from the adsorption portion of the isotherm. All the above calculations were carried out using the software supplied with the Micromeritics® ASAP 2000 instrument, and further details can be obtained from the instrument manual.[31] The interpretation of pore volumes follows the IUPAC recommended definitions with micropore diameters smaller than 2 nm, mesopores between 2 and 50 nm, and macropores having pore diameters larger than 50 nm.[32,33]

Thermal gravimetric analyses (TGA) were obtained on a T.A. Instruments, Inc., Thermal Analyst 2000 system under flowing nitrogen. This instrument was equipped with a Hi-Res TGA 2950 module, differential scanning calorimeter (model DSC 2910), and differential thermal analyzer (model DTA 1600). TGA temperature ramping was done employing the instrument's Hi-Res™ software. This software employs a variable temperature

ramping rate dependent on the rate of weight loss. The maximum temperature ramping rate was set at 10°C/min, with a resolution setting of 5.00. This enhances the resolution of weight changes, while minimizing run time and avoiding transition temperature overshoot.

Gas Adsorption Studies

Gas adsorption isotherms were obtained on the Micromeritics® ASAP 2000 Chemi system, or on a glass manifold line (Figure II-1). This manifold system consisted of a glass chamber of known volume; threaded Teflon high vacuum stopcocks (Ace Glass, 8190 series); a Welch vacuum pump and mercury diffusion pump; two pressure heads from MKS Baritron, type 390HA (one capable of measurements from 1-1000 torr, the other from 10^{-5}-1 torr); MKS Baritron type 274 channel selector, 270B signal conditioning unit, and a 390A sensor head; and various condensers and connecting tubing. The system itself was not thermostatted, but temperatures were found not to vary more than ±1°C over the course of a run.

The procedure to obtain isotherm data on the glass vacuum line, known as the successive addition technique, is a static, gas volumetric technique. It employs a known volume and changes in pressure to determine the amount of gas adsorbed. Initially, after the sample tube has been connected to the vacuum line *via* an o-ring seal, the entire system is evacuated and the sample degassed. After closing the valve to the sample, the manifold (V_m) and known volume (V_k) are filled with helium, a gas that is assumed to be non-adsorbing (see Figure II-2 for further detail of specific volumes). The valve to V_k is closed, the gas pressure recorded as P_1, and the manifold evacuated. Knowing the volume and pressure of the gas contained in V_k, opening the valve to V_k and

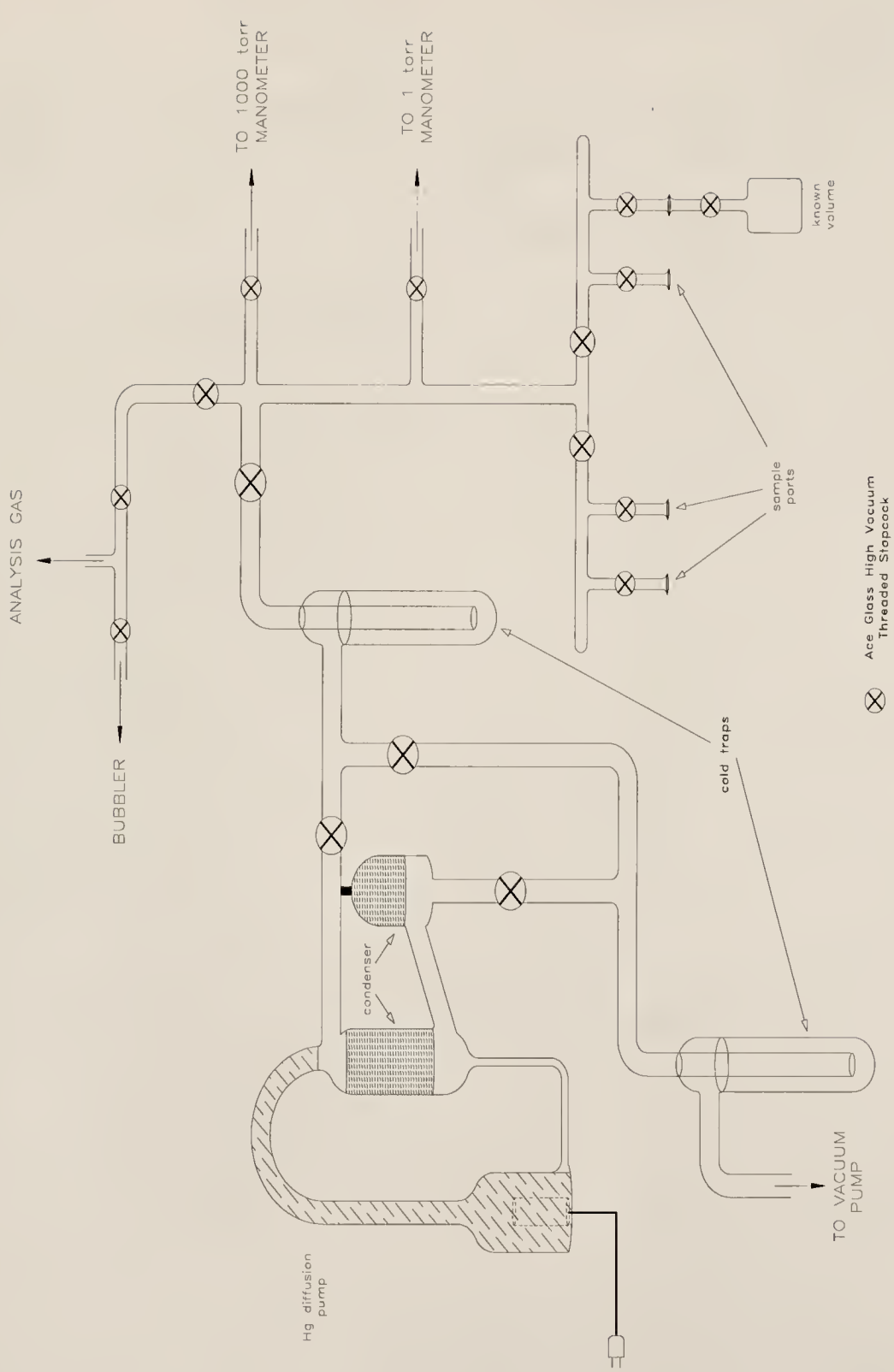

Figure II-1. Schematic of Glass Manifold for Adsorption Isotherm Measurements

allowing it to equilibrate with V_m yields P_2, the equilibrium gas pressure. Assuming ideal gas behavior, V_m was then determined by the following equations:

$$n_{gas} = P_1V_k/RT \qquad \text{(II-1)}$$

where n_{gas} is the total number of moles of gas in the system, R the ideal gas constant, and T the temperature (in Kelvin). Since R, T and n_{gas} stay constant, when V_k is opened up to V_m:

$$P_1V_k = P_2(V_k+V_m) \qquad \text{(II-2)}$$

which rearranges to

$$V_m = V_k\left\{\frac{P_1}{P_2} - 1\right\} \qquad \text{(II-3)}$$

This series of steps can now be repeated, where P_2 becomes P_1, the valve closed and V_m again evacuated, and then reopening V_k to V_m gives a new value for P_2. This sequence is repeated a total of five times, with progressively lower gas pressures, to give a determination of V_m over the entire range of experimental pressures, as well as a measure of the accuracy and reproducibility of these measurements.

Next, it is necessary to determine the free space volume (V_s), which encompasses the volume above the sample in the sample tube and the volume between and within sample particles (sometimes referred to as void volume). This procedure, continued from above, is done in a similar fashion as in determining V_m, however, this time V_m is used as the known volume to find V_s. An initial pressure exists in the manifold (P'_2) and in the sample volume (P'_1). Obviously, for the first data series $P'_1 = 0$. V_m is then opened to V_s, and a new pressure is obtained (P'_3). The initial moles of gas present can be expressed as

$$n_s = P'_1V_s/RT \qquad \text{(II-4)}$$

$$n_m = P'_2V_m/RT \qquad \text{(II-5)}$$

$$n_3 = P'_3(V_s+V_m)/RT \qquad \text{(II-6)}$$

since $n_3 = n_s + n_m$:

$$\frac{P'_1 V_s}{RT} + \frac{P'_2 V_m}{RT} = \frac{P'_3 (V_s + V_m)}{RT} \qquad \text{(II-7)}$$

which rearranges to

$$V_s = V_m \left\{ \frac{P'_3 - P'_2}{P'_1 - P'_3} \right\} \qquad \text{(II-8)}$$

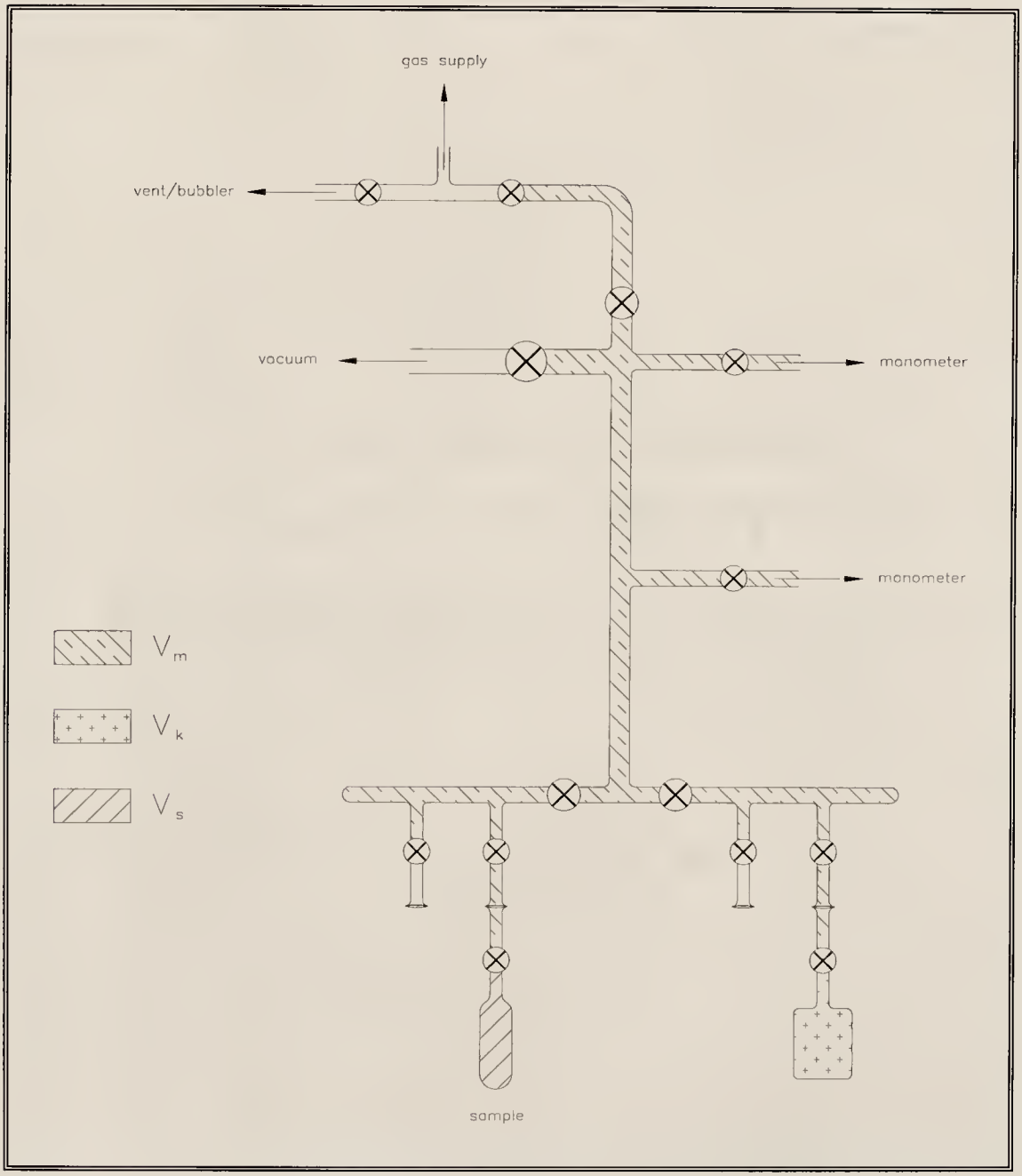

Figure II-2. Exploded View of Specific Volumes V_k, V_m and V_s from Glass Manifold

This series of measurements is then repeated over the entire experimental pressure range (0-760 torr), as was done in the determination of V_m, by the following method. After closing the valve connecting V_m and V_s, the manifold is dosed to a higher pressure yielding a new value for P'_2. The previous value of P'_3 becomes the P'_1 value for this data series, and a new value for P'_3 is obtained when V_m and V_s are allowed to equilibrate. As before, the values obtained for V_s over this entire pressure range are averaged, giving an estimate of the precision of these measurements. A large deviation may be indicative of strong adsorption of helium by the sample. This was not observed for any of the samples investigated.

With V_m and V_s now known, gas adsorption isotherms can be obtained using the particular adsorbate of interest. Data were obtained in a similar fashion as to that in the determination of V_s. After the manifold, known volume and sample volume were evacuated, the sample valve was closed and V_m again determined from V_k (Eqns. II-1 through II-3 and procedure outlined therein). This was repeated to help minimize any errors due to non-ideal behavior of the adsorbate gas, as well as for verification of prior results. Any large deviation from the value of V_m determined using helium would be indicative of the probe gas not behaving ideally, or it strongly adsorbing to the walls and seals of the manifold itself. This was not observed with any of the gases used in these studies.

After determination of V_m with the adsorbate gas, pressures were obtained in a fashion similar to that used for determination of V_s with helium. The initial pressure contained in the manifold (P''_2), which was filled to specific incremental pressures, and that contained in the sample volume (P''_1) were measured (again $P''_1 = 0$ for the first data series), and then V_m and V_s were opened to one another and allowed to equilibrate. This gave rise to the

equilibrium pressure measurement, P''_3. The number of moles of gas adsorbed by the solid (n_{ads}) was found from the difference in the number of moles present initially in the gas phase (n_{ini}) and that present after equilibrium was allowed to be established (n_{equil}):

$$n_{ads} = n_{ini} - n_{equil} \qquad \text{(II-9)}$$

where

$$n_{ini} = \frac{P''_2 V_m}{RT} + \frac{P''_1 V_s}{RT} \qquad \text{(II-10)}$$

$$n_{equil} = \frac{P''_3 (V_m + V_s)}{RT} \qquad \text{(II-11)}$$

Substituting equations II-10 and II-11 into II-9 gives

$$n_{ads} = \frac{(P''_2 V_m + P''_1 V_s) - P''_3 (V_m + V_s)}{RT} \qquad \text{(II-12)}$$

This value was then divided by the mass of solid sample to give an amount adsorbed per gram of adsorbent.

Pressure readings were recorded in torr, but were all divided by 760 to yield pressures in units of atmospheres (atm). Equilibrium was considered to be established when the pressure reading did not change ±2 units over a period of 30 seconds (values were recorded to four significant figures).

The Micromeritics® ASAP 2000 Chemi system performs its analyses and calculations in a similar fashion. Further details on the free space determination, adsorbed gas volumes and equilibration intervals can be found in the ASAP 2000 Chemi reference manual.[34] Equilibrium was considered attained for runs on this instrument when the pressure change per ten second time interval was less than 0.01% of the average pressure during that time interval. All adsorption isotherms were reported at pressure values between 0

and 1 atm, as most interest in these materials involves applications under standard atmospheric pressures.

Results and Discussion

Elemental Analyses

Because of the variety of sources and precursors for the various carbons under study, an initial determination of their physical composition was desirable. Since all of these materials have been pyrolyzed under relatively high temperatures, it can be assumed that their chemical composition is mainly carbon, with small amounts of hydrogen and oxygen, as well as nitrogen if it was present in the original polymeric precursor as in the case of PPAN. Mechanistic details on the decomposition under pyrolysis conditions for polymeric precursors of these materials are well characterized and have been reported.[13,35,36] Other chemical components are assumed to have been present in the original material as impurities, or incorporated during their preparation. All characterizations and isotherms were obtained on the same batch and lot number of a specific material.

Elemental analyses were done on all carbons as received, without further washing or treatment. The rationale was that this would most likely be the way these materials are used in the development of large scale production for a commercial catalyst or adsorbent system. The majority of the carbons exhibited less than 5% weight loss upon drying. Exception to this was observed for N-211, PPAN, and AX21. However, CHN analyses were obtained on all the materials as received without predrying, except in the case of AX21, for which both a wet and dry sample were submitted (Table II-1). In all cases,

Table II-1. Elemental Analyses for Carbons Under Study

	%C	%H	%N	total %CHN	approx. % weight loss upon drying[a]
PPAN	70.18	1.66	5.31	77.15	23
A-572	91.13	0.33	0.00	91.46	5
A-563	83.57	1.70	0.00	85.27	4
N-211	85.24	0.46	0.39	86.09	10
BPL	88.82	0.50	0.70	90.02	3
F-300	89.60	0.34	0.55	90.49	5
Kureha	95.56	0.67	0.04	96.27	4
DOW 493	87.25	7.05	0.02	94.32	5
AX21	44.43	2.60	0.07	47.10	53
AX21 (dried)[a]	87.13	0.31	0.15	87.59	--

[a] Dried under standard conditions for gas adsorption experiments, which involves degassing at 200°C under a vacuum of $<10^{-3}$ torr for a minimum of 8 hours.

the weight loss upon drying accounts for the majority of the remaining mass balance. Because of this, it was assumed that most of this weight loss occurs simply due to loss of adsorbed water, and, to a much lesser extent, adsorbed atmospheric gases. Any residue left after CHN analysis was attributed to metal salt impurities, as alluded to earlier, or other functionalities existing due to activation treatments. These may include groups containing oxygen, sulfur, phosphorous or chlorine. It is well accepted in the literature that these types of functionalities can exist on carbon surfaces,[12] but specific analyses for other functional groupings or metal salts were not done on these materials. The data presented in Table II-1 gives a relative comparison of the purity and hydrophilicity of these various carbonaceous adsorbents.

Surface Area and Pore Volumes

In employing highly porous solids as adsorbents and catalyst supports, an accurate determination of the physical structure of the surface, internal porosity and interconnecting channels is desirable. One of the standard techniques used for the determination of this information employs the N_2 adsorption and desorption isotherms obtained at 77K. Nitrogen is most often chosen as the adsorbate in these measurements because its small molecular size allows it access to small pores. Furthermore, it is easily handled, economical, approximately spherical, and inert, hence not likely to participate in chemisorption. Other gases can be used, the most common of which are krypton or argon.

Various theories exist to interpret isotherm data leading to the determination of surface areas, pore sizes, and pore volume distributions.[37,38] Determination of surface area turns out to be very complex in the absolute sense, however. Factors that may affect the determination of surface areas from standard methods that contribute to the inaccuracies can include irregular surface features, the fact that most surfaces of interest are energetically heterogeneous, resolution of the method, and the size of the probe molecule being used.[39] Although certain assumptions have to be made in the interpretation of gas isotherm data, the relative ease of data acquisition and the non-destructive nature of the technique give N_2 adsorption a large advantage over other methods such as mercury porosimetry.

The BET equation (Eqn. II-13) was employed in determining surface areas from gas adsorption data obtained on these carbons, employing N_2 gas as the adsorbate, with the sample container immersed in a Dewar containing liquid N_2 (at 77K).

$$\frac{X}{n_{ads}(1-X)} = \frac{1}{C \cdot n_m} + \frac{(C-1)}{C \cdot n_m} \cdot X \qquad \text{(II-13)}$$

The relative pressure, X, is P/P_0, where P is the measured equilibrium pressure (in torr) and P_0 is the adsorbate saturation pressure at the given temperature. The value n_{ads} is the molar amount adsorbed at the relative pressure X. The values of n_m, the monolayer capacity, and C, a constant dependent on isotherm shape, are both determined from the best fit linear plot of $\frac{X}{n(1-X)}$ vs. X. After determination of n_m and C, the surface area can then be calculated from

$$S.A._{BET} = n_m \cdot N_A \cdot \sigma \qquad \text{(II-14)}$$

where N_A is Avagadro's number (6.022×10^{23}), and σ is the cross-sectional area of the probe molecule. For N_2, a value of $\sigma = 0.162$ nm^2 was used. This is yet one more point of debate in the usage of gas adsorption data for the determination of surface areas, and several publications have discussed how the cross-sectional areas of adsorbed gases vary dependent on both adsorbent and temperature.[40,41] The appropriate conversion factors are combined with Equation II-14, and the final value divided by the mass of solid in the experiment yielding a value for the BET surface area ($S.A._{BET}$) in units of m^2/g.

The multi-point methods used in these studies for surface area determination are derived strictly from equations II-13 and II-14. For this multi-point method, analysis of the BET equation (Eqn. II-13) finds that plotting T versus P/P_0 yields a straight line, where T is

$$T = \frac{1}{\left[n_{ads}\left(\frac{P_0}{P} - 1\right)\right]} \qquad \text{(II-15)}$$

where n_{ads} is the number of moles of gas adsorbed per gram of solid at the measured relative pressure. The least-squares fit analysis of the line passing through the points chosen generates the slope (S) and y-intercept (Y_{int}), where

$$S = (C-1)/C \cdot n_m \qquad \text{(II-16)}$$

$$Y_{int} = 1/C \cdot n_m \qquad \text{(II-17)}$$

Simultaneous solution of the two equations gives n_m and C, where n_m is then used to calculate the S.A.$_{BET}$.[42] The Micromeritics software employs this relationship to find surface areas, employing the volume of gas adsorbed instead of the number of moles.[31] These two quantities are related simply by the molar gas volume. Therefore, in the case of the isotherms measured on this instrument, Equation II-15 becomes

$$T = \frac{1}{\left[V_{ads}\left(\frac{P_0}{P} - 1\right)\right]} \qquad \text{(II-18)}$$

and the S.A.$_{BET}$ (in units of m^2/g) is calculated from the slope and intercept of this line by

$$S.A._{BET} = \frac{\sigma \cdot N_A}{22414 \cdot 10^{18} \cdot (S + Y_{int})} \qquad \text{(II-19)}$$

Data points from the adsorption isotherm chosen for the determination of the S.A.$_{BET}$ are typically chosen between relative pressures of 0.05 and 0.30. Below this region it is found that BET theory predicts adsorption values below experimental values. Micropore filling arising from high adsorption potentials is the major cause of this inaccuracy. Above $P/P_0 = 0.30$, multilayer adsorption occurs, and BET theory is found to predict an adsorption value that is too high.

In this research, five points were chosen from the region of the isotherm that yielded the best fit line in the BET transformation plot (Eqn. II-18). Although the chosen data region, $0.01 < X < 0.07$, for these carbons occurred near and below the lower limit for BET analysis previously mentioned, these limits are not exact and do vary from solid to solid. The presence of large micropore volumes also affects the choice of this data set. In these analyses, the data series that yielded the best fit line for the transformation plot was used. For all the samples, the correlation coefficient for the 5-point line chosen

was found to be greater than 0.99999. As previously mentioned, the application of BET theory is based on several assumptions, and surface area determination is very difficult in the absolute sense. Therefore, for these materials the choice of the best fit line and the use of the same data region for each solid was assumed to be the most appropriate for making relative comparisons. The experimental data set used in applying BET and the pore-volume theories (BJH and HJ) should always be kept in mind when making quantitative comparisons based on these types of reported values.

Table II-2. BET Surface Areas and Pore Volume Data from BJH Adsorption Curve

CARBON	Surface Area (m^2/g)	Pore Volumes (cc/g)			BET C constant
		micropores	mesopores	macropores	
PPAN	880	0.334	0.119	0.090	1685
A-572	1159	0.428	0.284	0.207	866
A-563	606	0.221	0.206	0.226	1850
N-211	762	0.263	0.188	0.050	888
BPL	1075	0.432	0.079	0.009	313
F-300	1026	0.390	0.143	0.022	416
Kureha	1382	0.557	0.062	0.007	287
DOW 493	1340	0.498	0.314	0.324	328
AX21	2745	1.160	0.318	0.016	83.2

The data presented in Table II-2 shows the determined surface areas and pore volume distributions for the carbons analyzed. As was mentioned earlier, although these materials do not possess uniform pore structures, they were found to contain unique and uniform pore size distributions. Reference to the

pore volume distribution curves in Appendix A is made here, as well as the data presented in Table II-2. From this it can be seen that a variety of carbonaceous materials with a large diversity of relative surface areas and pore volumes have been considered.

The initial steep slope of the experimental isotherms (see Appendix A) is attributed to a large enhancement to the energy of adsorption due to the presence of pores with diameters of only a few molecular diameters (with reference to the probe molecule), and narrow openings to larger pores in the internal volume of the porous solid. This large interaction potential arises from the close proximity of opposing walls, resulting in a large volume of the adsorbed gas being concentrated in the micropore volume at pressures below its normal saturation pressure, to the point of condensation of the adsorbate. This large potential, which might be accounted for by the occurrence of chemisorption, was ruled out in the case of these carbons as all of the N_2 isotherms were found to be completely reversible.

Following this steep slope in the adsorption curve attributed to micropore filling, the isotherm levels off. The knee in the curve in this region occurs near the monolayer coverage, or filled micropores in the case of microporous solids. In this leveled region of the isotherm, monolayer and multilayer formation occurs, which is followed by another steep increase in the slope. This second large increase in adsorption is attributed to mesopore filling due to capillary condensation. The final leveling off of the adsorption curve represents attainment of the adsorption capacity of the porous solid. The multilayers thus formed more closely resemble the bulk liquid than the monolayer that is idealized in the application of classical adsorption theories. However, the narrowness of the pores in a solid may disturb the condensed phase so as to modify it from the bulk liquid or impose steric effects on the

packing of the molecules.[43] For these reasons, the usage of BET theory for surface area determination is not considered an absolute method. For similar samples run under identical conditions, however, relative comparisons are considered valid. It is on this assumption that direct comparisons were made for the various carbons and the data presented in Table II-2.

The overall shape of the N_2 isotherms (Appendix A) can be classified as Type II or Type IV according to the BDDT classification scheme.[44] Exception to this can be seen in the case of Kureha, BPL and AX21, which more closely resemble the Type I isotherm. Analysis of the data in Table II-2 and the pore distribution curves in Appendix A shows that these three solids are almost entirely microporous. These classifications are indicative of porous solids, and interpretation of the various regions of these isotherms follows the description in the previous paragraph. In general, reversible isotherms exhibiting a steep increase in adsorbed volumes at low relative pressures are indicative of highly porous materials and thus, the presence of micropores.[37,38] This steep increase will yield a greatly enhanced value for the BET C value (> 300), and a surface area that may be erroneously high.

The difference between these three isotherm types is that Type I isotherms are generally observed for solids that are mainly microporous. A steep increase is observed in the initial low pressure region of the isotherm, with a leveling off over the remainder of the pressure range. The shape of the Type II and IV isotherms are very similar, where Type IV is generally seen to level off near $P/P_0 = 1.0$ and a hysteresis often observed, yielding further insight into the pore size distributions and shapes. More detail on the meaning and importance of these various isotherm types can be found in the literature.[37,38,39]

The hysteresis effect arises from a surface tension phenomenon due to the condensed phase of the adsorbate. The narrower the pores, the greater the

curvature on the condensed surface, and the lower the vapor pressure of the condensed phase. Therefore, upon desorption of an adsorbed gas, a lower pressure must be reached before the adsorbate desorbs and a hysteresis loop is thus observed. A similar but opposite effect would arise from narrow entrances to larger pores (ink-bottle pores). The restricted opening, and hence the small diameter and greater curvature of the surface of the condensed phase at the pore opening, would make it necessary for a greater pressure to be reached before the pore would fill. The rapid filling of this pore volume would result in an erroneously high value for the volume of the smaller pore size, which was derived from the pore entrance diameter. This would also contribute to the occurrence of a hysteresis in the adsorption/desorption isotherm.

The relationship between the vapor pressure and the condensed film surface radius, in addition to the thickness of the adsorbed layers, provides the basis of BJH theory.[30] Pore volume distribution plots of the BJH desorption data can be found in Appendix A. The y-axis in these plots, dV/dlog(D), is generated from the following equation:

$$\frac{dV}{d\log(D)} = \frac{V_{pI}}{\log(D_{pI}/D_{pI+1})} \qquad \text{(II-20)}$$

where V_{pI} is the adsorbed gas volume (cm^3/g @ STP) at data point I, and D_{pI} and D_{pI+1} are the pore diameter range over which the BJH calculation was done. Graphed in this fashion, the change in pore volume per change in magnitude (change per decade) of pore diameter is represented.

From this graphical data, it was observed that the majority of the carbons analyzed generally have a bi-modal distribution of pore size ranges, where the relative maxima vary from carbon to carbon. For instance, A-572 was found to be bi-modal, with a distinct amount of its pore-volume contained in pores < 20Å in diameter, and the rest between 250-400Å, with a maximum

around 320Å. In the case of Kureha, almost all of its pore volume is contained in the micropore region (< 20Å), with a small peak at ~40Å. The BJH pore volume distribution plots compliment the data reported in Table II-2, and show these materials have a limited, well defined pore structure. This information can be used to further help in determining which adsorbent would be the most appropriate choice for a specific application.

In general, it is proposed that the BJH desorption data is more representative of the surface than the adsorption data. However, both data sets are subject to error from effects of narrow pore openings into larger pores and failures in the assumptions made by the model. The BJH model assumes a cylindrical pore shape, which obviously cannot be rigidly correct as the majority of these pores consist of irregular spacings between carbon particles. Consequently, the reported pore sizes and volumes cannot be taken as absolute, but may be interpreted as a statistical average of irregular pore shapes.[30] It is therefore more important in making comparisons of a variety of solids to be consistent in data manipulation, and for these experiments the BJH adsorption curve was used to calculate mesopore and macropore volumes. For point of interest, the mesopore and macropore volumes determined from the BJH desorption curve are reported in Table II-3. However, for purposes of later discussion the values reported in Table II-2, based solely on the BJH adsorption curve, will be the only values used.

The BET C constant is related to the increased effect on the heat of adsorption for these systems. For the determination of a reliable value of n_m, the monolayer coverage, it is beneficial to have a sharp knee in the initial portion of the isotherm, which also results in an increased value of C. However, the ideal adsorptive for these types of measurements would be

Table II-3. Pore Volume Data from BJH Desorption Curve

CARBON	Pore Volumes (cc/g)	
	mesopores	macropores
PPAN	0.203	0.009
A-572	0.496	0.001
A-563	0.441	0.002
N-211	0.022	0.215
BPL	0.113	0.003
F-300	0.158	0.008
Kureha	0.090	0.002
DOW 493	0.427	0.196
AX21	0.354	0.006

spherically symmetrical and tend not to localize on the surface. Non-localization demands a low value for C, as a large value is indicative of strong interactions between the adsorbate and adsorbent. The stronger the interaction between the two, the more an effect the adsorbent lattice has on the orientation and geometry of the adsorbed molecule.[45] The BET C value has also been related to the enthalpy of interaction by the following equation:[46]

$$\ln C = (\Delta H_{ads} - \Delta H_l)/RT \qquad \text{(II-21)}$$

where ΔH_{ads} is the adsorption energy and ΔH_l the heat of liquefaction of the adsorbate. However, it is generally accepted that, although the value of C may give an indication of the magnitude of the adsorbent-adsorbate interaction and the isotherm shape, this value is not usually directly translatable to adsorption enthalpies.[32]

It was observed from the data in the last column of Table II-1 that these types of adsorbent materials readily adsorb moisture and atmospheric gases.

Because of this, degassing at elevated temperatures under vacuum before isotherms are obtained is necessary. The data in Table II-4 illustrates the effect of degas temperatures on surface area and pore volume for PPAN. It has been reported that for degassing of microporous, carbonaceous materials temperatures of at least 300°C should be employed.[33] However, original analyses included some of the polymeric precursors to the carbons reported that were known to be thermally unstable at these higher temperatures (see Figures II-3 and II-4). For this reason, a lower temperature of 200°C was chosen for these gas isotherm studies. From the data presented in the following table, it was observed that increasing the degas temperature had its greatest effect on increasing the surface area and micropore volume.

Table II-4. Degas Temperature Effects on Surface Area and Pore Volumes for PPAN

Degas Temp.	Surface Area	Pore Volumes (cc/g)			BET C
(°C)	(m^2/g)	micropores	mesopores	macropores	constant
110	806	0.305	0.120	0.086	1549
200	880	0.333	0.119	0.090	1685
300	925	0.351	0.118	0.094	1714

TGA, Pyrolysis and Pore Volumes

Samples were obtained, courtesy of the Rohm and Haas Company, that were similar in chemical composition to the precursor materials for the syntheses of Ambersorb® adsorbents, for the purpose of studying the thermal, surface area, and pore volume characteristics of the polymeric materials used as precursors for the variety of carbons evaluated. Although these results cannot be assumed to be representative of all of the materials listed, they were

considered representative of this class of compounds. These analyses were found to yield interesting information about the effects of functionality and thermal treatments on the resultant pyrolyzed solids.

Two solids were analyzed with a variety of elemental analyses, surface area and pore volume studies, and thermal gravimetric analyses (TGA). One of these materials, referred to as A-POLY, was a macroreticular copolymer of styrene and divinylbenzene, with no additional functionality. The other, A-SO4, was a similar polysulfonated copolymer. Both of these materials were in bead form, made through suspension polymerization, and were used as received without any further treatment.

Table II-5. Elemental Analyses for A-POLY and A-SO4

	%C	%H	%N	total %CHN	approx. % weight loss upon drying
A-POLY	91.66	8.07	0.00	99.73	1
- pyrolyzed[a]	92.56	3.44	0.00	96.00	---
A-SO4	39.19	5.22	0.00	44.41	12
- pyrolyzed[a]	82.78	2.09	0.00	84.87	---

[a] The CHN results for the pyrolyzed samples were obtained from the chars resulting from the TGA analyses (Figs. II-3 and II-4) on the original polymeric materials.

The two polymeric materials were both subjected to pyrolysis conditions, and weight loss as a function of temperature was analyzed employing TGA. Note that the major difference between these two materials is that A-SO4 has been sulfonated, where A-POLY has not. It was observed that without functionalization, this type of polymer system readily degrades at temperatures near 300°C, with ~7% of the original mass left at 600°C (Figure II-3). This translates to a 7.0% carbon yield under these conditions. However, the

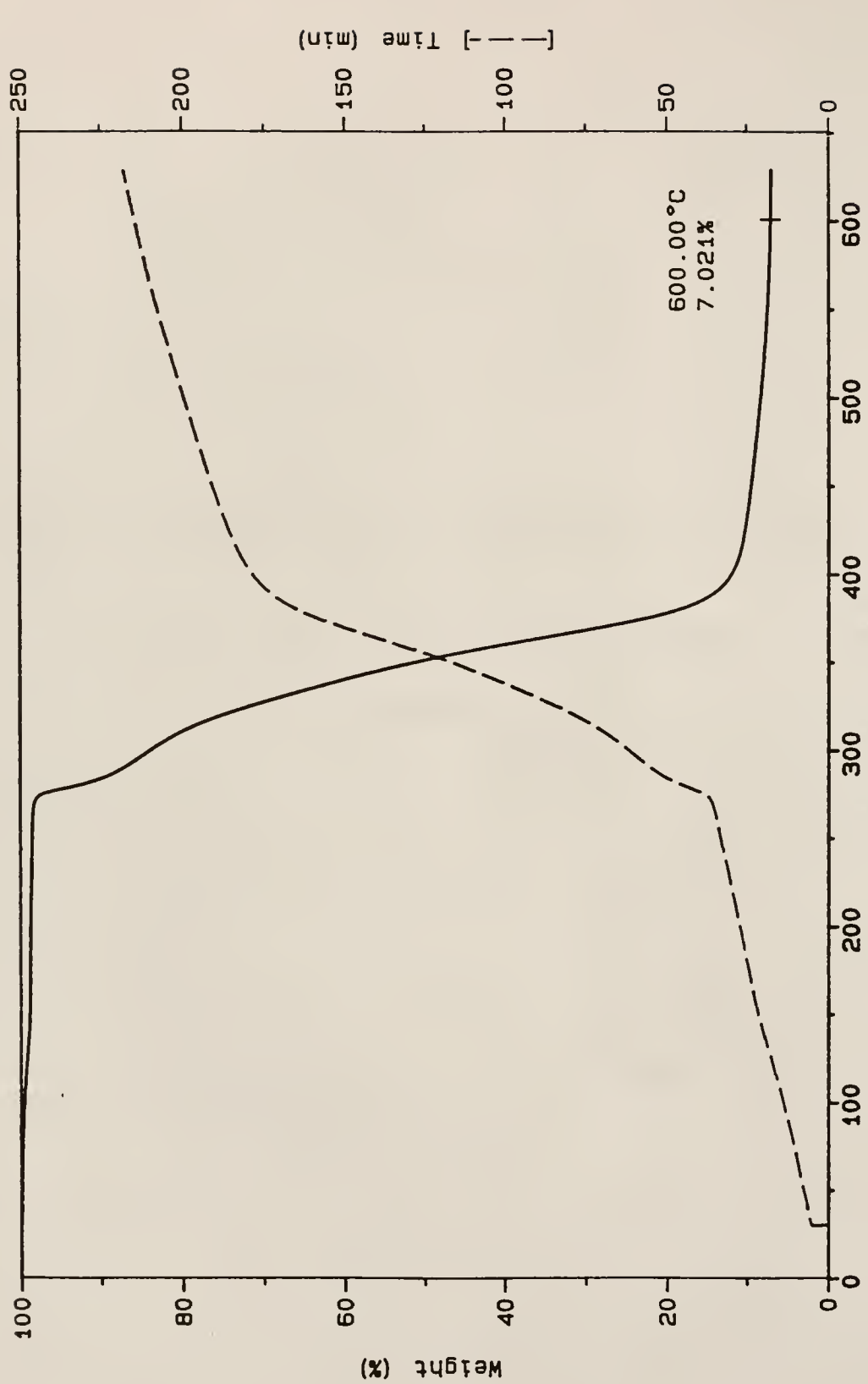

Figure II-3. TGA Results for A-POLY

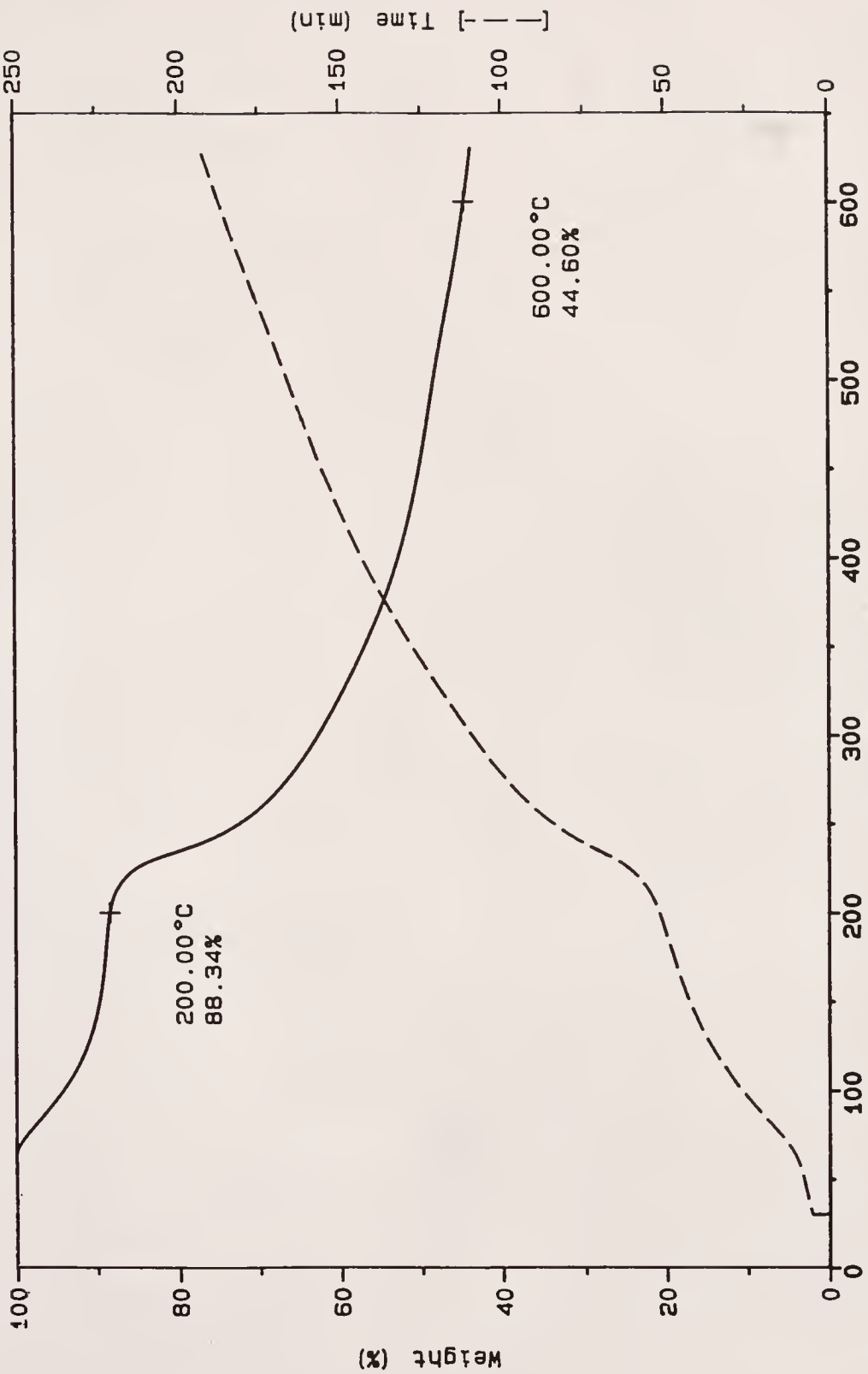

Figure II-4. TGA Results for A-SO4

sulfonation of these polymers greatly increases their thermal stability, where ~45% of the original mass still remains at 600°C (Figure II-4). This represents a 94.2% carbon yield. Elemental analyses for these two polymers and their resulting chars are presented in Table II-5. One can infer from this information that approximately 44% of the mass of A-SO4 was due to the presence of the sulfonate groups. The data from the last column in Table II-5 shows that functionalization of this polymer greatly enhances its tendency to adsorb atmospheric moisture. The initial weight loss in Figure II-4 between room temperature and 200°C is attributed to the loss of this moisture, and this value agrees well with the observed weight loss reported in the table. The second phase of weight loss, observed above 200°C, is reported to be due to the loss of the sulfonate functional groups,[36] and this is in agreement with the results observed in the TGA. At 600°C, approximately 55% of the original mass has volatilized, which is in agreement with the loss of sulfonate functionality and adsorbed moisture inferred from the CHN data.

To observe how pyrolysis temperatures affect pore distributions and surface areas, a series of experiments was performed with A-SO4 varying the maximum temperature by increments of 50°C up to 600°C. These runs were done by placing ~1.5g of A-SO4 in a porcelain boat, placing this inside a quartz tube in a tube furnace, and performing the pyrolysis under flowing N_2 gas. The tube furnace (Hevi-Duti Electric Company, type M-3012) was controlled with an Omega CN-2042 programmable temperature controller. All samples were purged with nitrogen before elevating the temperature, and the ramp rate was constant for all, at 2°C/minute. The sample was held at the maximum temperature for 15 minutes, and then allowed to cool at the same rate of 2°C/minute down to room temperature. Surface area and pore distributions were obtained on all the resultant carbons in the same manner as previously

outlined. However, the degas temperature for all these samples was lowered due to the thermal instability of A-POLY and A-SO4. For comparison purposes this temperature was kept constant for all samples at 110°C.

Table II-6. Pyrolysis Temperature Effects on Surface Area and Pore Volumes for A-SO4[a]

Pyrolysis Temperature (°C)	Surface Area (m^2/g)	Pore Volumes (cc/g)			BET C constant
		micro-	meso-	macro-	
A-POLY[b]	77	0.006	0.265	0.191	42.8
A-SO4[b]	43	0.005	0.130	0.137	88.6
300	426	0.152	0.207	0.236	599
350	536	0.194	0.227	0.255	729
400	623	0.228	0.239	0.265	849
450	652	0.240	0.246	0.257	1061
500	692	0.255	0.260	0.250	1355
550	716	0.262	0.246	0.249	1659
600	690	0.252	0.229	0.238	1987

[a] Degas temperature changed from normal for these samples. Conditions were kept at 110°C under $<10^{-3}$ torr vacuum for a minimum of 8 hours.
[b] Unpyrolyzed polymers as received.

Table II-6 shows the changes in surface areas and pore features from the original polymeric materials as a function of the pyrolysis temperature. It can readily be seen how increases in temperature increased all of these parameters up to about 550°C. After this point, increases were no longer observed, except for the BET C value, and changes occurring above this temperature were much more subtle, involving structural rearrangements and additional loss of hydrogen. This was verified by the data presented in Table II-7, where a

definite trend of rising %C and falling %H was seen as pyrolysis temperatures increased. Further illustration of these changes in pore volumes is given in Figure II-5.

Table II-7. Elemental Analyses for Pyrolyzed A-SO4

Pyrolysis Temperature (°C)	%C	%H	%N	total %CHN
300	66.93	2.94	0.00	69.87
350	73.53	2.89	0.00	76.42
400	77.38	2.84	0.00	80.22
450	81.07	2.87	0.00	83.94
500	84.19	2.78	0.00	86.97
550	86.80	2.57	0.00	89.37
600	88.89	2.27	0.00	91.16

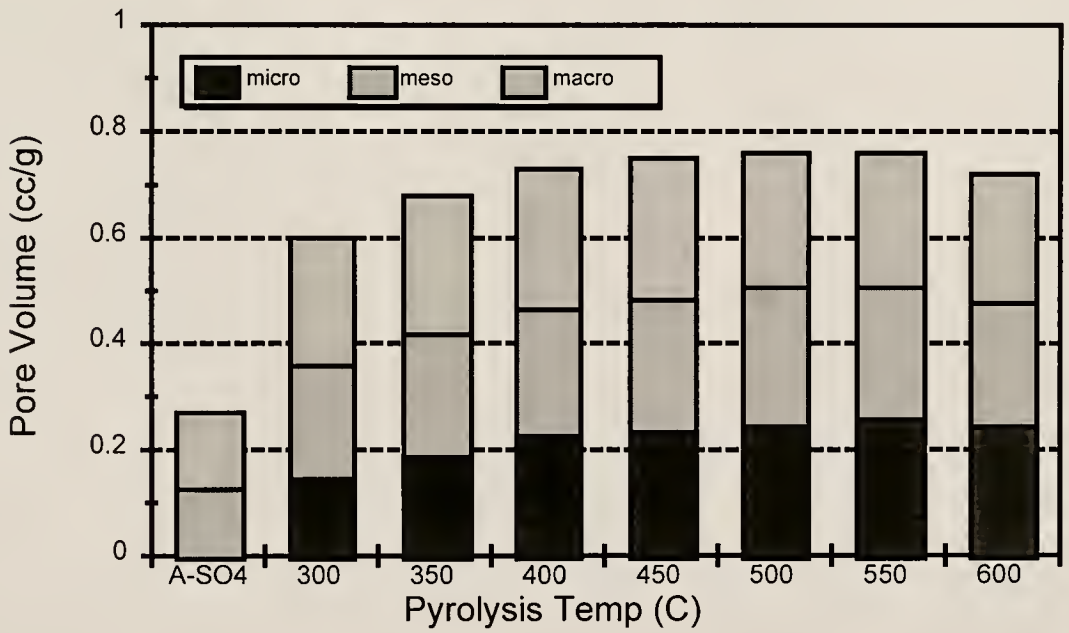

Figure II-5. Pyrolysis Temperature Affects on Pore Distributions for A-SO4

Gas Adsorption Isotherms

To gain further understanding of the adsorption characteristics of these carbonaceous materials, a series of gas adsorption isotherms was obtained at room temperature employing a variety of gases. The tabular data for these adsorption isotherms, as well as isotherms obtained at other temperatures, are summarized in Appendix B. Figure II-6 compares the N_2 adsorption isotherms obtained on all nine carbons at room temperature. Relative comparisons of the affinity and capacity of these materials can be made from this data. Attempts to correlate the adsorption capacities with any of the previously reported surface area, pore volumes or the BET C constants yielded no apparent trends for this data. Similar data is reported in Figure II-7 for room temperature CH_4 adsorption, except for data for F-300 and a limited data set for PPAN. The capacity of all of these solids was higher for CH_4 than N_2, yet again no direct correlation for the relative ordering could be made with any of the physical parameters previously found.

In comparing the N_2 adsorption data with that of CH_4, the relative affinities and capacities of some of the solids change as a function of both the adsorbate and equilibrium pressure. This is most obvious in the CH_4 adsorption data for BPL and N-211. Since no physical parameter, such as micropore volume or surface area, can be employed to adequately explain this shift in adsorption behavior, the chemical functionality of the surface and the adsorbate must have decided effects on the adsorption process. It is of interest in comparing these adsorbents to be able to better quantify the adsorption affinity and capacity they would have under various conditions. Therefore, it is obvious that other parameters must be considered when attempting to choose the best adsorbent/support for a specific application.

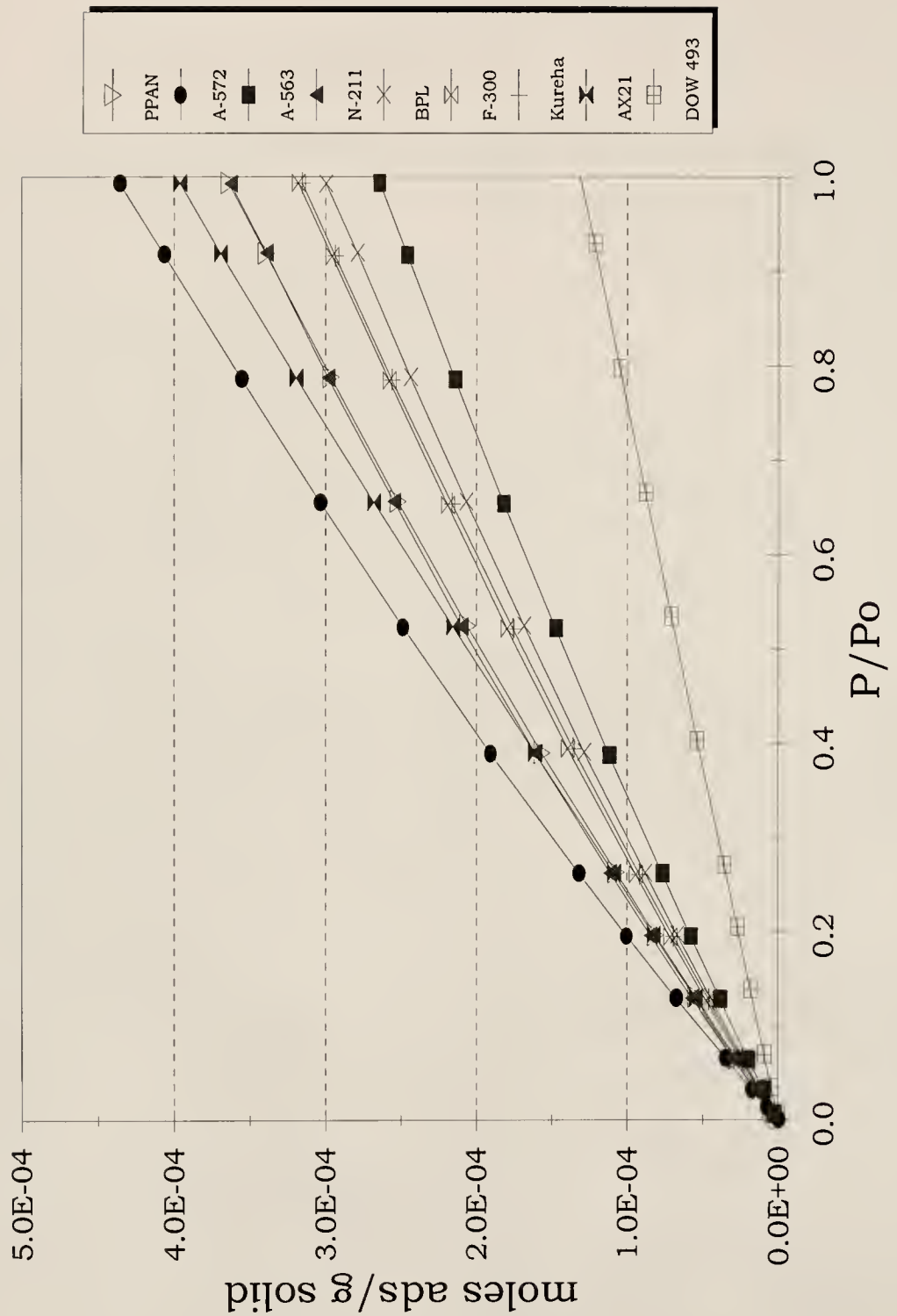

Figure II-6. Room Temperature N_2 Adsorption Isotherms for Various Carbons

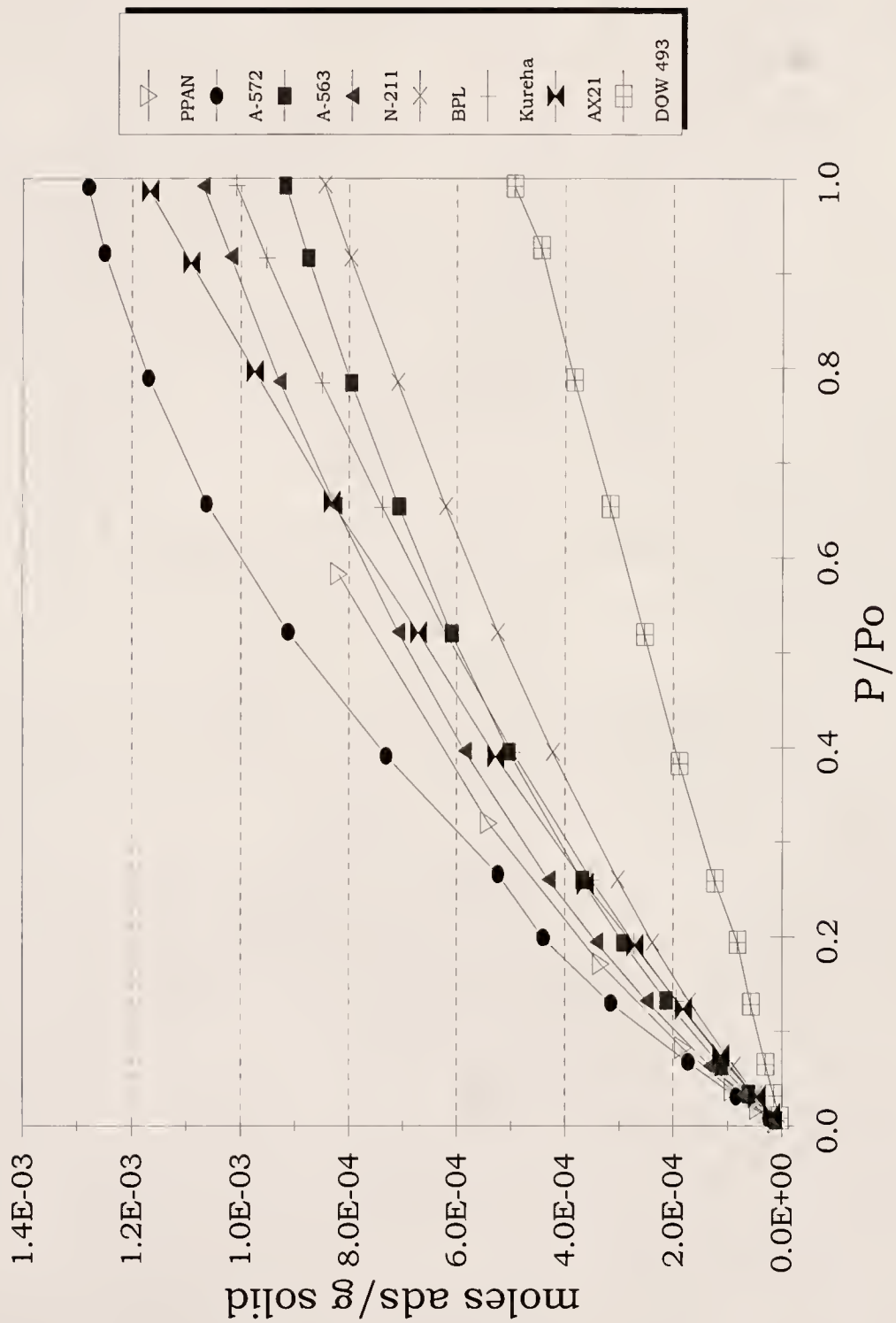

Figure II-7. Room Temperature CH_4 Adsorption Isotherms for Various Carbons

Conclusion

Referring to Table II-1, despite the large variety of source materials and the pyrolysis and treatment conditions the original polymers were exposed to, the elemental compositions of most of the resultant carbonized materials were very similar. However, it can be seen from the data presented in Table II-2, all the variables in chemical treatments and pyrolysis conditions have a decided impact on the porosity and surface features of these carbons. From this it was concluded, as stated in the introduction, that through varying a large number of parameters a carbonaceous adsorbent can be tailored to have specific capacities and affinities for a wide variety of chemical compounds, both dependent on their shape and size, and chemical functionality. Varying these parameters would have a large impact on how these materials behave as adsorbents, catalysts, and catalyst supports.

In addition to the surface area and porosity differences observed in these materials, their affinities and capacities for various adsorbates is also dependent on the synthesis of these materials. It was found that for two fairly non-interactive probes, N_2 and CH_4, differences in adsorption characteristics were observed that cannot be accounted for simply by the measured physical parameters of these adsorbents. It is therefore likely that the adsorption character of these materials, although affected by parameters such as surface area and pore volumes and distributions, is highly dependent on their chemical properties such as surface functionality, elemental composition and acidity. This observation has been observed in the development of heterogeneous catalyst systems.[47,48,49] It would therefore be desirable to develop another model to complement existing theory that would allow for more quantitative

and predictive ability of the adsorption characteristics of these types of solids. Such a model is developed in the following chapter.

The composition of the remaining mass of these solids, both as additional functionality and residual metal salts (ash content), was not well characterized in these studies. From the CHN analyses of these materials (Table II-1) it was found that several have significant amounts (>5% by mass) of other elements incorporated in their structure or on their surface. A more detailed analysis for trace metals is warranted, as it has already been surmised that the chemical functionality of these materials is very important in their adsorption behavior. The presence of trace metals would also have a large impact on the catalytic behavior of these solids.

The shape of the isotherms and hysteresis loops can help in elucidating information about the structure, shapes and sizes of the pores in these materials.[32,37,50] Although pore shapes and sizes have not been fully developed here, a large amount of information has been gained about the relative porosity, surface area and adsorption characteristics of the nine carbons studied. The BET theory and interpretation of isotherms have been discussed in great detail to understand the large amount of information gained from gas adsorption data. Further analysis of the BJH model and Harkins-Jura theory employed to determine pore size distributions is beyond the scope of this work. However, a good understanding of the BET equation (Equation II-13) is helpful in understanding the informative value of the interpretation developed from the isotherms presented in Figures II-6 and II-7 in Chapter III.

CHAPTER III
GAS-SOLID ADSORPTION EQUILIBRIA

Introduction

Porous supports have been examined in great detail for applications in the area of heterogeneous catalysis. Porosity, pore size, surface area, and the accessibility to the internal surface area are all important factors facilitating reaction pathways on solids. As was found in Chapter II, however, direct correlation of a solid's adsorption behavior cannot be determined from its physical structure alone. Certain pore structures may affect concentration of reactants near active catalyst sites. The same concentration effect may occur with reaction products, which could inhibit the reaction. Therefore, an understanding and quantitative measure of a solid's capacity and affinity for various adsorbates are essential in understanding and developing a rational selection process for solid materials.

The general phenomenon of adsorption involves the enrichment of one or more components at an interfacial layer. Gas-solid equilibria are typically characterized by three types of adsorption interactions: absorption, chemisorption and physisorption. Absorption occurs when the adsorptive molecules penetrate the surface layer of the solid and enter the bulk structure. Chemisorption involves irreversible bond formation to the solid, and is generally associated with large enthalpies of adsorption (10-50 kcal/mol or greater). The chemisorbed molecules can be removed, but this often requires higher temperatures than the adsorption conditions, and the desorbed species

may evolve chemically different than the original chemisorbed compound. An example of this is seen when O_2 strongly binds to charcoal at room temperature. It desorbs at elevated temperatures, but as CO and CO_2. Physisorption, which will include the process of reversible chemisorption for this discussion, involves the reversible adsorption of molecules on a surface. This adsorption process is dependent mainly on intermolecular interactions such as induced dipoles, permanent dipoles, quadrupolar interactions, and electrostatic forces. Interactions between the interface and adsorbent are usually found to be most significant for the first monomolecular layer formed.[51,52] Therefore, it is found that most physisorption processes involve adsorption enthalpies that approach the enthalpy of condensation for the adsorptive.[53]

As described earlier in Chapter II, up to three processes may be present in the physisorption isotherm. These are micropore filling, monolayer and multilayer adsorption, and capillary condensation. The size and shape of the pores in the solid, the adsorbate diameter, temperature, and the equilibrium gas pressure of the adsorbate all have an effect on which process is occurring. To examine the effect of pore sizes on adsorption, Everett and Powl[54] calculated interaction energies as a function of pore size based on the Lennard-Jones potential model. In cylindrical pores five adsorptive diameters or less in size, the model predicts increasing adsorption energies with decreasing pore size. Preferential micropore adsorption occurs because of these higher adsorption energies. Furthermore, if the temperature is below the critical temperature of the adsorbate, capillary condensation is possible in pores larger than four adsorptive diameters.

The BET equation (Eqn. II-13) has proven to be one of the most successful in interpreting and predicting gas adsorption isotherms. Extended

from the Langmuir and Kelvin equations, it better accommodates multilayer formation and porous surfaces.[55] As discussed previously, this model does have limitations on its applicability and the assumptions made in its derivation. In addition, the value of the BET C constant and its physical meaning have often been debated. This constant appears to be a complex quantity related to the isotherm shape, surface coverage, the ratio of equilibrium constants for the various adsorption sites and processes, and contributions from the enthalpies and entropies of adsorption of the monolayer and multilayer. Literature attempts to interpret the BET C value have led to various proposals,[56] but none appear universal in obtaining thermodynamic information about gas-solid interactions.

The focus of this research was to develop a method complementary to existing theory for the analysis of adsorption data. The goal of this analysis was to obtain thermodynamic data for the interaction of the adsorptive molecules with the strongest binding sites on the solid surface. For these studies, the adsorption isotherms of two carbonaceous adsorbents that had been previously well characterized in this research group were focused upon. Pyrolyzed polyacrylonitrile (PPAN) and Ambersorb® 572, lot# 2125 (A-572) were chosen. More information on the physical characteristics and adsorption behavior of these two solids can be found in the previous chapter.

Experimental

All gas adsorption isotherms were obtained in the exact manner as that described in Chapter II, employing the glass vacuum line (Fig. II-1) or the Micromeritics® ASAP 2000 Chemi system. Adsorption isotherms were obtained at temperatures ranging from -93°C to 75°C. Low temperature isotherms were

obtained by immersing the sample in a Dewar filled with a slush made from liquid N_2 and an appropriate solvent. Toluene was the solvent for the -93°C isotherms, and acetonitrile for the -42°C runs. An ice/water mix was used for isotherms obtained at 0°C. Variance of less than ±1°C was observed for these systems during the course of a run. For isotherms obtained at room temperature (25°C) or higher, a heating mantle was employed to regulate the temperature. For these systems temperature control was not as precise, with variations of ±2°C observed. The numerical data for all the obtained isotherms for the various gases and temperatures are tabulated in Appendix B.

Results and Discussion

Supports and Adsorptives

Two chemically different porous carbonaceous adsorbents and a series of different gases were focused on to better characterize the processes involved in gas-solid adsorption equilibria. A-572, derived from sulfonated, macroreticular polystyrene, and PPAN, an adsorbent derived from pyrolyzed polyacrylonitrile, where characterized in detail in Chapter II. It was observed that these two materials differ in both their physical composition (Table II-1) and surface areas/pore distributions (Table II-2). Additionally, their adsorption behavior towards N_2 and CH_4 (Figs. II-6 and II-7) at room temperature were observed to differ in a fashion not solely accounted for by the physical characterizations just mentioned.

The gases used in the adsorption measurements discussed in this chapter are summarized in Table III-1 and were chosen to provide a range of polarity, polarizability and size. The nonpolar N_2, slightly polar CO, and the

quadrupolar CO_2 were chosen to investigate the influence of polarity on the application of the developed adsorption model and to provide an indication of the importance of these properties on adsorption by these two solids. N_2 and CO are non-condensible gases in this study because their isotherms were obtained above their critical temperatures. These adsorptives will therefore be subject only to gas-solid, micropore filling, and multilayer interactions, with no possibility of capillary condensation occurring. CO_2 is, however, a condensible adsorptive at room temperature, so there also exists the possibility of capillary condensation with this adsorbate.

Table III-1. Summary of Adsorbate Gases and Associated Physical Properties[57]

Gas	Mol. Wt. (g/mol)	Polariz-ability (A^3)	Dipole Moment (debye)	Molar Volume (mL/mol)[a]	Critical Temp. T_c (°C)	Boiling Temp. T_{bp} (°C)	ΔH_v (kcal/ mol)
He	4.00	0.205	0	32	-268.0	-268.9	0.0194
N_2	28.01	1.74	0	35.4	-146.9	-195.8	1.33
CO	28.01	1.95	0.112	34.9	-140.2	-191.5	1.44
CO_2	44.01	2.91	0	40.0 (@ -37°C)	31.04	-78.44	6.03 (subl)

[a] Molar volumes of the liquids at their normal boiling point (unless otherwise noted).

Equilibrium Analysis and Adsorption Model

The measured isotherms were analyzed using an equilibrium model derived by analogy to a multiple site Langmuir adsorption model. The resulting equation is given below:

$$n_{tot} = \sum_i \frac{n_i K_{i,ads} P_{atm}}{(1 + K_{i,ads} P_{atm})} \qquad \text{(III-1)}$$

where n_{tot} is the total number of moles of gas adsorbed per gram of solid; n_i the available capacity of process i; $K_{i,ads}$ the equilibrium constant for the adsorption process i; and P_{atm} the equilibrium gas pressure in atmospheres. From the experimental isotherms where n_{tot} and P_{atm} were measured, a modified simplex

routine (Appendix C) was used to solve equation III-1 for the values of n_i and $K_{i,ads}$.

It has previously been found in using this data fitting routine that a very shallow minimum in the solution series results from solving simultaneous equations for data involving even two processes.[58] In addition, it is an accepted limitation of the simplex approach that misleading data may arise due to the minimization of a complex equation in local or relative minima.[59] Our experience in solving Equation III-1 for room temperature gas adsorption data found a shallow surface and uncertain quantities for n_i's and K_i's for up to three processes. Employing six parameters to fit these relatively simple curves yields values for n_i and $K_{i,ads}$, but one must critically evaluate the physical meaning of the determined values. In the Cal-Ad method,[58,60] adsorption and calorimetric data are solved simultaneously to better define the minimum. The adsorption enthalpies of physisorption processes for most carbon adsorbents are so small that this approach cannot be employed. Instead, a series of isotherms were measured at various temperatures. Assuming the n_i values are temperature independent, each isotherm at a different temperature introduces only new K_i's as unknowns, leading to a better definition of the minimum in the solution of the combined data sets.

The reproducibility and precision in the adsorption measurements were determined from three successive experiments in which N_2 adsorption by A-572 at 25°C was followed by evacuating and repeating the N_2 adsorption experiment on the same sample. The adsorption isotherms were found to be very reproducible. At higher equilibrium pressures ($P_{atm} > 0.05$), the relative error (δ) in the average number of moles of N_2 adsorbed per gram of A-572 was less than 0.5%. At lower equilibrium pressures ($P_{atm} < 0.05$), the relative error was somewhat larger, with $\delta < 3\%$. This larger relative error arises from the very

small volumes of gas adsorbed and the limits of sensitivity of the pressure transducers. Two successive adsorption isotherms were also obtained for CO on A-572 at T = -93°C. At this low temperature, CO leads to much higher volumes of gas adsorbed at lower pressures. However, as observed in the N_2 data, the greatest differences in successive runs were observed at the lower equilibrium pressures. For the two CO adsorption isotherms a $\delta < 4\%$ was found for $P_{atm} < 0.05$. In this type of data analysis, it is essential to add processes only until the adsorption data is fit to the precision and accuracy to which it is known. The relative errors discussed above were used as the criteria for the minimum number of processes needed to fit the adsorption data. The procedure for obtaining n_i's and K_i's for the gases N_2 and CO in this study is outlined as follows:

(1) The isotherms for N_2 and CO at -42°C were fit to two processes using the above criteria, leading to values for all four parameters (n_1, n_2, K_1, K_2). At this temperature, the value for n_1 is best defined[61] as the data points range from zero to near full capacity for process 1. Further explanation of this assumption will follow, along with an interpretation of the physical meaning of the different processes. In addition, the K_i's sufficiently differ so that the two processes are felt to be well distinguished.

(2) The -93°C isotherms required three processes to fit the data to within experimental error. The value for n_1 was fixed to the value obtained in Step 1. This lower temperature data provides a better definition of n_2, so this value was not fixed, although the value of n_2 obtained in Step 1 gives a good approximation of the maximum for this value. This resulted in values for n_2 and n_3, as well as K_1, K_2, and K_3 for this temperature. At this temperature, processes 1 and 2 both contain

data points over the majority of their capacity range. Therefore, the values of n_2, K_1 and K_2 are felt to be well defined for this data set. Process 3 is not as well characterized as there exist a limited number of data points in the region where process 3 is occurring. Because of this, n_3 and K_3 are not believed to be as accurately known. This is a limit imposed by the apparatus and experimental data set, as it was not possible to take measurements above $P_{atm} = 1.0$, where process 3 is occurring to the largest extent.

(3) The above two isotherms (at -42° and -93°C) were then reanalyzed, employing a total of three processes. Since n_1, n_2 and n_3 have already been determined, these values were not allowed to vary. This procedure was also used on the room temperature data. This final step yields values for all K_i's at the three different isotherm temperatures.

In addition to finding the $K_{i,ads}$'s at various temperatures, Step 3 constitutes a final check to determine if meaningful parameters for n_i's have been obtained. If the values found for n_1, n_2 and n_3 from Steps 1 and 2 are well defined, it should be possible to fit all the data sets to within the precision of the experimental measurements. A second check results from plotting the natural logarithm of the K_i values versus the reciprocal temperature (in Kelvin). This relationship, known as the van't Hoff equation, should yield a straight line whose slope is proportional to the enthalpy of adsorption. Although different temperatures were used for the CO_2 adsorption data, the same basic procedure was followed for fitting this data. In this case, however, a good data fit was obtained with three processes for the 0°C data, and the n_i's obtained here were used in the simplex analysis for the other three temperatures.

Further detail and discussion of this method, and determination of what is considered a good fit of experimental data, are found in Appendix D. This is exemplified and discussed with a sample set of data taken from Appendix B.

It is important to realize that the $K_{i,ads}$ values found from this procedure were derived from static adsorption data, where the established criteria for equilibria (see Chapt. II, Experimental - Gas Adsorption Studies section) generally observed 4-5 minutes passing between each obtained data point. If these materials are allowed to stay in contact with the adsorbates for several hours, the reported adsorption capacities are found to increase, but by a relatively small amount (< 10%). However, this rapid equilibrium process is of greatest interest for these types of adsorbents when considering separation and catalytic applications.

Adsorption Isotherms

Figures III-1 through III-3 show the adsorption isotherms at various temperatures for PPAN and A-572 with N_2, CO and CO_2, respectively. In all cases the adsorption isotherms were observed to become more linear, and the capacities of the adsorbents decrease, with increasing temperature. The numerical data in all the isotherms were fit to Equation III-1 as previously outlined, producing the best values for n_1, n_2, and n_3, and the different values of K_1, K_2, and K_3 for all the measured temperatures. The isotherms for all three adsorbates, on both solids at all the temperatures measured, could be fit within the accuracy of the experimental measurements using three processes. As previously mentioned, the numerical data for these, as well as several other isotherms for all nine of the carbons studied in Chapter II, are tabulated in Appendix B.

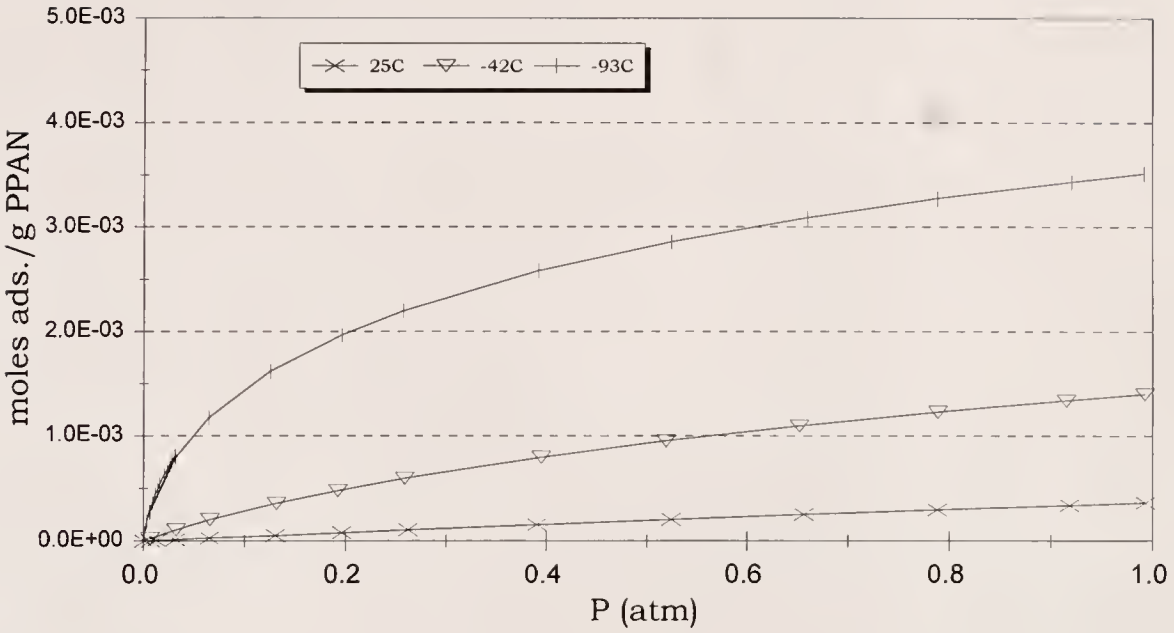

(a)

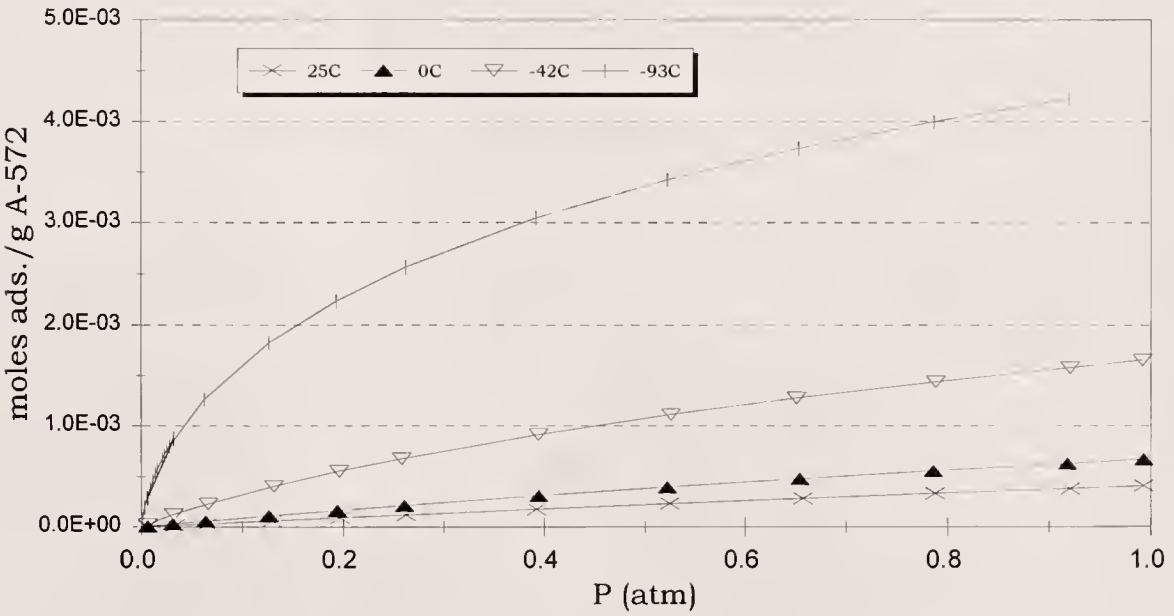

(b)

Figure III-1. N_2 Adsorption Isotherms at Various Temperatures for (a) PPAN; (b) A-572

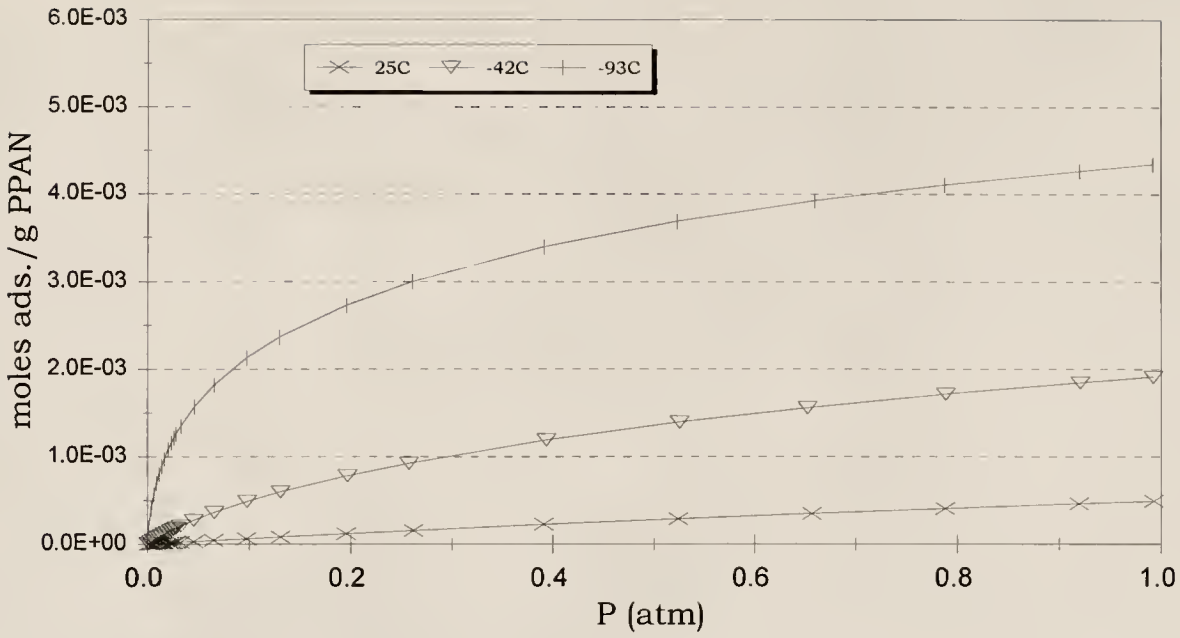

(a)

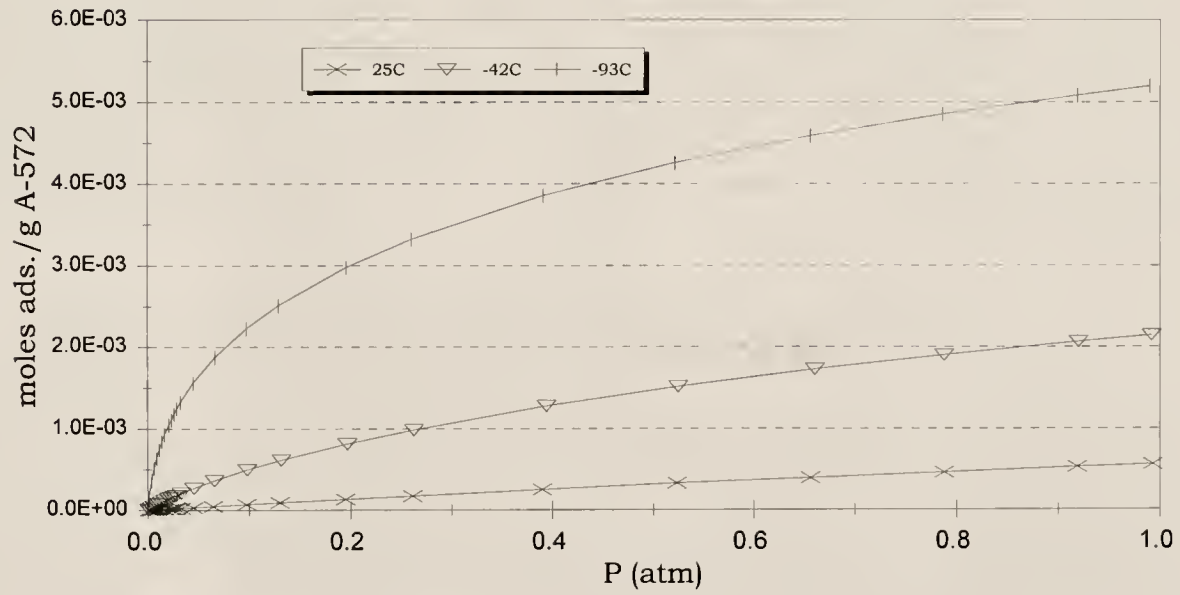

(b)

Figure III-2. CO Adsorption Isotherms at Various Temperatures for (a) PPAN; (b) A-572

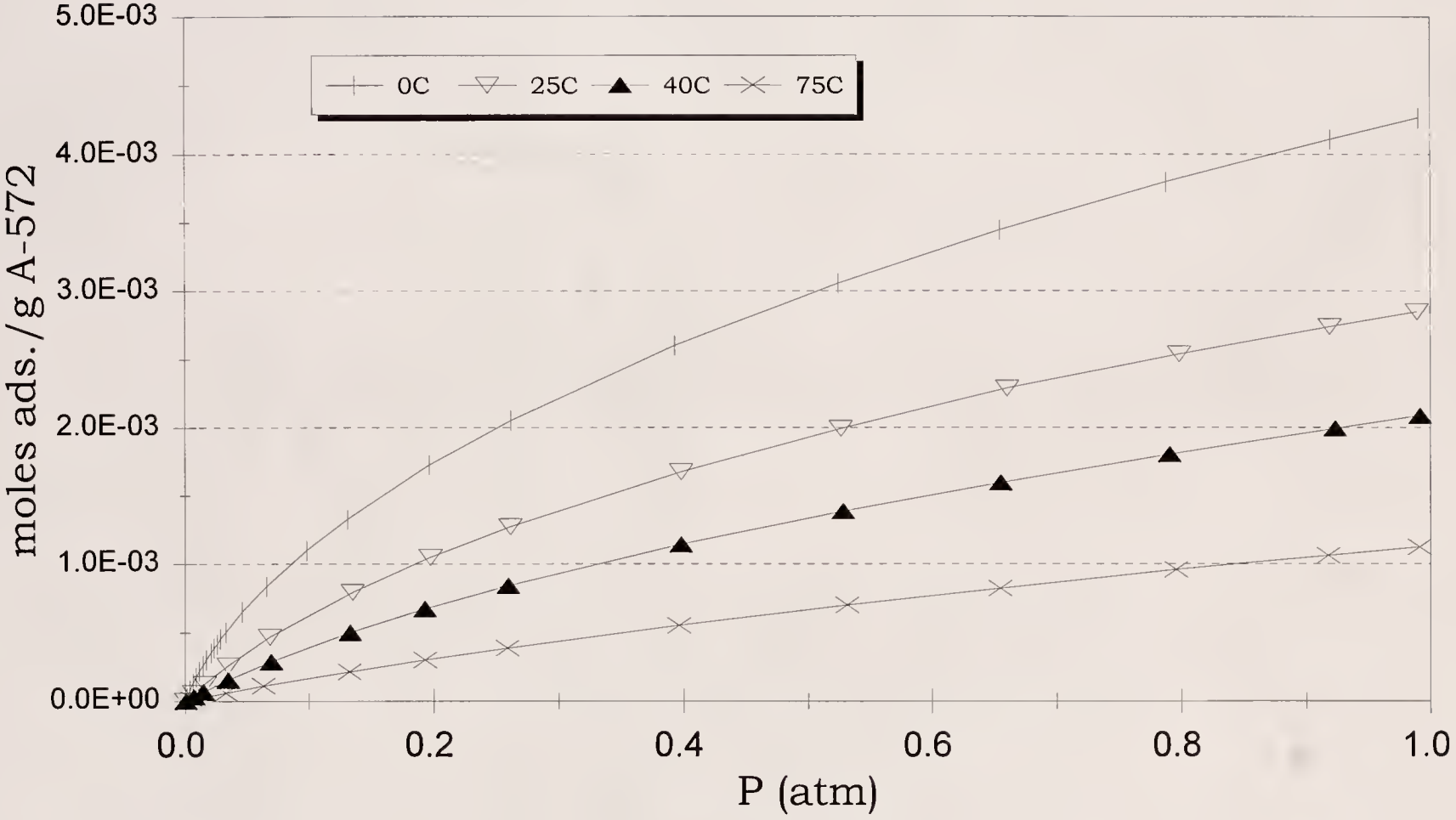

Figure III-3. CO_2 Adsorption Isotherms at Various Temperatures for A-572

Table III-2. Gas-Solid Adsorption Equilibria Parameters for PPAN and A-572

Solid	Gas	Process	n_i [mmol/g]	$K_{i,ads}$ -93°C	-42°C	0°C	25°C	40°C	75°C
A-572	N_2	1	0.46±0.06	89.4±10.9	4.56±0.11	0.94±0.01	0.55±0.01		
		2	1.78±0.01	8.77±0.04	0.78±0.03	0.13±0.01	0.042±0.003		
		3	5.34±0.02	0.76±0.01	0.12±0.01	0.052±0.001	0.042±0.001		
	CO	1	0.53±0.01	184±44	8.26±0.30		0.66±0.02		
		2	1.82±0.06	16.7±0.6	1.12±0.07		0.056±0.005		
		3	4.94±0.20	1.36±0.20	0.17±0.02		0.054±0.002		
	CO_2	1	0.18±0.01			57.4±5.5	16.0±1.6	7.37±0.89	3.10±0.14
		2	1.38±0.02			6.39±0.07	2.80±0.08	1.63±0.09	0.52±0.01
		3	8.69±0.20			0.50±0.01	0.23±0.01	0.14±0.01	0.064±0.002
PPAN	N_2	1	0.43±0.01	106±10	4.66±0.08		0.30±0.01		
		2	1.53±0.01	9.41±0.50	0.74±0.02		0.15±0.01		
		3	3.63±0.03	0.88±0.10	0.11±0.01		0.015±0.001		
	CO	1	0.56±0.01	250±152	8.95±0.29		0.72±0.03		
		2	1.79±0.04	19.3±0.5	1.13±0.08		0.05±0.01		
		3	3.65±0.53	1.35±0.20	0.15±0.04		0.05±0.01		

Table III-2 summarizes the n_i and $K_{i,ads}$ values determined for the isotherms shown in Figures III-1 through III-3. In the table, n_i is the capacity of the solid for the specific adsorption process i, expressed in millimoles of gas adsorbed per gram of solid (mmol/g). The n_i values are a measure of the capacity of each process, and are functions of the pore size and pore distribution of the solid, as well as the adsorbate size. The reported K_i values measure the affinity of a specific process on the solid for the gaseous probe. It is well known that for solid materials, surface interactions are not easily characterized due to the solid being energetically heterogeneous.[56,62] This is especially true for highly porous materials such as those studied here. With this in mind, it is important to recognize that the K_i's found are likely to be average values for adsorption processes at different solid sites whose K_{ads}'s can not be differentiated by this type of data analysis. It is also likely that although the K_i's are significantly different as to separate them into three different processes, the second and third processes are occurring before adsorption process 1 is complete.

The enthalpies of adsorption for the three processes on the individual solids have been determined using the well known relationship between the thermodynamic parameters of enthalpy (ΔH) and entropy (ΔS), and the equilibrium constant K, which in this case will all be adsorption values:

$$-RT\ln K_{ads} = \Delta H_{ads} - T\Delta S_{ads} \qquad \text{(III-2)}$$

where R is the gas constant and T the temperature in Kelvin. Dividing both sides of Equation III-2 by -RT yields

$$\ln K_{ads} = \frac{-\Delta H_{ads}}{RT} + \frac{\Delta S_{ads}}{R} \qquad \text{(III-3)}$$

Assuming ΔH_{ads} and ΔS_{ads} are constant over the experimental temperature range, a plot of $\ln K_{ads}$ vs. $1/T$ should yield a straight line whose slope is $-\Delta H/R$

and intercept is $\Delta S/R$. The results are summarized in Table III-3, and a graphical plot of this analysis for CO_2 on A-572 is shown in Figure III-4. In this graph, the points shown are the experimental data, and the lines generated from the least-squares fit analyses. The least-squares fit of the resultant plots are given as a footnote to Table III-3. The proposed model (Eqn. III-1) is further verified by the linearity of these data series, as shown in Figure III-4. Additionally, the values calculated for ΔH_{ads} are consistent with those expected for physisorption.

Table III-3. Summary of $-\Delta H_{ads}$ (kcal/mol) from $\ln K_{ads}$ vs. 1/T Plots

	A-572			PPAN	
Process	N_2[a]	CO[b]	CO_2[c]	N_2[d]	CO[e]
1	4.7 ± 0.1	5.1 ± 0.04	7.4 ± 0.6	5.3 ± 0.2	5.3 ± 0.1
2	4.5 ± 0.3	5.1 ± 0.4	6.3 ± 0.3	3.8 ± 0.2	5.3 ± 0.5
3	3.0 ± 0.1	3.0 ± 0.3	5.4 ± 0.3	3.6 ± 0.2	3.0 ± 0.4

[a] Process 1: lnK = 2370 (± 66)/T - 8.64(± .11)
Process 2: lnK = 2270 (± 158)/T - 10.22(± .21); lnK at 25°C was omitted because it is poorly defined.
Process 3: lnK = 1509 (± 27)/T - 8.54(± .04); lnK at 25°C was omitted.
[b] Process 1: lnK = 2562 (± .1)1/T - 9.00(± .03)
Process 2: lnK = 2548 (± 219)1/T - 11.2(± .3)
Process 3: lnK = 1492 (± 154)1/T - 8.0(± .2)
[c] Process 1: lnK = 3739 (± 323)1/T - 9.7(± .2)
Process 2: lnK = 3196 (± 163)1/T - 9.8(± .1)
Process 3: lnK = 2705 (± .59)1/T - 10.6(± .03)
[d] Process 1: lnK = 2665 (± 81)1/T - 10.1
Process 2: lnK = 1892 (± 123)1/T - 8.3
Process 3: lnK = 1808 (± 119)1/T - 10.2
[e] Process 1: lnK = 2665 (± 39)1/T - 9.3
Process 2: lnK = 2695 (± 238)1/T - 11.9
Process 3: lnK = 1512 (± 188)1/T - 8.2

The determination of accurate and meaningful numbers for the three processes is in part based on the ability of Equation III-1 to predict the observed isotherms. Additionally, measuring a large number of data points over a large range in pressures allows for the best possible solution of the data fitting routine for the three processes. In the case of CO on either solid, it is

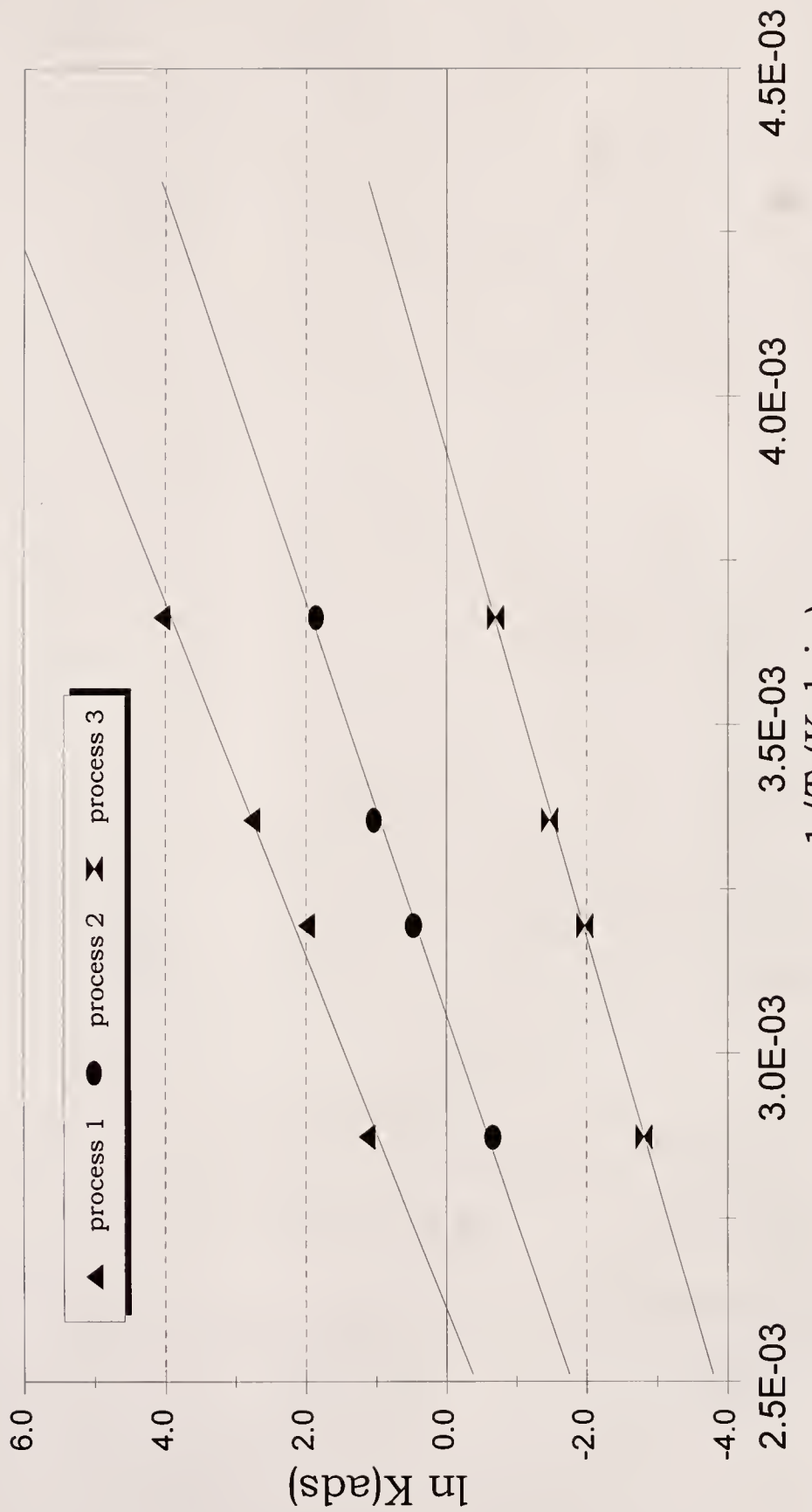

Figure III-4. $\ln K_{ads}$ vs. 1/T Plots for CO_2 Adsorbed on A-572

important to note that the final n_i's and K_i's were within 10% of those based solely on the -93°C isotherm. It has already been noted that the n_i values for CO_2 were derived exclusively from the 0°C isotherm. Both these results indicate that if enough adsorbate is adsorbed by a solid in the region of the isotherm where a specific process is dominant, reasonable estimates of n_i are possible from measurements at only one temperature. If this is not the case, as seen with the N_2 and CO data, isotherms at various temperatures must be obtained to better isolate the individual processes.

Interpretation of the Processes Involved

The equilibria, enthalpies, BET surface areas, and porosimetry values of A-572 were utilized to provide an interpretation of the physical nature of the three processes. Because it is the most thoroughly characterized of the two solids, the interpretation of the processes involved is illustrated with A-572. PPAN was studied with N_2 and CO to afford a comparison of adsorbents. The different values of $K_{1,ads}$, $K_{2,ads}$, and $K_{3,ads}$ for A-572 are consistent with different interaction potentials for different adsorption processes. At low pressures, adsorption of the gas into the small micropores, and the most energetic sites of the solid, should be the dominant adsorption process. As a measure of the affinity of the adsorbate for these sites, K_1, increases in the order $N_2 < CO < CO_2$ at any given temperature (Table III-2). The adsorption enthalpies increase in the same order (Table III-3) and are directly proportional to the polarizability of the gas molecules (Table III-1). This result suggests that the predominant interaction of the adsorbates studied with this solid involves dipole and induced dipole type interactions.

The assignment of process 1 to adsorption in the smallest pores is supported by the literature,[54,63,64] and by pore resolved NMR porosimetry results.[65] In the NMR spectra, it is observed that the smallest pores of A-572 fill first when CH_3CN is adsorbed from a dilute CCl_4 solution. This is a direct observation that shows the equilibrium constant for this process is the largest. For all of the systems in Table III-2, K_1 is almost an order of magnitude larger than K_2.

Process 2 is attributed to adsorption in the larger micropores and mesopores of the solid. For N_2 and CO on A-572, the enthalpies for processes 1 and 2 are the same, within experimental error. The predominant contribution to the enthalpy in process 2 is the solid-adsorbate dispersion interaction. N_2 and CO are similar in size, and therefore it is reasonable to assume they have access to the same internal pore volume. This then indicates that the increased interaction potentials arising from the close proximity of pore walls in the microporous region have only a small enthalpic, but a large entropic component. With the larger molecule CO_2, the enthalpic contribution to process 1 is 1.1 kcal/mole larger than that for process 2. The small pores involved in the solids studied apparently have dimensions that lead to a larger enthalpic interaction for the CO_2 molecule. For the smaller, less polarizable molecules N_2 and CO, the enthalpic contribution is small and the process is driven more by entropic contributions.

The predominant contribution to the enthalpy of process 2 for CO, N_2, and CO_2 arises from the dispersion force interactions of these molecules with the carbon surface. The values of both n_1 and n_2 are larger for CO than for N_2. Due to variation in the adsorbate sizes, the quantities n_1 and n_2 will consist of varying combinations of micropores for different adsorbates. Stronger interactions enable CO_2 to adsorb more strongly than CO, and CO to adsorb

more strongly than N_2. If this consideration is limited to process 1 as previously defined, this would result in larger values of n_1 and K_1 for CO over N_2, as observed. The K_1 and K_2 values for CO_2 are much larger than those found for the other two gases, which is consistent with the above arguments. However, the n_1 and n_2 values for CO_2 are smaller than those reported for both CO and N_2. The smaller n_1 and n_2 values are accounted for by CO_2 being a much larger molecule and, therefore, not having access to the same micropore volume as does N_2 or CO.

Process 3 includes adsorption on the remaining surface and larger pores, multilayer formation, and capillary condensation in cases where isotherms are obtained below the critical temperature of the gaseous adsorbate. As was previously mentioned, there exist a limited number of measured data points under the temperature and pressure conditions where process 3 is thought to be dominant for these solids. Additionally, since the measured isotherms were never observed to level off, the total capacity of the solid was never reached. Because of this, the values for n_3 and K_3 are considered approximations, and not as well defined as those for processes 1 and 2.

A polarized surface molecule could lead to multilayer adsorption even though isotherm temperatures are above the critical temperature of the adsorbate. Whether the adsorbed molecules are all on the surface or on surface and bilayer sites is often of minor concern. Therefore, in processes where the solid-adsorbate interactions are comparable to the adsorbate-adsorbate interactions, it is difficult to distinguish the contribution from multilayer adsorption and surface bound interactions. In this case, the two interactions may proceed concurrently and with a comparable K_{ads}. However, for most adsorbent and catalytic applications the concern is with the capacity and affinity of the various processes.

Using an adsorbate cross-sectional area of 16.2 Å^2 for nitrogen, the values of n_1 and n_2 for A-572 correspond to a surface area of 45 and 155 m^2/g, respectively. The value of n_3 corresponds to 519 m^2/g. A similar analysis for CO using an adsorbate area[66] of 15.0 Å^2 gives 48, 164, and 446 m^2/g from the values of n_1, n_2 and n_3, respectively. In both these cases, process 3 is attributed to adsorption by the larger pores and remaining surface. Comparing the results from this data analysis with those from BET theory suggests that only a small portion of the total surface area for A-572 ($S.A._{BET}$ = 1159 m^2/g) is occupied under these experimental conditions. Knowing that a large amount of the reported $S.A._{BET}$ is because of the large micropore volume of this solid, it appears that all of the adsorption occurring under these conditions is in the microporous region. The Micromeritics® software reports a value of 1080 m^2/g for the micropore area of A-572. This number is calculated based on the difference between the reported total surface area ($S.A._{BET}$) and that calculated for the external surface area. This external area is defined as the surface area of the solid excluding that of the micropores. The value for the external area is calculated from the slope of the Harkins-Jura t-plot analysis, including what is referred to as surface area and density correction factors.[67]

Comparing the n_i values to the total amount of CO and N_2 adsorbed for the various isotherms (e.g., ~1.7×10^{-3} moles/g at P_{atm}=1.0 and -42°C on A-572) shows that up to an equilibrium pressure of 1.0 atm all of the adsorbate can be accommodated by the n_1 and n_2 values. At the lowest temperature, -93°C, this is not the case. However, the n_1 and n_2 processes still have the capacity for over half of the amount of gas adsorbed. These observations were found to be true for both solids. On the basis of these observations and the previous statements regarding the number of experimental data points that correspond to specific processes, the quantitative thermodynamic data for process 3 is

seen to be poorly defined at the temperature and pressure regions studied. This is caused by only a fraction of n_3's capacity actually being occupied.

When similar calculations are done with the CO_2 data, using a cross-sectional area[66] of 21.8Å^2, the corresponding surface areas are 24 and 181 m^2/g for processes 1 and 2. An area of 1140 m^2/g is calculated based on the n_3 value. The total area thus calculated from n_1, n_2, and n_3 for these three processes exceeds the reported S.A.$_{BET}$. Thus, CO_2 must involve both adsorption by the solid surface and multilayer processes. Both n_1 and n_2 are smaller for CO_2 than for either N_2 or CO, as expected from its larger size. However, n_3 is much larger, and provides the only clear manifestation of a multilayer process in the systems reported in Table III-2.

It is of interest to note that the enthalpies of process 3 are larger than the enthalpies of vaporization of the liquids. From this observation, the polarization of a surface bound molecule must increase the enthalpy of interaction of a second layer with the surface layer. In general, if multilayer formation occurs in each of the processes, the $K_{i,ads}$'s are comparable to those for surface adsorption of those processes. The interaction potentials that give rise to the different processes influence not only the surface interactions, but also the multilayer interactions. However, this multilayer interaction beyond the monolayer coverage has been found to decrease rapidly with distance,[51,52] and therefore it is not likely that many areas on the surface of these solids contain more than a bilayer at the pressures studied.

Comparison of PPAN and A-572

Although the two adsorbents chemically differ in both their structural composition and porosity, it is of interest to note that PPAN was very similar to

A-572 in its adsorption characteristics towards the gases studied. In general, values for n_1, n_2, K_1, and K_2 where found to be very similar for the two solids. Thus, the nitrogen functionality of PPAN appears to do little to change the interaction of the solid surface with the adsorbed N_2 or CO. As observed before, the adsorption characteristics, and more specifically the trends observed for these two solids n_i and $K_{i,ads}$ values, do not appear to have any direct correlation to any of the surface area or porosity values previously determined using standard gas adsorption theory.

The BET model was developed to account for multilayer adsorption by assuming that the Langmuir equation, which involves only monolayer adsorption, applies to each layer. Following Adamson,[56] the BET C constant is related to the ratio of equilibrium constants for both the monolayer and multilayer adsorption. It is also related exponentially to the difference in the enthalpies of adsorption of the monolayer and the multilayer. Therefore, C encompasses several processes and thus is difficult to relate to the affinity or strength of interaction of an adsorbate with the solid. Although BET deals with multilayer formation, it assumes the surface is energetically homogeneous. As previously discussed, this is not the case with most solids.

In the multiple process equilibrium model presented here (Eqn. III-1), the BET C constant is essentially being separated into components for surface adsorption in pores of different sizes and multilayer formation. By interpreting the isotherms as a combination of energetically different processes, distinction is also being made between energetically different sites on the surface of the solid. A significant advantage of this model is that $K_{i,ads}$ for micropore filling is a true thermodynamic quantity and can be related to physical properties, (e.g., polarizability, etc.) of the adsorbate. Thus, this method of analysis provides a complementary method to existing theory of interpreting adsorption isotherms.

From this analysis, a thermodynamic measure of gas-solid equilibria and a thermodynamic basis for understanding adsorption processes have been developed.

It is of interest to note that both adsorbents were cycled through adsorption experiments and degassing at 200°C up to fifteen times. No changes were observed after repeated analysis on the same sample in the overall surface area or pore size distribution from the original sample. This thermal stability and physical integrity is important when considering separation and catalytic applications.

Conclusion

The affinities of three gases for two porous solids have been compared using a multiple process equilibrium analysis. For the non-condensible adsorbates N_2 and CO, a multiple process adsorption model is able to separate the processes of adsorption in small micropores, adsorption by larger micropores and mesopores, and adsorption by the remaining surface. The enthalpies of interaction for condensible adsorptives indicate that multilayer condensation may accompany surface adsorption for each process and is clearly involved for CO_2 in process 3. Comparison of the affinity of the solids for large and small probe molecules is complicated, however, by the fact that a different distribution of pore sizes comprises processes 1 and 2 for different size probes.

The $K_{i,ads}$ and n_i values for different adsorptives provide a quantitative characterization of the forces involved in porous solid-gas equilibria. For a given adsorbent, quantitative comparisons of the $K_{i,ads}$'s for different adsorbates will give insight into the polarizability, polarity, and donor-acceptor properties

of the solid surface. Comparison of the $K_{i,ads}$ and the $\Delta H_{i,ads}$ values provides insight into the fundamental nature of the interaction of the adsorbent and adsorptive molecules, and allows a quantitative means of selecting solids for adsorption or catalytic applications. The gas-solid interactions studied here were found to be predominantly physisorption. Accordingly, the carbonaceous adsorbents studied here are expected to be effective in the separation of molecules that differ in polarizability.

The excellent fit of the data for the non-condensible gases to the three process model, using the same n_1, n_2, and n_3 values for isotherms at all temperatures studied, suggest that the n_1 and n_2 values obtained are accurate measures of the available capacity for these different processes. It should also be considered that the values found from this data analysis may prove to be more useful in comparing the adsorption behavior of different solids. For applications as adsorbents, catalysts, or catalyst support materials, the absolute surface area and pore structure of a solid are not necessarily the most important parameters to be measured. Instead, the effective or accessible surface area and pore volumes for a specific adsorbate are of greater interest. The n_i values are a measure of the capacity of this effective pore volume. The $K_{i,ads}$ and subsequent $\Delta H_{i,ads}$ are measures of the strength of these interactions.

Kinetic factors are also important in the practical applications of solids in separation and catalytic processes. However, this aspect of the problem was not addressed in these studies.

CHAPTER IV
HETEROGENEOUS WACKER CATALYSIS

Background

Palladium catalyzed oxidation of olefins is a well known synthetic approach in homogeneous catalysis.[68,69] One of the better known applications arose from the discovery by Smidt *et al.*[70] of the homogeneous catalytic oxidation of ethylene to acetaldehyde. Most often referred to as the Wacker process after the German company that first commercialized the process, it involves an aqueous co-catalyst system of $[PdCl_4]^{-2}$ and $CuCl_2$. Pd(II) is reduced to Pd(0) upon the oxidation of ethylene to acetaldehyde, and is then reoxidized by Cu(II). The catalytic cycle is completed by the rapid oxidation of Cu(I) back to Cu(II) by O_2.[71,72] The overall process is represented by the following equations:

$$C_2H_4 + PdCl_2 + H_20 \rightarrow CH_3CHO + Pd(0) + 2HCl \quad \text{(IV-1)}$$

$$Pd(0) + 2CuCl_2 \rightarrow PdCl_2 + 2CuCl \quad \text{(IV-2)}$$

$$CuCl + 2HCl + \tfrac{1}{2}O_2 \rightarrow 2CuCl_2 + H_2O \quad \text{(IV-3)}$$

$$C_2H_4 + \tfrac{1}{2}O_2 \rightarrow CH_3CHO \quad \text{(IV-4)}$$

The proposed mechanism involves the displacement of a Cl^- from the palladium complex followed by coordination of ethylene. This activates the olefin for hydration by the solvent, water. Addition of another H_2O molecule to the palladium complex follows, accompanied by loss of HCl. Finally, through a reductive elimination step, acetaldehyde is lost and reduced Pd(0) remains.

One of the major disadvantages to the industrial homogeneous system is the production of chlorinated oxygenates as unwanted by-products.[73] In addition to the presence of chloride as the counterion, it has been suggested that the presence of copper is a major contributor to the formation of these undesired by-products. A variety of research has been done investigating the replacement of both copper and chloride ion in this catalyst system. It has been reported that this system is very susceptible to the counterion and oxidant, and that different product distributions are obtained with changes in these variables.[74,75,76] As shown in Eqn. IV-2, the importance and function of copper in this catalytic system is in the regeneration of the active palladium species. Halide free catalysis systems have been reported, and other species have been found that can serve the function of Cu(II) in this system. These include vanadium oxides,[77] heteropolyacids,[78] peroxides, benzoquinone derivatives,[79] and activated charcoal.[80] Considering that the function of copper may be met by carbonaceous materials, it is feasible that doping a specific adsorbent, like those discussed in Chapter II, with Pd(II) salts would yield a functioning catalytic system for Wacker-type catalysis. Due to carbon's unique chemical and physical properties, it may also prove advantageous over more traditional supports (e.g., zeolites or silica) to employ a high surface area carbonaceous support as a heterogeneous oxidation catalyst and/or catalyst support.

For this study Ambersorb® carbonaceous adsorbents were chosen. Ambersorb® adsorbents have previously shown catalytic activity towards both oxidation and reduction applications,[81,82,83] as well as resistance to self-oxidation in the presence of an oxidative atmosphere. Studies have shown these materials to have high affinities and capacities for a variety of organic substrates.[84] Gas adsorption studies indicate high surface areas and pore

volumes that would be advantageous for catalytic applications (see Chapter II). All the reactants and products for the Wacker oxidation can be easily handled in the gas phase, and therefore lend themselves well to a gas flow system with an immobile Pd(II) solid catalyst. For these reasons it was felt that Ambersorb® adsorbents would be excellent candidates for the support of Pd(II) salts that could lead to a heterogeneous Wacker catalyst system.

Experimental

Ambersorb® 572 (lot# 2201) was employed as the carbonaceous support for this series of experiments. Metal salts were dispersed onto the support by pore-filling, also known as the incipient wetness method. This involves making a concentrated solution of a soluble salt of the metal species in an appropriate solvent, usually deionized water. Aliquots of the solution are added to the solid until its surface appears wetted, avoiding excess liquid so as to not suspend the solid in the solution. The wetted solid is then dried under vacuum until it appears dry. This procedure is repeated until the entire salt solution has been added. The final catalyst is then dried under vacuum at 100°C. This technique is used in hopes of concentrating the active catalytic species in the internal volume and/or microporosity of the support. As was previously discussed, the micropore regions in these types of solids are thought to be very important in catalytic processes.

Catalyst systems for the oxidation of ethylene to acetaldehyde were evaluated in a gas flow system (Figure IV-1). Reactant gases, which included moist air and an ethylene/nitrogen mix (ranging from 10-20% C_2H_4 in N_2), were combined before coming in contact with the catalyst bed. To assist in gas mixing and heat transfer to the reactant stream, enough glass beads were

placed on top of the catalyst bed to fill the remainder of the reactor tube. Water was introduced into the system by passing the air stream through a glass bubbler fitted with a coarse air diffuser. The amount of moisture in the air stream was regulated by either placing the bubbler in a Dewar containing ice water, leaving it at room temperature (RT ~ 25°C), or heating the bubbler slightly with thermal tape to increase the vapor pressure of water in the bubbler. Catalyst temperature was regulated with an Omega solid state temperature controller (model CN310) and variable transformer (Staco, Type 3PN1010) connected to an oven that surrounded the reactor tube. Temperatures did not vary more than ±2°C from the set-point on the temperature controller during the course of a run. The reactor flow system was constructed entirely of glass. The reactor tube was 40 cm long, constructed of a 10 mm I.D. glass tube. Connections were made at both ends *via* 10/30 ground glass joints, and a coarse glass frit was mounted in its center on which the catalyst bed was supported. A thermocouple, surrounded by a glass jacket, was mounted directly below the glass frit and used for oven temperature control and monitoring reactor temperature. The reactor gas flow was in a downward direction, as diagrammed in Figure IV-1.

A Hewlett-Packard 5890 gas chromatograph (g.c.), equipped with an Alltech RSL™-160 capillary column and flame ionization detector were used in the analyses and identification of organic reactants and products from the catalyst flow system. This non-polar, 100% dimethylsiloxane polymeric phase separates organic analytes mainly on the basis of their boiling points. This is a product line no longer used by Alltech. The same phase can now be found sold as Alltech's AT-1, or Hewlett Packard's HP-1 capillary columns. The column used was 30m in length, 0.32 mm O.D. and 5μm film thickness, with He as the carrier gas and a 3m deactivated silica guard column on the injector end.

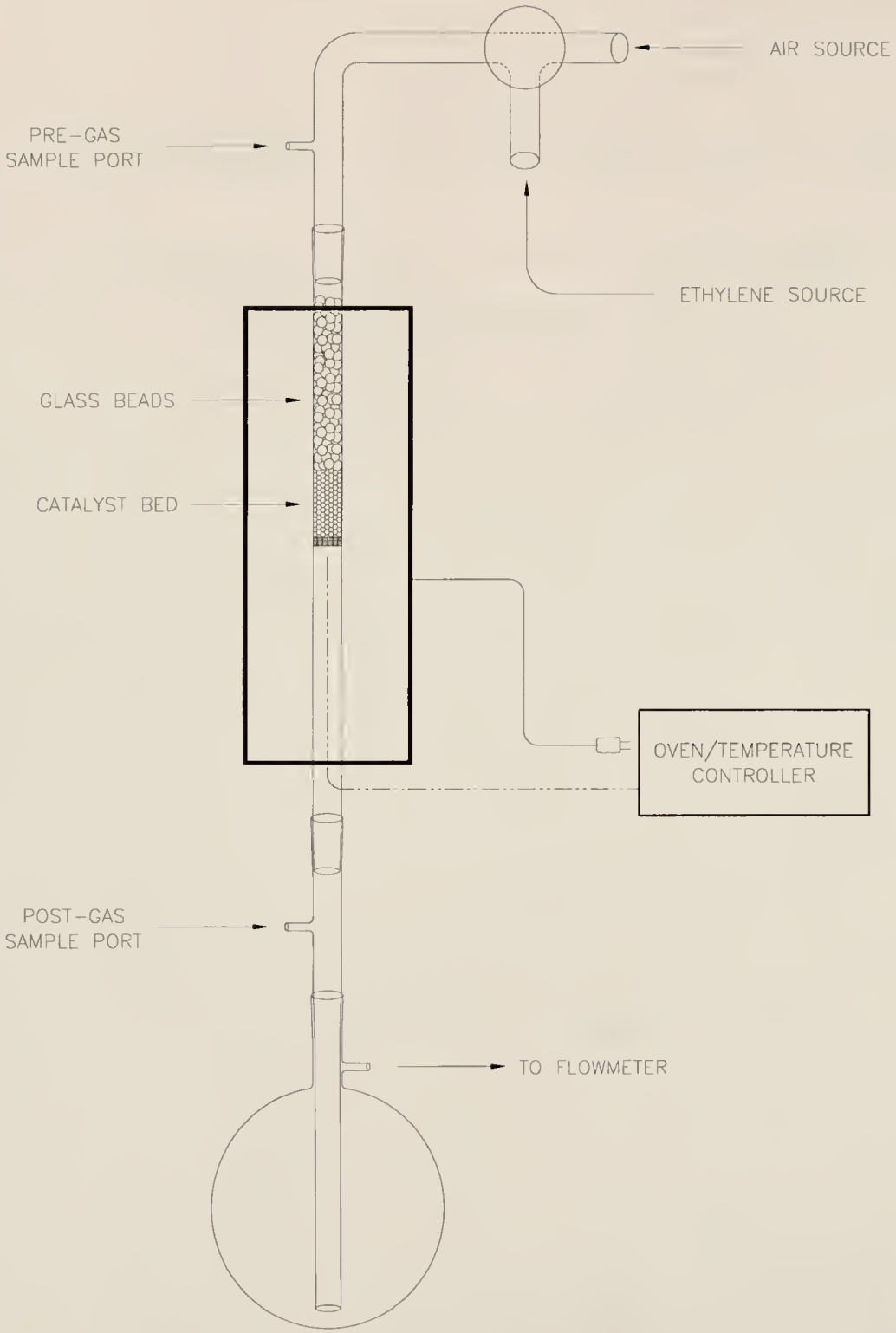

Figure IV-1. Gas Flow Apparatus for Catalyst Screening

Gas samples were taken both before and after the catalyst bed, which allowed for calculation of conversions and selectivities. A Varian 3700 g.c., equipped with a Carboxen™ 30 foot, 60/80 mesh packed column and a thermal conductivity detector was also employed for monitoring N_2, O_2, CO and CO_2. This was done for purposes of mass balance and to monitor any possible over oxidation of ethylene or the carbon support under reaction conditions.

Preparation of $H_2[PdCl_4]$ Catalyst: (HPd-572)

To 0.31g of $PdCl_2$ was added 1.0 mL concentrated $HCl_{(aq)}$ and 4.0 mL distilled H_2O. The resultant solution was pore-filled onto 5.0g of Ambersorb® 572. The resultant solid was dried under vacuum at 100°C for one hour before use in any catalysis runs. The doping level in the resultant catalyst was $3.5x10^{-4}$ moles Pd(II)/g of carbon (3.7 wt%).

Preparation of $Na_2[PdCl_4]$ Catalyst: (NaPd-572)

To 0.26g of $PdCl_2$ was added 1.0 mL concentrated $HCl_{(aq)}$ and 1.0 mL distilled H_2O. To the resultant brown solution was added 0.18g NaCl (~2 moles Na(I) per mole Pd(II)), dissolved in ~2 mL H_2O. This solution was evaporated to dryness over a steam bath, the resultant solid (presumed to be $Na_2[PdCl_4]$) dissolved in a water/ethanol mix (1/1), and then this solution was pore-filled onto 5.0g of Ambersorb® 572. The resultant solid was dried under vacuum at 100°C for one hour before use in any catalysis runs. The doping level in the resultant catalyst was $3.0x10^{-4}$ moles Pd(II)/g of carbon (3.2 wt%).

Preparation of $Na_2[PdCl_4]$ + $CuCl_2$ Catalyst: (NaPd-572+Cu)

To 1.04g of the NaPd-572 catalyst was added 0.51g of $CuCl_2 \cdot 2H_2O$, dissolved in 3 mL of a water/ethanol mix (1/1), by the pore-filling method. The resultant solid was dried under vacuum at 100°C for one hour before use in any catalysis runs.

Preparation of $NH_3/Na_2[PdCl_4]/CuCl_2$ Catalyst: (CuPd-572)

Prior to pore filling, the carbon was washed with 6M $NH_{3(aq)}$, and allowed to stay in contact with this solution for ~1 hour. This was followed by repeated rinsing of the solid with distilled H_2O until a pH-neutral effluent was observed, dried under vacuum at 100°C, and pore-filled with a solution containing both Pd(II) and Cu(II) salts. The $Na_2[PdCl_4]$ was made in similar fashion as in the preparation of NaPd-572. To 0.23g of $PdCl_2$ was added 1.0 mL concentrated $HCl_{(aq)}$ and 1.0 mL distilled H_2O. To the resultant brown solution was added 0.15g NaCl, dissolved in 2.0 mL H_2O. This solution was evaporated to dryness over a steam bath, the resultant solid dissolved in water, and 1.10g $CuCl_2 \cdot 2H_2O$ was added to this solution. This liquid mixture was then pore-filled onto 5.0g of the NH_3 washed Ambersorb® 572. The resultant solid was dried under vacuum at 100°C for one hour before use in any catalysis runs. The doping level in the resultant catalyst was 2.5×10^{-4} moles Pd(II)/g of carbon (2.7 wt%), and 1.3×10^{-3} moles Cu(II)/g of carbon (8.2 wt%).

Materials

The C_2H_4 gas employed (Matheson) was C.P. grade (99.5% pure). Compressed air and N_2 gases were standard research grade. All were used as received without further purification. $PdCl_2$ (Aldrich) was reported as 99% pure

and used as received. All other reagents used were of common laboratory grade, obtained from Fisher Scientific, and used without any further purification unless otherwise noted.

Run Conditions

Typical catalyst run conditions used between 0.5-1.0g of catalyst in the flow reactor system. Reaction temperatures were varied between 25° and 150°C. It was found that above 125°C, significant amounts of CO_2 were produced, arising from either oxidation of the support, or over-oxidation of the organic substrates. The best reaction temperature for these catalysts was found to be around 75°C. Total gas flows ranged between 2.0 and 10.0 mL/minute, with C_2H_4 concentrations typically ranging from 1-3% of the total gas flow.

Results and Discussion

HPd-572 Catalyst Results

Initial catalysis runs employed the $H_2[PdCl_4]$ doped Ambersorb® 572 (HPd-572). Reaction conditions were varied in attempts to yield the most active catalyst system. Using 1.0g of the HPd-572 catalyst with a bed height of 2.0 cm, flow rates were varied over ranges from 2-10 mL/minute. Catalyst temperatures were varied from 50°-150°C, and the moisture content from the described method with the water bath temperature ranging from RT (~5% humidity) to a heated bubbler at 75°C (~25% humidity). Relative amounts of air and C_2H_4 were varied from concentrations in which O_2 was a limiting reagent, to experiments where O_2 was present in large excess. Conversion of

C_2H_4 did not exceed 20%, and the selectivity to CH_3CHO was less than 25%. Several additional products were found by g.c. analysis. However, since the desired activity was not observed and the production of chlorinated alkanes and ethers is known to occur from acid catalyzed reactions with olefins, no further attempt was made at identification or quantification. In the homogeneous industrial process it is reported[76] that small amounts of acetic acid, 2-chloroethanol, chloroethane, chloroacetaldehydes and acetaldehyde condensation products are the most often observed by-products. It has been assumed that the minor by-products formed in this reaction are also composed of these compounds.

Appreciable activity was not observed in this system until temperatures exceeded 125°C, and this also resulted in the production of large amounts of CO_2. Analyses of g.c. data showed almost complete consumption of O_2 at temperatures above 125°C, unaccompanied by a proportional increase in aldehyde or other oxygenated organic products. Since no noticeable decrease in the carbon mass of the support was noticed over the course of the run, the production of CO_2 at these elevated temperatures is attributed to complete oxidation of the organic substrates. It was also observed that turning off the C_2H_4 in the gas feed caused an increase in the amount of CO_2 observed in the postgas stream. Again, since no measurable decrease in the support mass was observed over the course of a run, this was assumed to be due to the complete oxidation of adsorbed organics on the support. Returning the C_2H_4 feed to its original levels resulted in an immediate decrease in CO_2 production, back to its original levels at a given temperature. Based on calculated turnover numbers (T.O.N.)† for the amount of palladium present in this catalyst, this system was

† A turnover, or turnover number (T.O.N.) in catalysis terminology is determined by taking the number of moles of desired product produced, and

not found to be catalytic. The low activity it did exhibit was found to quickly taper off within three hours of the beginning of the reaction. Although the overall activity of HPd-572 was very low, the catalyst system was found to be more active at the slower flow rates (2-3 mL/min).

Initial observations found the support to have a high affinity for adsorbing organic substrates, as it was at least 1 hour before any organic analytes were observed in the post-catalyst gas stream for all of the catalyst systems analyzed. Additionally, the adsorption capacities and affinities of these supports[84] indicate they will not only adsorb and concentrate organic reactants, but will have even higher affinities for the products of this reaction. Due to this observation, no quantitative data for reported conversions or selectivities were obtained until adsorption equilibrium was considered to be reached. This was determined from an approximate mass balance of the amount of organic reactants measured in the pre-catalyst gas sample, compared to that measured after the catalyst bed. During the initial stages of a catalyst run, where adsorption was occurring to a large extent, it was obvious that the majority of the organic reactant was not accounted for in post-gas analyses.

NaPd-572 Catalyst Results

Because of the low activity of HPd-572 and the apparent production of acid-catalyzed products, the next catalyst screened was designed to eliminate possible effects due to the presence of Brønsted-Lowry acidity. In this system

---

dividing this by the number of moles of active catalyst species. A T.O.N.$\leq$ 1 would be indicative of a stoichiometric reagent, with values higher than 1 corresponding to catalytic agents. This number is often expressed per unit time, where the T.O.N. is simply divided by the given amount of time of the reaction.

the sodium salt of tetrachloropalladate was employed as the pore-filling salt (NaPd-572). Reaction temperatures were generally kept below 100°C, since results with HPd-572 had shown no benefit in going to higher temperatures, and flow rates were also kept low (3.0 mL/min). Using 0.5g of the catalyst, with a bed height of 1.3 cm and the water bubbler kept at RT, this system was run under the typical reaction conditions described earlier (see Run Conditions).

Initially, the NaPd-572 catalyst showed activity towards acetaldehyde production at 50°C. The activity of this system was found to maximize around 75°C, with ~70% conversion of C_2H_4 and >90% selectivity towards CH_3CHO. Other products included very small amounts of CO_2, and trace organic products. Determination of original conversions and selectivities were initially calculated as much lower, as large amounts of ethanol were observed in the post-gas analyses. It was later determined that the observed ethanol was not the product of a reaction of C_2H_4, but residual adsorbed solvent from the pore-filling preparation of the catalyst. This was further verified by the drying of a batch of this catalyst overnight at 200°C under flowing air, and then subjecting to normal run conditions with wet air and C_2H_4/N_2 mix. At temperatures below 100°C, CH_3CHO was the only observed organic product, and no ethanol was observed in the post-gas of the air dried NaPd-572.

To further verify that all the acetaldehyde produced originated from the ethylene, a mixture of air and ethanol vapors were passed over the catalyst under standard run conditions. Under these conditions, no reaction with ethanol was observed. This confirmed the observation that all the CH_3CHO produced arose from direct oxidation of C_2H_4, with the residual ethanol from pore-filling being unreactive. The presence of residual ethanol from pore-filling made it impossible to determine if ethanol was produced during this reaction.

The large amount of ethanol remaining in this catalyst once again points to the strong adsorptive capabilities of this support.

When the reaction with NaPd-572 was carried out above 100°C, a variety of heavier organic components (determined from g.c. elution times) were observed, along with a decrease in conversions and selectivity to acetaldehyde. No further analyses to identify these trace compounds were undertaken. As was previously observed in the HPd-572 catalyst, lower temperatures are more desirable for minimizing CO_2 production. Lower reaction temperatures are also advantageous when considering overall costs for industrial scale processes. Although this system was found to be catalytic, exhibiting 3 T.O.N. in optimal conditions, its activity was observed to decline rapidly after a period of 5 hours, leading to conversions of C_2H_4 of <5%.

A series of eight runs on the same sample of the NaPd-572 catalyst (0.50g, under standard reaction conditions: 3.0 mL/min gas flow, 75°C) were evaluated in an attempt to regenerate the catalyst to initial reactivity levels. These included a variety of overnight treatments with air at elevated temperatures (200°C), in hopes of reoxidizing the palladium and/or carbon surface, as well as extended exposure to a humid air stream at room temperature. Results of the air treatments saw a partial return of catalyst activity, with about 5-10% conversion of C_2H_4, 100% selective to CH_3CHO, but this activity steadily declined over a period of 4 hours. Moist air treatments were more successful, leading to a return of ~40% conversion, again with 100% selectivity towards CH_3CHO. As was observed previously, however, catalyst activity declined steadily after the first few hours of the reaction, dropping to <5% conversions after ~5 hours.

From these observations, it appears that the loss of activity is in part caused by poor retention of enough water for the system to remain active under

run conditions. Heating the water bubbler to 75°C to increase the overall humidity in the system prolonged catalyst life to ~5 hours, yet conversions still dropped off to <5% after this period of time. From these results, it would appear that the reoxidation of the active palladium species by the carbon support is not totally efficient under reaction conditions. Regardless, although some measure of activity was observed to return after the various attempts at regeneration, none restored the catalyst to its original conversion levels. Once this catalyst system was started, even when conversions were very low (<5%), CH_3CHO was always observed in the post-gas stream. However, instead of continued catalytic activity, this could simply be from the desorption of adsorbed product, which is feasible considering the previously observed adsorptive capacity of the support.

NaPd-572+Cu Catalyst Results

Unsuccessful attempts to regenerate the NaPd-572 system and its limited lifetime suggested the addition of a better oxidant for Pd(II), such as a Cu(II) salt, to this catalyst system may improve its overall activity. The resultant catalyst, NaPd-572+Cu, was screened in the same fashion as the other catalysts. A total gas flow of 3.0 mL/min, and a reaction temperature of 75°C were used on 0.50g of catalyst with a bed height of 1.1 cm. This catalyst showed almost no activity initially (<5% conversion to CH_3CHO). However, after an overnight exposure to moist air at 200°C activity was observed. Acetaldehyde production occurred at temperatures as low as 50°C. Selectivities greater than 98% were observed up to 125°C. The conversion of C_2H_4 maximized around 75°C, at about 80%. As previously observed, however,

the activity of this system was found to rapidly decline after ~4hrs. This system was found to be catalytic, producing 17 T.O.N. of acetaldehyde.

NaPd-572 Without Ethanol Catalyst Results

To further characterize and determine the effects ethanol may have on the reactivity of this catalyst system, another batch of the NaPd-572 catalyst was made using methanol and water in place of the ethanol/water mix used as the pore-filling solvent (see Preparation of $Na_2[PdCl_4]$ Catalyst). Additionally, the catalyst was dried in a vacuum oven overnight at 100°C prior to use, to ensure removal of the pore-filling solvents. The standard reaction conditions and setup were used, as previously described. Two different runs were done using this prepared catalyst.

The first experiment on this catalyst involved heating the water reservoir to 50°C, as it was previously noted that not enough water was being retained by the system to remain active if the water bubbler was not heated. The activity of this system was quite high, with conversions of ~80% and >95% selectivity to CH_3CHO at 75°C. As before, however, the activity of this catalyst was observed to rapidly decline after ~6 hours. This system was found to be more active than the catalyst made with ethanol, exhibiting ~10 T.O.N.

The second experiment with this batch of catalyst was meant to determine ethanol's effect on the reactivity of the system. In this case, a 1/1 ethanol/water mix was placed in the bubbler through which air passed, instead of distilled water only. This introduced both water and ethanol vapors to the catalyst bed during the course of the reaction. Using the standard run conditions, the presence of ethanol was observed to severely limit the conversion of C_2H_4. Overall conversions of C_2H_4 never exceeded 30%, and the

appearance of other organic products was also observed. This is not completely surprising, as the existence of another organic substrate would obviously allow for the production of other compounds in this catalyst system. Additionally, it was observed from pregas and postgas analyses that a large amount of the ethanol in the feed gas stream was simply being adsorbed by the support. No significant evolution of ethanol was noticed until the catalyst temperature was taken above 100°C. Both of these experiments point to the presence of ethanol being undesirable in this catalyst system.

CuPd-572 Catalyst Results

In an effort to combine all of the observations previously seen with the various Wacker-type catalysts supported on Ambersorb® 572, a base washed catalyst was made containing both copper and palladium salts (CuPd-572). Base washing with aqueous ammonia was done in hopes of removing any residual acidity from the solid that might exist, considering its precursor is a sulfonated ion-exchange resin. And as observed in the case of the NaPd-572+Cu catalyst, although this system was observed to be catalytic without copper present, addition of this ion greatly increased its activity.

Under standard reaction conditions, which included total flow rates of 3.0 mL/min, temperatures ranging from room temperature to 100°C, C_2H_4 concentrations of ~2%, and employing a heated water reservoir at 50°C (resulting in ~5-10% humidity after considering dilution of air stream with C_2H_4/N_2 gas mix), experiments were done with 0.50g of catalyst, and a bed height of 0.95 cm. This catalyst system was found to be the most active of all those tested. Initially, activity was observed at room temperature, and as before maximized at 75°C. The system was run continuously over a period of

10 days, and during this time activity was never observed to decline. Conversion of C_2H_4 was found to be >90%, with greater than 98% selectivity towards CH_3CHO production. During this time period, it was found that the catalyst produced more than 120 T.O.N.

Small amounts of CO_2 were observed, but no other organic products were indicated by g.c. analysis. However, further tests indicated that chlorine was lost during the reaction. This is surmised from elemental analyses of the CuPd-572 catalyst. Results for the catalyst before use found it to contain 9.83% Cl^- by mass (theoretical value is 10.2%). Analysis of the catalyst after the 10 day experimental run found it to contain 6.24% Cl^-. This is a 37% decrease in the amount of chloride ion, and is not accounted for in the detected products. This is assumed to occur either because the chlorine-containing by-products are in such low concentrations that they are below the detection limits of the g.c. detectors, or that these products are adsorbed and retained on

Table IV-1. Summary of Heterogeneous Wacker Catalyst Conditions and Results

Catalyst	HPd-572	NaPd-572	NaPd-572+Cu	CuPd-572
Dopant Level (g metal/g carbon)	0.0037g Pd(II)	0.0032g Pd(II)	(see prep. of catalyst)	0.0027g Pd(II) 0.0082g Cu(II)
Total Gas Flow (mL/min)	2-10	3.0	3.0	3.0
Catalyst Temp. (°C)	75-150	50-125	50-125	25-75
C_2H_4 Conversion	15% max.	70% max.	80% max	>90%
Selectivity to CH_3CHO	<20%	>90%	>98%	>98%
Turn Over Number	not catalytic	3	17	>120
Catalyst Lifetime	---	5 hrs.	4 hrs.	>10 days

the carbon surface under reaction conditions. Regardless, only small amounts of materials were made, and this loss of Cl^- did not appear to affect catalyst activity. More long-term studies of this catalyst are warranted to further understand this observation.

Table IV-1 summarizes the results for the various catalyst systems studied, excluding the observations from the second sequence of experiments done on the NaPd-572 catalyst made without ethanol.

In an effort to further qualify the effect of moisture content on this system, and gain further evidence that a traditional Wacker-type mechanism was being followed, the water feed to the system was turned off for a brief period of time. This was done by simply routing the air flow around the aqueous bubbler. The effects of this, which are further detailed in Figure IV-2, show a decrease in the conversion of C_2H_4 concurrent with a drop in the humidity of the system. As soon as the water feed was reintroduced to the system, the catalyst returned to its original activity level.

Porosimetry and Surface Area Studies

The presence of micropores in these types of carbonaceous supports is thought to be advantageous for heterogeneous catalysis applications. As discussed in Chapter II, these microporous regions allow for areas of concentration of reactants. Ideally, these are localized around active catalyst sites. Accessibility to these areas is also of great importance. Therefore, the size of the substrates must be kept in mind, as well as the presence of mesoporous and macroporous regions on the solid that would facilitate transport to and from these microporous regions. From the observations made on the catalyst systems developed here, it would appear that the choice of

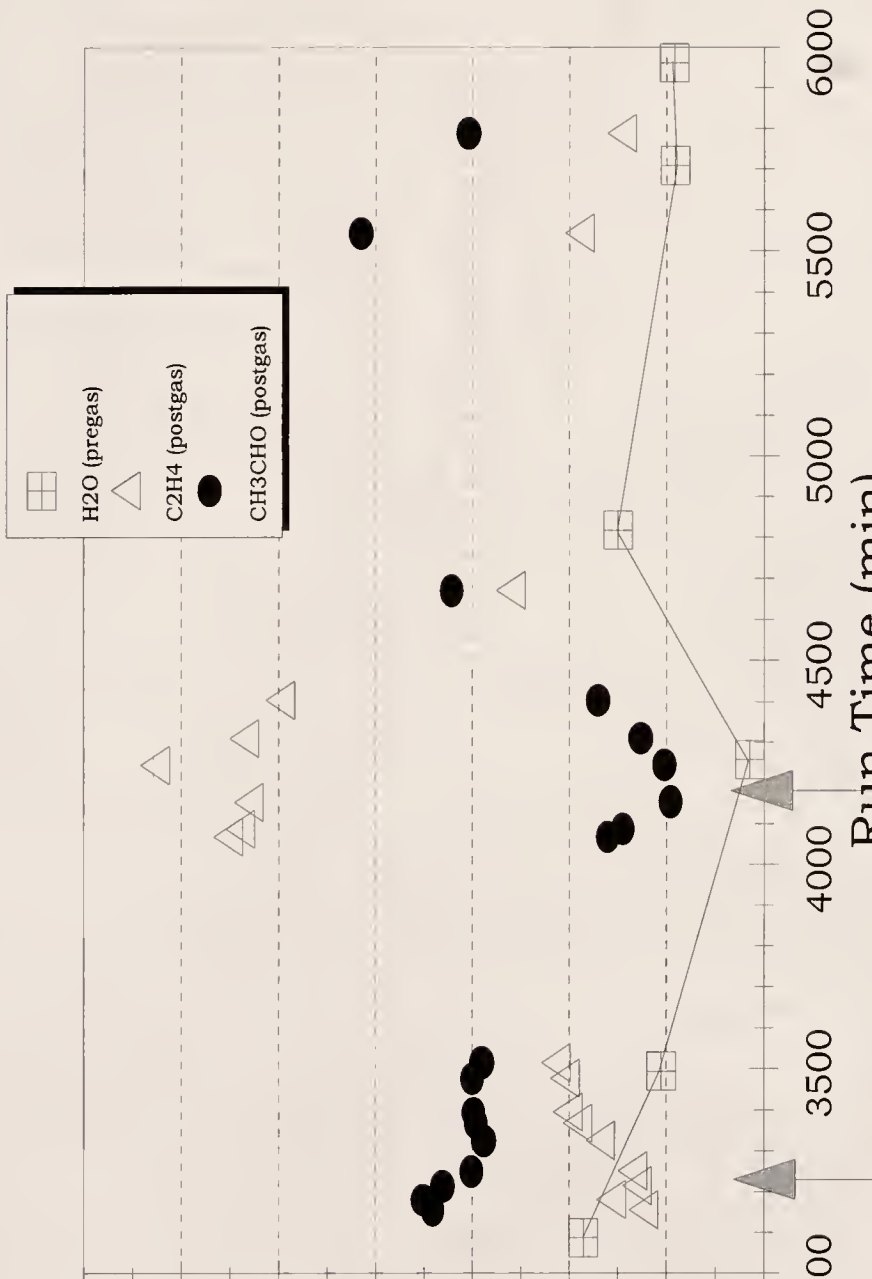

Figure IV-2. H_2O Effects on CuPd-572 Catalyst and Production of CH_3CHO

Ambersorb® 572 as a support for this heterogeneous catalyst system facilitates these important processes. This was determined from the large adsorption of ethylene that was initially seen in the beginning of a reaction, as well as the retention of ethanol by this support that was observed in the case of the NaPd-572 catalyst system. The development of an active catalyst system (CuPd-572) also indicates these processes are occurring with some degree of efficiency.

In an effort to further determine where the pore-filled salts reside on this support, a series of surface area and porosity studies were done on these catalysts. This data is summarized in Table IV-2. These values were obtained in the same manner as those reported in Chapter II, with the only difference being the degas temperature for all the samples listed was chosen to be 110°C.

Table IV-2. Surface Area and Pore Volume Data for Wacker Catalysts

CARBON	Surface Area (m^2/g)	Pore Volumes (cc/g)			BET C constant
		micropores	mesopores	macropores	
A-572[a]	1236	0.457	0.324	0.242	995
NaPd-572	857	0.314	0.262	0.175	970
% Difference (from A-572)	30.7	31.3	19.1	27.7	---
CuPd-572	566	0.205	0.232	0.162	1077
% Difference (from A-572)	54.2	55.1	28.4	33.1	---

[a] This is a different lot number (#2201) and degas temperature (110°C) than the sample reported in Chapter II (lot #2125, 200°C degas).

As can be seen from the data, a decrease in all the physical parameters is observed upon doping A-572 with the various salts. Although this decrease is not specific to just the micropores, it is this region of the pore structure that undergoes the largest change. This is evidence that the majority of the pore-filled salts are residing in, or blocking the entrances to the micropore volume of the support.

Further Characterization of Ambersorb® Carbonaceous Adsorbents

Magnetic susceptibilities and electron paramagnetic resonance (EPR) spectra were obtained on two different Ambersorb® carbons in efforts to further understand the activity of these materials as catalysts and catalyst supports, and gain further insight into the interaction of the metal dopants with the carbons. Magnetic susceptibilities were obtained using a Johnson Matthey magnetic susceptibility balance (model MSB-1). This employs a method where the magnetic susceptibility of a sample is determined by the force the sample exerts on a suspended permanent magnet, which is the equal but opposite force determined by the traditional Guoy balance method where the force exerted on the sample by a fixed permanent magnet is measured.[85] Table IV-3 summarizes the results of the measured mass susceptibilities (X_g) of the two carbons with and without metal dopants.

No corrections were made to the measured values for the volume susceptibility of air or diamagnetic contributions from chloride or water present in the samples. Close analysis of the data in Table IV-3 does yield some interesting observations. A negative value for X_g is found for A-563/2144, which is indicative of a diamagnetic compound. However, a single sharp EPR peak was obtained for this material at 190K, with a g value of 2.005. Since the

Table IV-3. Mass Susceptibilities of Ambersorb® 563 and 572 With Dopants

Sample[a]	X_g (c.g.s.)
A-563 (lot #2144)	-2.08×10^{-7}
A-563/2144 with 5% Cu(II)[b]	2.62×10^{-7}
A-572 (lot #2201)	4.82×10^{-6}
A-572/2201 with 5% Cu(II)[b]	3.88×10^{-6}
CuPd-572 catalyst	5.65×10^{-6}
$CuCl_2 \cdot 2H_2O$ solid	7.89×10^{-6}

[a] All samples were ground to a fine powder using a Wig-L-Bug (Crescent), to minimize errors from inhomogeneous packing and trapped air volume between sample particles.
[b] The 5% doping level of Cu(II) was a weight percent pore-filling value, using $CuCl_2 \cdot 2H_2O$ as the dopant.

reported X_g is so small, it is most likely that the measured diamagnetic character of A-563/2144 is a bulk property arising from either diamagnetic contributions from the matrix, magnetic anisotropy of the sample, or perhaps anti-ferromagnetic coupling of the carbon free radicals to some trace metal in the solid. The existence of a definitive EPR signal shows that this solid is paramagnetic, however, and the g value is typical of carbon free radicals.

Three EPR spectra were obtained at 190K for pure $CuCl_2 \cdot 2H_2O$, a 5% Cu(II) glass made from a 2:1 ethylene glycol:water mix, and for A-563/2144 with 5% Cu(II). As would be expected, a very broad, unrefined peak is observed for the pure copper salt, and the hyperfine splitting typical of Cu(II)-d^9 ion is not seen until the sample is dispersed in the glass and is magnetically dilute.[86] The hyperfine structure of Cu(II) is observed in the case of the doped A-563/2144, along with a single sharp peak associated with the pure carbon. Although little information can be derived about the electronic interaction

between the metal ion and the carbon support, the appearance of the hyperfine splitting does indicate that Cu(II) is well dispersed on the solid.

The A-572/2201 sample has a fairly large and positive X_g, typical of paramagnetic compounds. Its value of 4.82×10^{-6} c.g.s. is comparable to that of pure $CuCl_2 \cdot 2H_2O$ (7.89×10^{-6} c.g.s.). Of further interest here is that upon doping A-572/2201 with 5% Cu(II) ion, the magnitude of X_g decreased. An explanation for this occurrence is not obvious. The X_g value for the CuPd-572 catalyst is also reported here. No EPR was obtained on the A-572 carbons as it was not possible to obtain a lock on the instrument for this sample.

Conclusion

Surface area and micropore volume are considered to be very important factors in heterogeneous catalysis. It stands to reason that the greater the exposed surface area for the solid catalyst, the more likely the possibility of reactants coming in contact with an active site on the catalyst surface. Maximizing exposed catalyst surface area is the major limitation in developing a heterogeneous catalyst from a homogenous system. Employing a support that has synergistic effects on the desired reaction is of even greater benefit, and this was observed in the catalyst systems described. Included in these observed synergistic effects are the ability of the support to adsorb and concentrate organic reactants in the internal pore structure of the carbon, where most of the catalyst is believed to be present, and the support's ability to serve as an oxidative compound for the catalytic cycle.

The initial success of this system as an active Wacker-type catalyst opens up many other possibilities for further research. Obviously, there are many parameters to be considered in designing this type of heterogeneous

system. This in turn yields countless possibilities and parameters to be modified in tailoring a heterogeneous catalyst system for specific reactivities and reaction conditions. Included in these are the possibilities of replacing the chloride counterion with others, such as nitrate or acetate, which eliminates the possibility of forming undesired chlorinated by-products, and application of this catalyst to other systems of environmental and commercial interests. Although no chlorinated by-products were observed in the most active catalyst system, CuPd-572, evidence did exist that chloride was somehow being lost during the reaction. Changing the counter-ion in such a way would also have some effect on the overall reaction and product distribution, which could also prove desirable. The preferential oxidation exhibited by these catalysts for an organic substrate versus the support itself would also allow employing these supports at higher temperatures, without concern for their combustion.

It is often observed in dispersed heterogeneous catalyst systems like those reported here that the actual percentage of active catalyst species is much less than 100%. T.O.N.'s reported here were based on the assumption that all of the Pd(II) was active, which is probably not a true representation of this catalyst system. Further studies involving chemisorption and other surface methods would help in gaining a more complete picture of the actual catalyst surface and active sites. The possible error arising from this assumption is advantageous, however, as it shows that the reported catalytic activity of these catalysts is a conservative estimate of their minimum activity levels.

Results of the magnetic susceptibility measurements and EPR studies did not yield any conclusive data about the behavior of these supports, or the interaction of the metal dopants with the carbon. However, in conjunction with the physical properties and adsorption characteristics reported in Chapters II

and III, they provide another characterization of the behavior of these systems. The curious results from the EPR and susceptibility measurements definitely warrant further investigation into determining the effect these supports have on metallic species doped onto their surface, and the nature of the chemical interactions between the two.

CHAPTER V
CONCLUSION

The purpose of the research presented was to develop a greater understanding of the behavior and properties of carbonaceous adsorbents. Through the employment of a variety of physical methods such as elemental analyses, gas adsorption studies, and the determination of surface areas and porosities, a better understanding of the physical characteristics of porous carbonaceous materials has been gained. This included the determination of what have proven to be the most important factors of the adsorption characteristics of porous carbonaceous solids. It was found that the adsorption behavior of a solid is governed by a complex series of parameters. Surface area and pore distributions of a porous solid are definitely important in facilitating transport and adsorption behavior, but the chemical functionality of the carbon support[10,11,12,37,48] plays a much more significant role. The determination of what these various functionalities may be, where they exist on the surface of a solid, and their relative concentrations have proven to be difficult to determine by most modern instrumental methods. However, rapid advances are being made in methods to help characterize these types of materials, driven by their importance and successes in adsorbent and catalytic applications.

As observed in these studies, a large effort in the characterization of these nine different carbons through elemental analysis and interpretation of the standard N_2 gas adsorption isotherms at 77K yielded a substantial amount

of information for making relative comparisons of these adsorbents. A great deal has been learned about the determination of surface area and porosity of porous solids. An appreciation and deeper understanding of the theories that assist in interpretation of the interactions at the gas-solid interface were used to help understand and further characterize porous solids. This information was then used to assist in understanding the chemical behavior of carbonaceous adsorbents as heterogeneous catalysts and catalyst supports. The knowledge gained from these studies will contribute to the growing understanding of heterogeneous chemistry, which in many cases has been considered just as magical a process as the "philosopher's stone" of alchemy fame.

When comparisons of these solids with a variety of adsorptive gases were made, none of the measured physical parameters could be directly correlated with the observed adsorption behavior. The capacity and affinity of a carbonaceous adsorbent for a specific adsorbate were not solely dependent on the properties determined from elemental composition, surface area, pore volumes, or on the resultant C constant derived from the BET equation. These values were found to be better characterized by the use of n_i and $K_{i,ads}$ values.

The interpretation and data analysis presented in the proposed model (Eqn. III-1) is not claimed to be any simpler than the application of BET theory. However, it has found applications in being able to more readily analyze adsorption data and isolate the thermodynamic parameters involved in physisorption. This model is not intended to replace or disprove existing theory, but is intended to complement current interpretations of adsorption data. The values thus gained may prove to be more meaningful for comparison purposes when considering porous solids in catalytic and adsorption processes.

From the proposed model, a capacity (n_i) and equilibrium constant ($K_{i,ads}$) were obtained for what have been determined to be three different processes. An interpretation of the physical meaning of these three processes has been offered that is in agreement with current descriptions of adsorption isotherms. Obtaining these isotherms at various temperatures has allowed the calculation of the adsorption enthalpies ($\Delta H_{i,ads}$) for the three defined processes. These values of n_i, $K_{i,ads}$, and $\Delta H_{i,ads}$ can then be used to more directly compare and better choose an adsorbent for a specific application.

This process data may prove to be more meaningful than standard surface area and pore volume measurements when considering adsorption and catalytic applications. Knowledge of the pore sizes, volumes and shapes, and the absolute surface area is beneficial in characterizing porous solids. However, current methodology and theory involve many assumptions, and instrumental techniques become increasingly complex and expensive if one desires to characterize a surface absolutely. Additionally, for catalytic and adsorbent applications, it is more meaningful to know the adsorption behavior of a material versus its absolute physical structure. The development of the model presented in Chapter III allows for the collection of quantitative data about the adsorption characteristics of a solid from isotherm data that is relatively simple to acquire. The capacity and thermodynamic data obtained from this approach can then be compared directly between various solids. This data interpretation may prove more useful than determination of the absolute surface areas and pore volumes. What is likely of greater importance in many applications are the effective areas and volumes with which an adsorbate interacts. The values found for n_i give a quantitative measure of this. The $K_{i,ads}$ values give a measure of the strength of these interactions. Comparisons of four gaseous probes, N_2, CO, CH_4 and CO_2, exemplified the effects changes in

polarity and size will have on these adsorption parameters for porous carbons. Further application of this model to other gases and a larger variety of solids would, therefore, be of great interest.

Finally, the development and characterization of an active supported catalyst system employing a porous carbonaceous support was described. Knowledge of the adsorption characteristics and physical structure assisted in the choice of a carbonaceous adsorbent that would function as a working support in the Wacker reaction. Determination of the important factors involved in adsorption by porous carbons led to a greater understanding of the behavior of this heterogeneous catalyst system. This support was also found to have synergistic benefits for the catalysis which could replace the function of the oxidant Cu(II). The resultant catalyst system's activity equals or surpasses the activity of other reported heterogeneous Wacker systems.[80,87] The activity of this system shows that it is quite feasible to explore the development of a heterogeneous catalyst system derived by analogy to existing homogeneous processes. Additionally, the employment of carbon as a support in catalysis chemistry was shown to be feasible, and even beneficial when one can take advantage of carbon's unique physical and chemical behaviors.

APPENDIX A

N_2 ISOTHERMS (@77K) AND PORE VOLUME DISTRIBUTION CURVES OF CARBONACEOUS ADSORBENTS STUDIED

Graph (a): Adsorption and desorption plot of N_2 isotherm @ 77K.

(———) adsorption curve

(.....) desorption curve

Graph (b): Pore volume distribution plots from BJH desorption curve data.

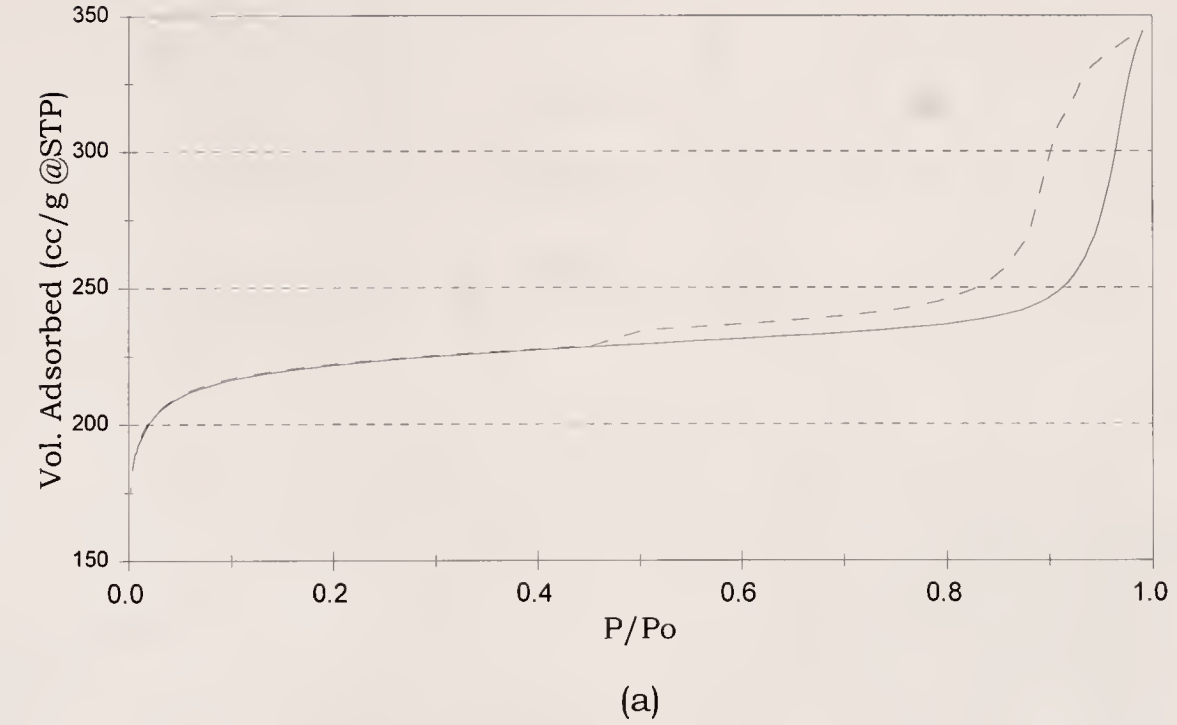

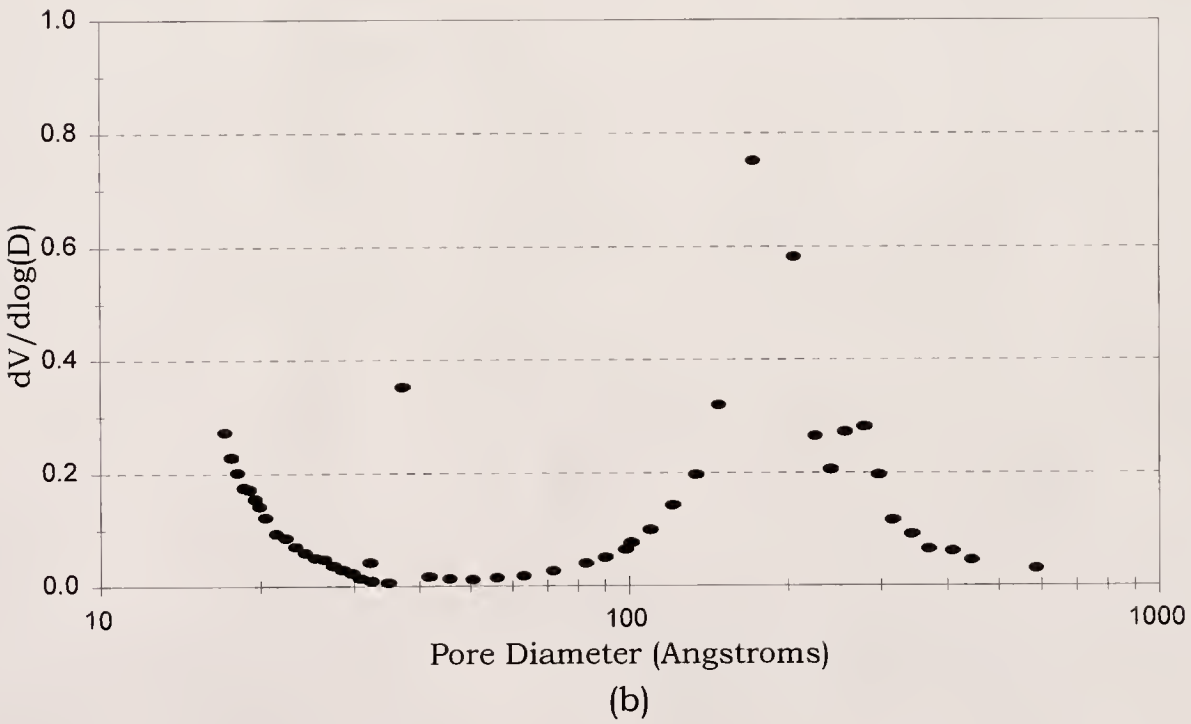

Figure A-1. (a) Nitrogen Isotherm; (b) Pore Volume Distribution for PPAN

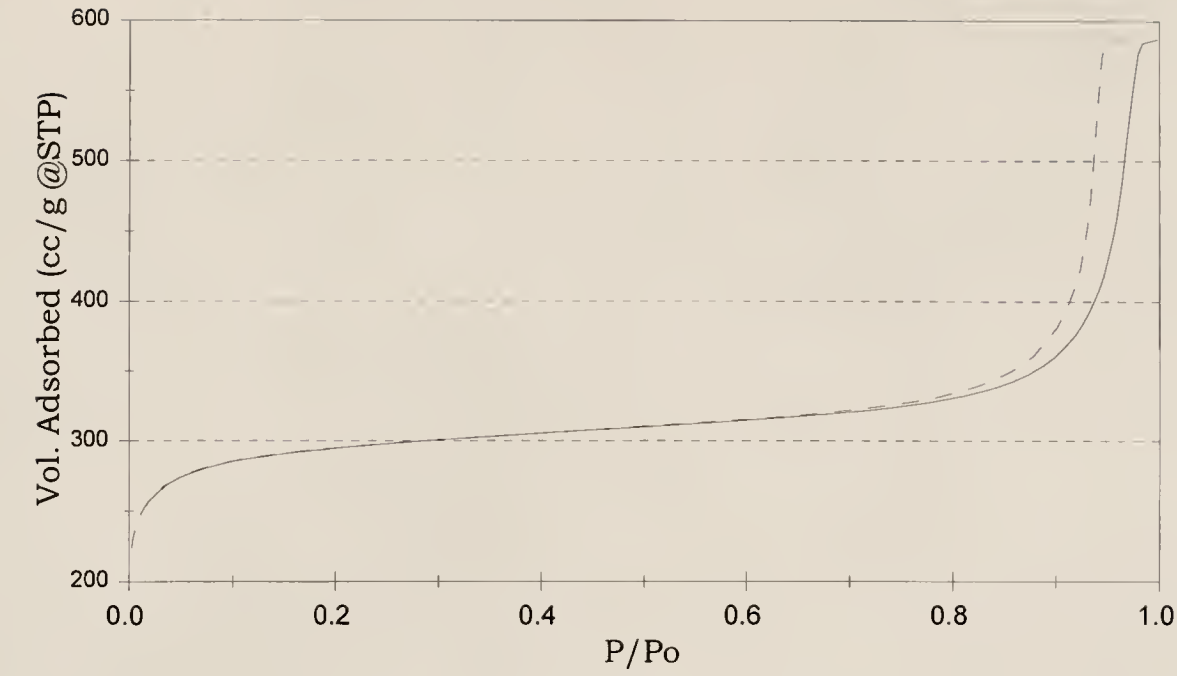

(a)

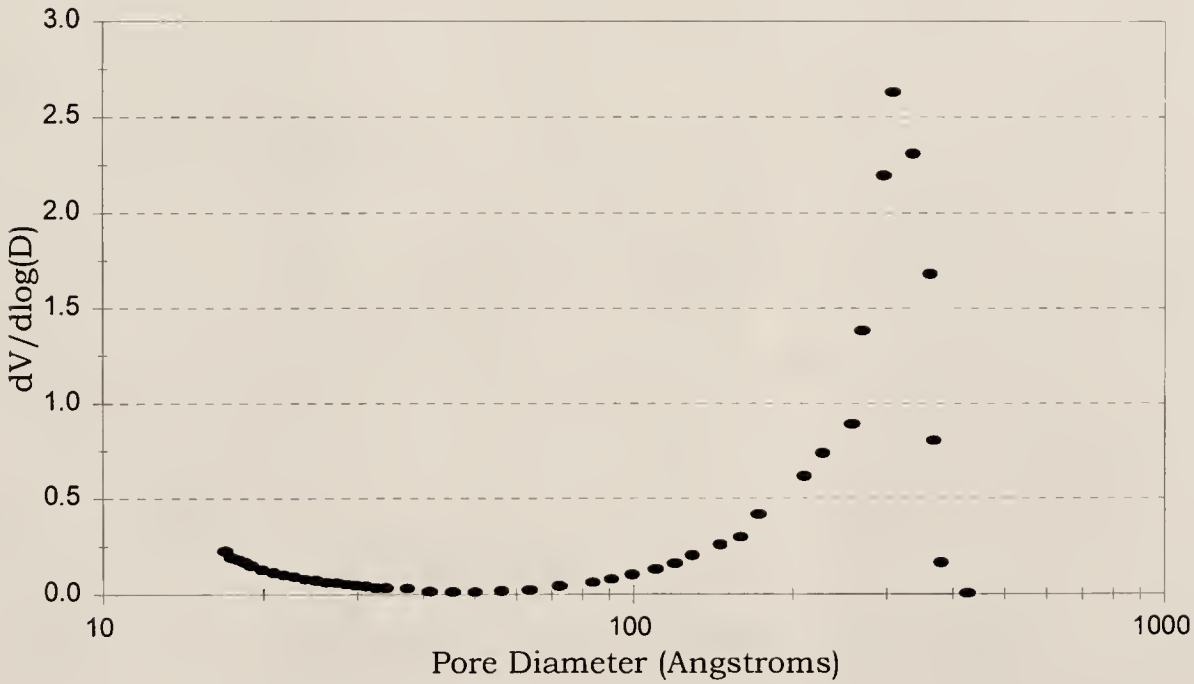

(b)

Figure A-2. (a) Nitrogen Isotherm; (b) Pore Volume Distribution for A-572

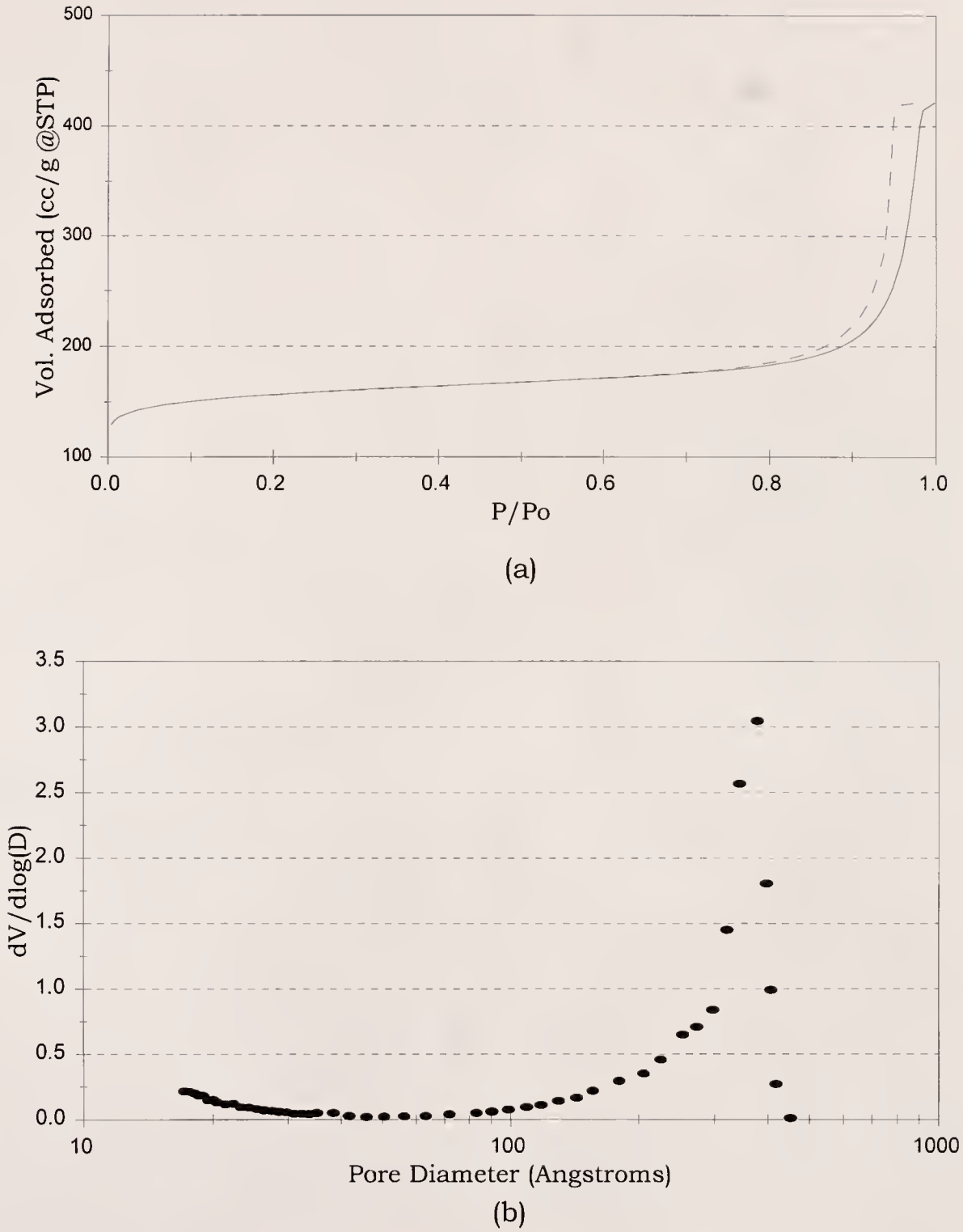

Figure A-3. (a) Nitrogen Isotherm; (b) Pore Volume Distribution for A-563

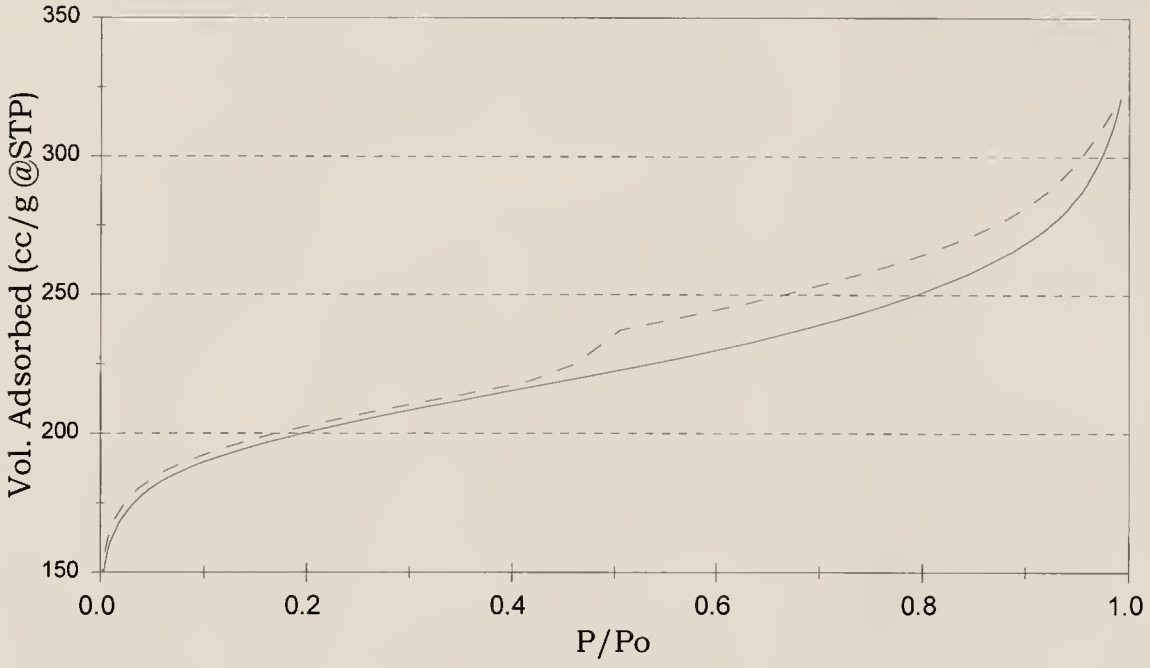

(a)

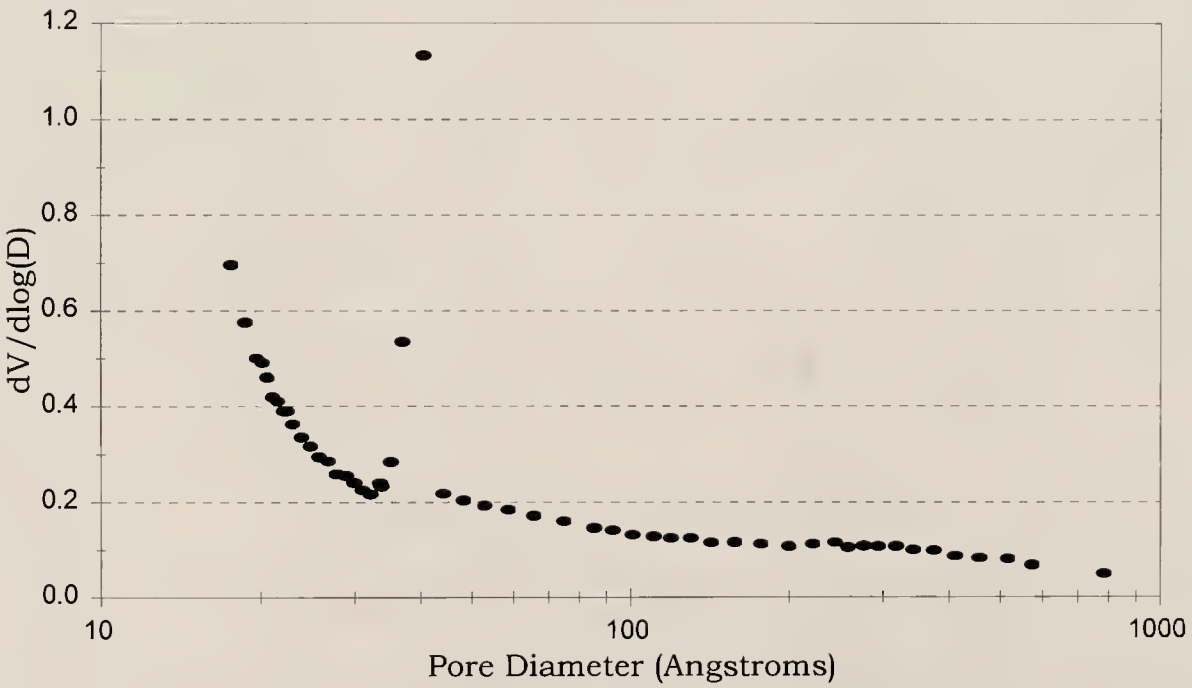

(b)

Figure A-4. (a) Nitrogen Isotherm; (b) Pore Volume Distribution for N-211

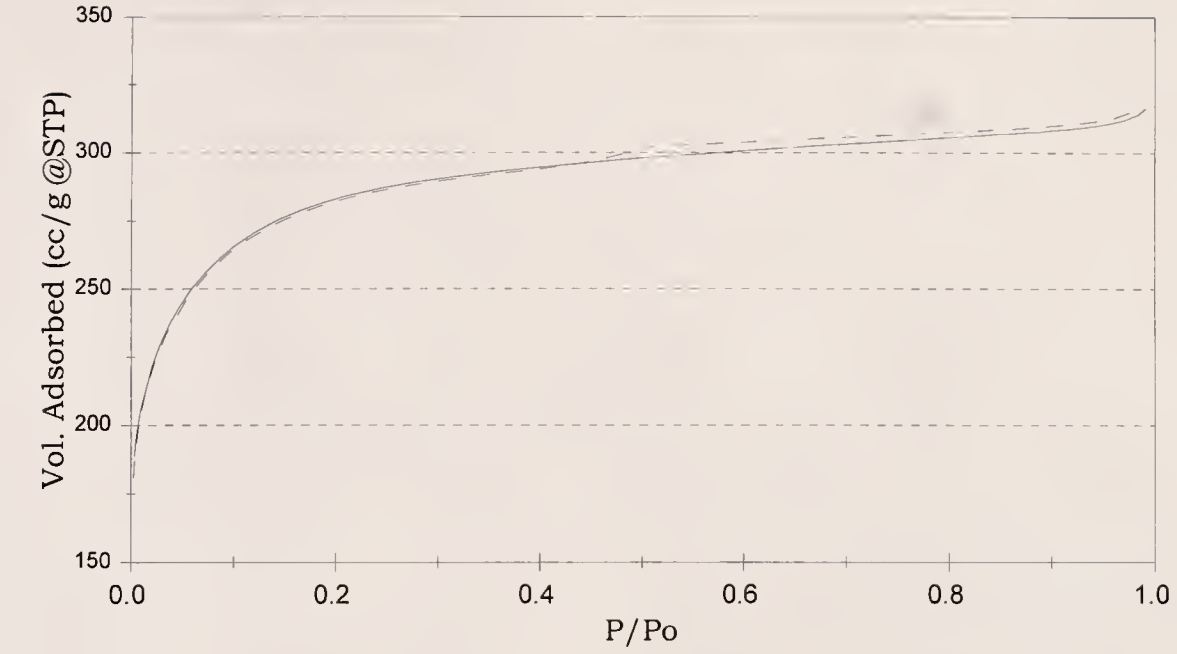

(a)

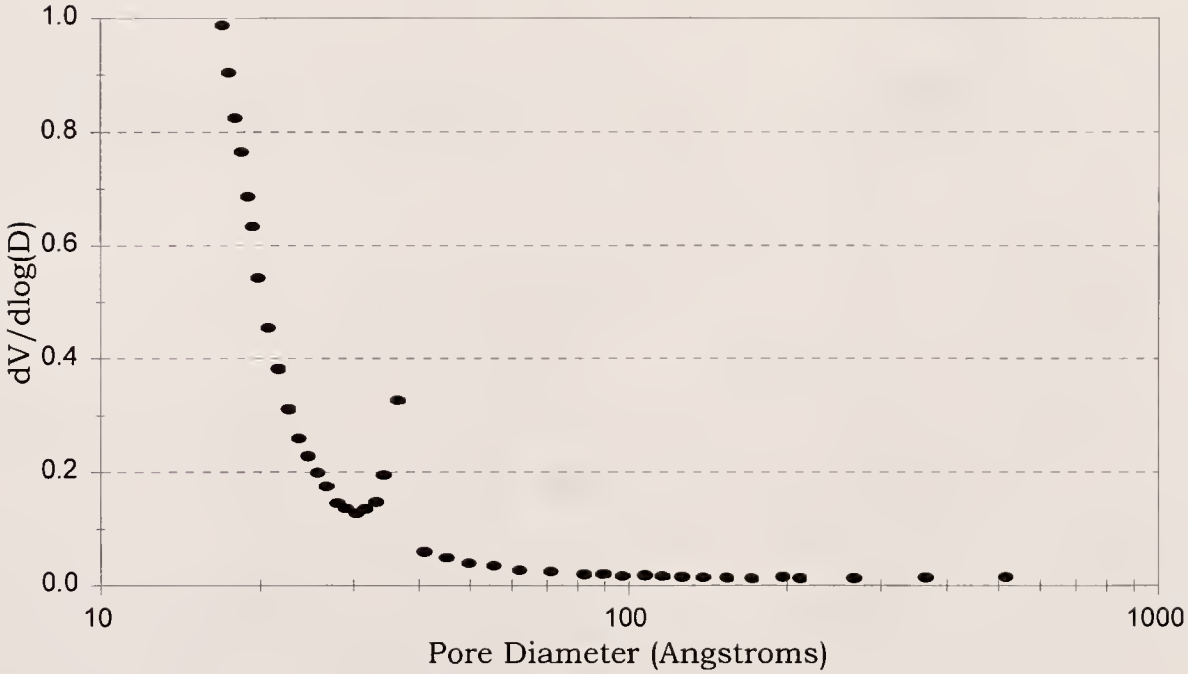

(b)

Figure A-5. (a) Nitrogen Isotherm; (b) Pore Volume Distribution for BPL

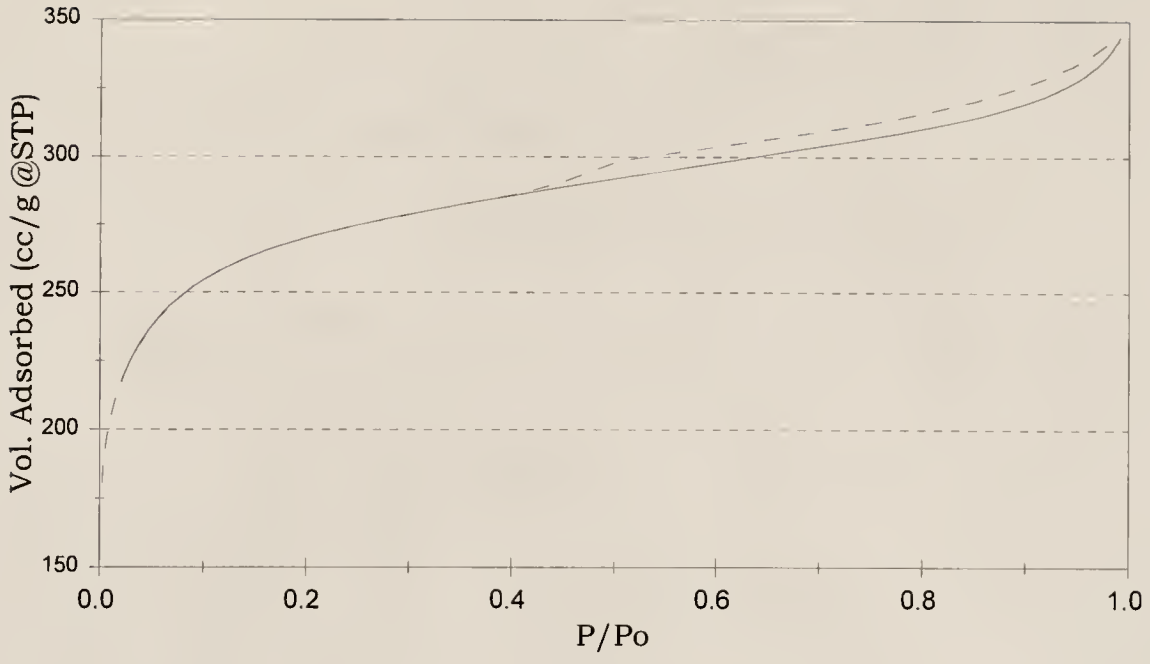

(a)

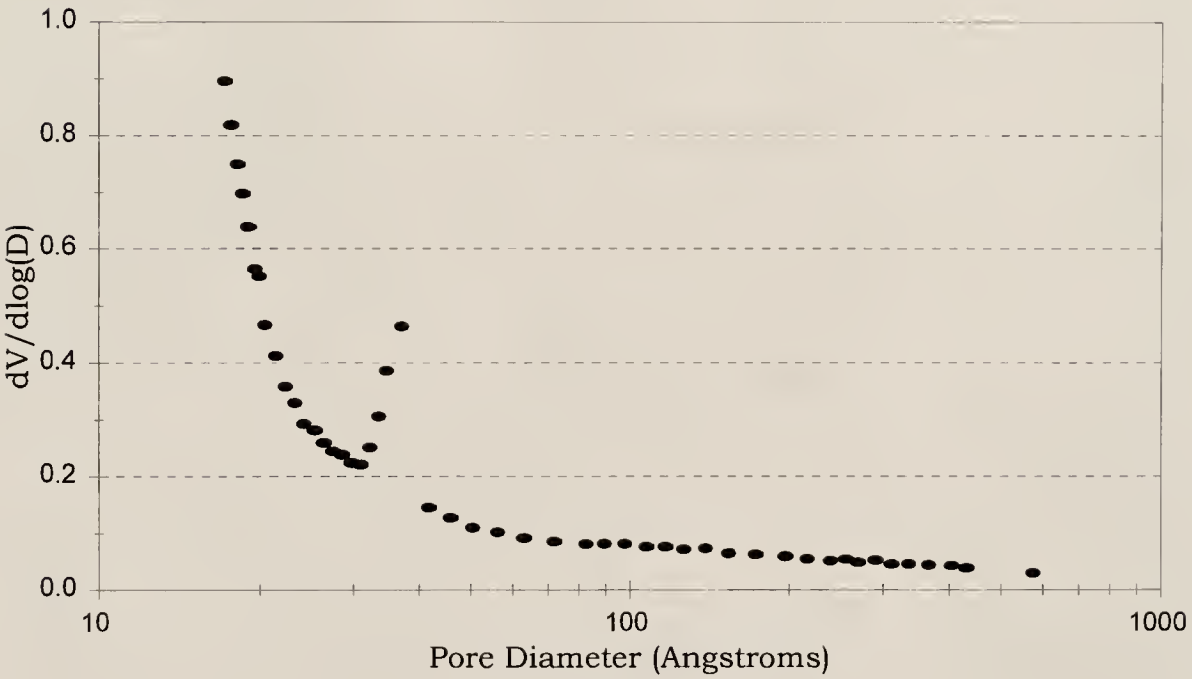

(b)

Figure A-6. (a) Nitrogen Isotherm; (b) Pore Volume Distribution for F-300

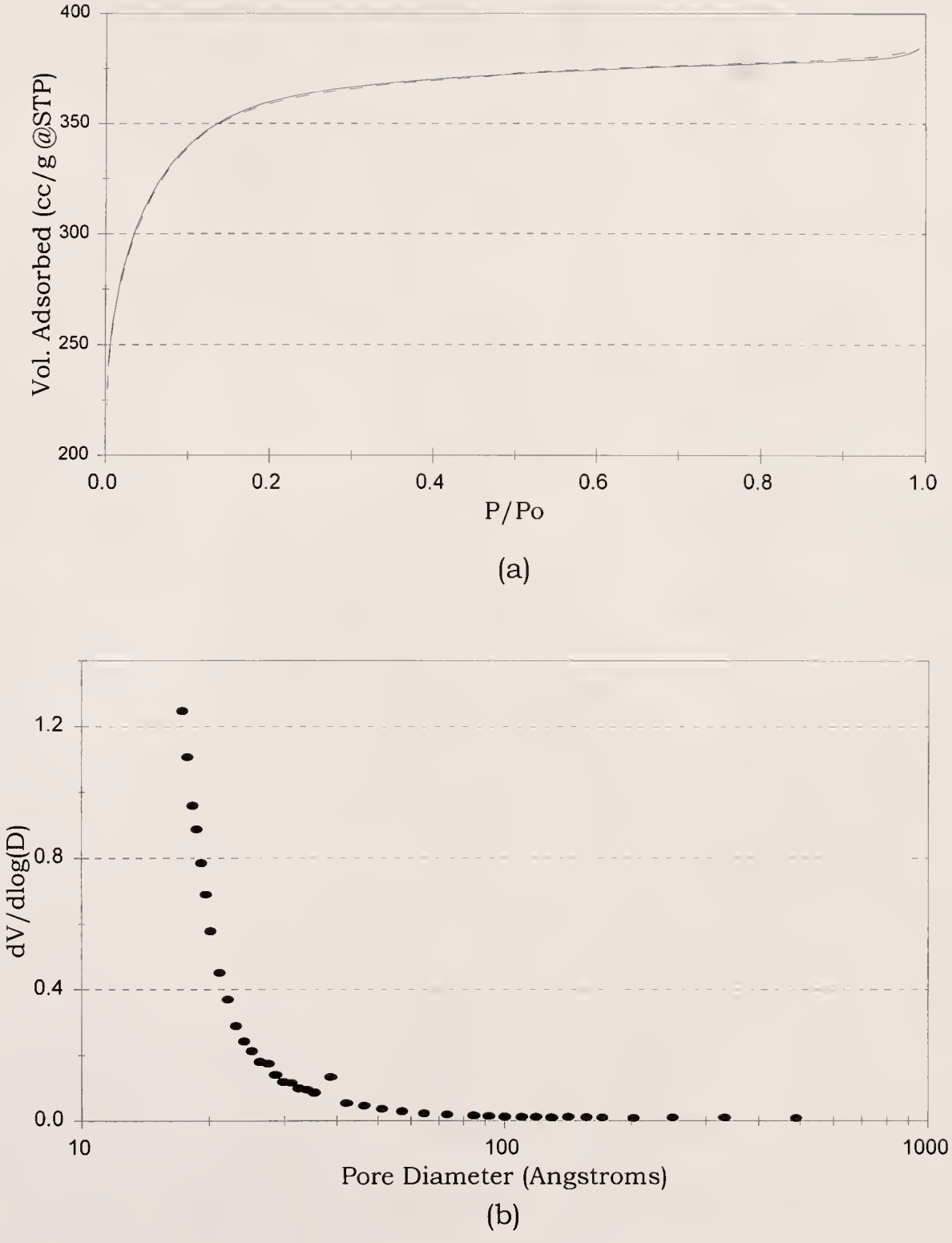

Figure A-7. (a) Nitrogen Isotherm; (b) Pore Volume Distribution for Kureha

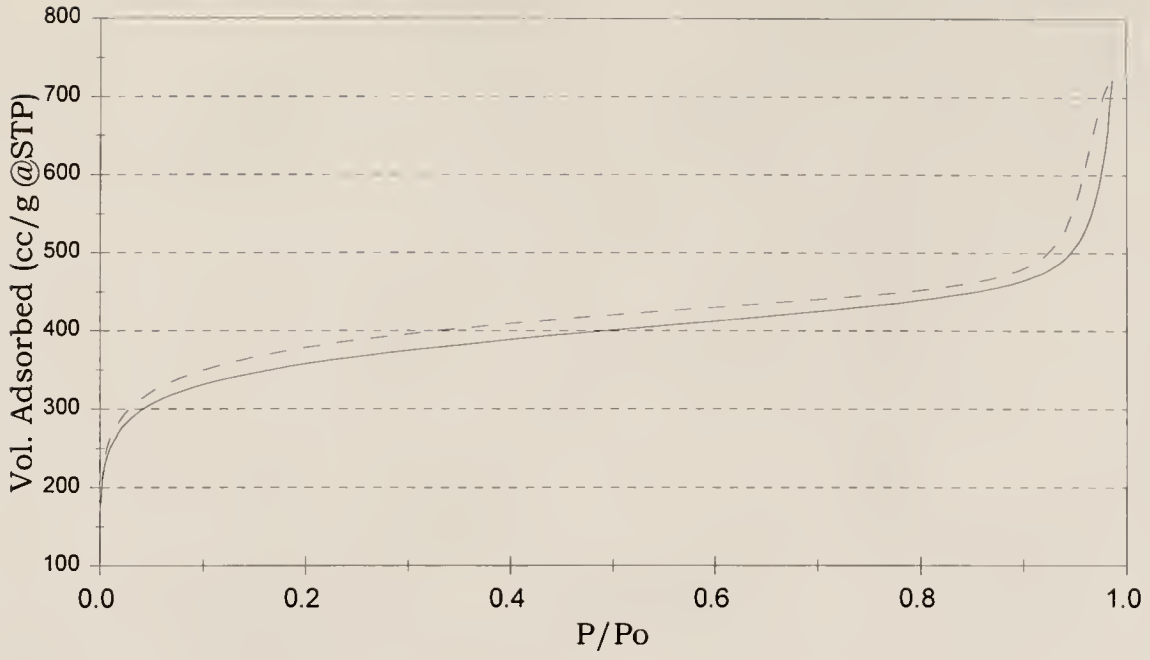

(a)

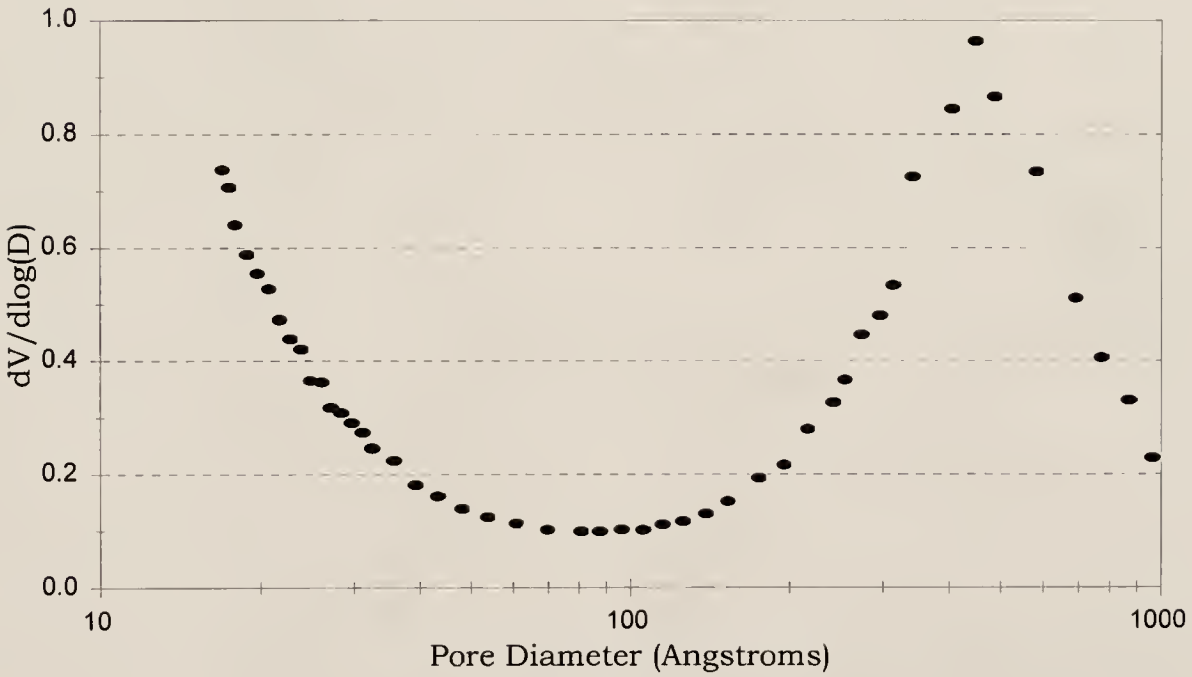

(b)

Figure A-8. (a) Nitrogen Isotherm; (b) Pore Volume Distribution for DOW 493

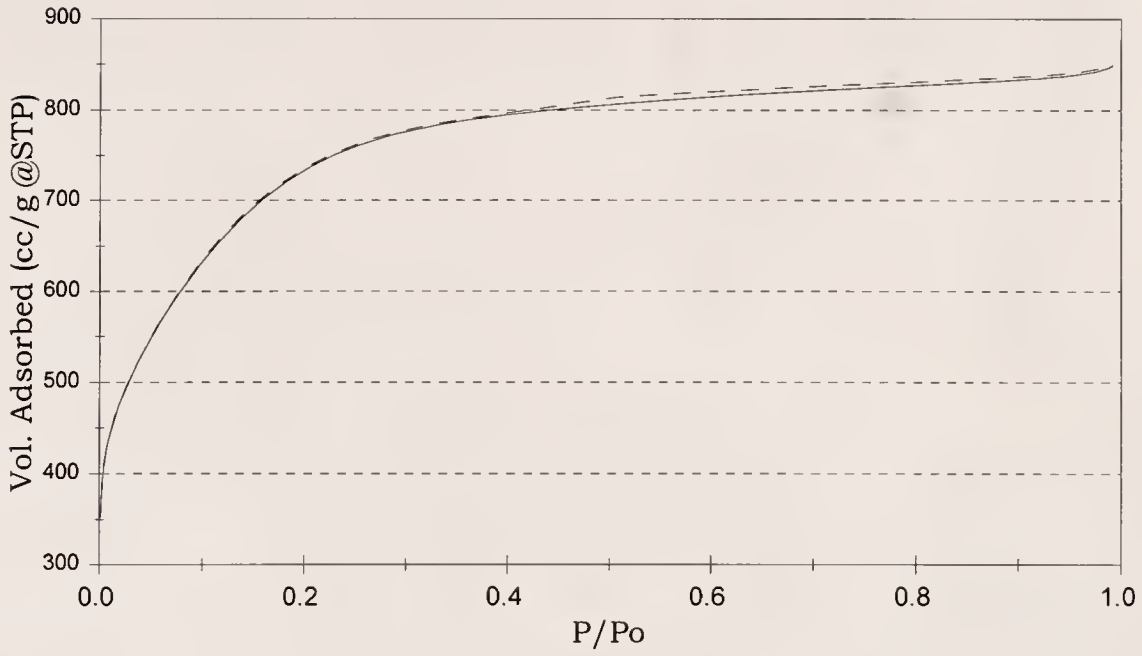

(a)

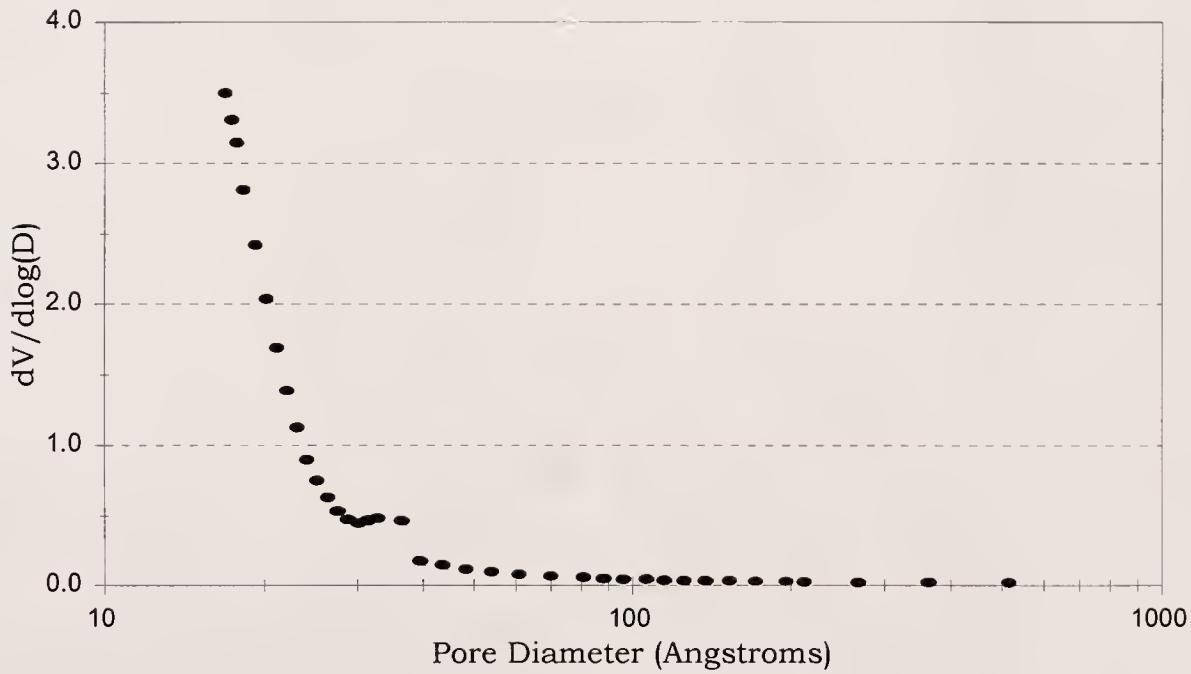

(b)

Figure A-9. (a) Nitrogen Isotherm; (b) Pore Volume Distribution for AX21

APPENDIX B

NUMERICAL ADSORPTION ISOTHERM DATA

Adsorption Isotherm Data for PPAN

N2 adsorption @ RT

P(atm)	moles ads (n/g)
6.8468E-03	3.1320E-06
3.3453E-02	1.5504E-05
6.5571E-02	2.9714E-05
1.3001E-01	5.7736E-05
1.9663E-01	8.5331E-05
2.6304E-01	1.1239E-04
3.9185E-01	1.6143E-04
5.2468E-01	2.1034E-04
6.5662E-01	2.5593E-04
7.8829E-01	2.9948E-04
9.1955E-01	3.4320E-04
9.9331E-01	3.6946E-04

N2 adsorption @ -42C

P(atm)	moles ads (n/g)
6.5025E-03	2.3650E-05
3.2427E-02	1.0856E-04
6.6246E-02	2.0452E-04
1.3211E-01	3.6045E-04
1.9302E-01	4.8177E-04
2.5922E-01	5.9749E-04
3.9559E-01	8.0043E-04
5.1991E-01	9.5534E-04
6.5178E-01	1.0981E-03
7.8903E-01	1.2319E-03
9.1539E-01	1.3412E-03
9.9269E-01	1.4039E-03

O2 adsorption @ RT

P(atm)	moles ads (n/g)
6.6618E-04	5.7806E-07
9.6037E-03	4.1082E-06
3.5142E-02	1.4134E-05
7.9720E-02	3.1369E-05
1.3144E-01	5.0838E-05
1.9888E-01	7.5646E-05
2.6667E-01	1.0001E-04
3.9502E-01	1.4409E-04
5.2496E-01	1.8683E-04
6.5671E-01	2.2947E-04
7.8770E-01	2.7049E-04
9.1768E-01	3.1035E-04
9.9346E-01	3.3373E-04

N2 adsorption @ -93C
-low pressure data

P(atm)	moles ads (n/g)
1.2745E-03	7.6109E-05
3.7786E-03	1.9042E-04
6.3086E-03	2.8182E-04
8.9624E-03	3.6289E-04
1.1956E-02	4.4093E-04
1.3998E-02	4.9075E-04
1.6447E-02	5.4541E-04
2.0802E-02	6.3173E-04
2.3524E-02	6.8238E-04
2.6382E-02	7.2983E-04
2.8492E-02	7.6510E-04
3.1622E-02	8.1234E-04

N2 adsorption @ -93C

P(atm)	moles ads (n/g)
6.3568E-03	2.7627E-04
3.1670E-02	7.9719E-04
6.4944E-02	1.1776E-03
1.2585E-01	1.6187E-03
1.9641E-01	1.9668E-03
2.5751E-01	2.1972E-03
3.9245E-01	2.5821E-03
5.2439E-01	2.8630E-03
6.5987E-01	3.0944E-03
7.8793E-01	3.2771E-03
9.2035E-01	3.4397E-03
9.9221E-01	3.5181E-03

H2 adsorption @ RT

P(atm)	moles ads (n/g)
7.6145E-04	0.0000E+00
6.1830E-03	2.6786E-07
1.3065E-02	6.5179E-07
3.5054E-02	1.8750E-06
7.0754E-02	3.8527E-06
1.3758E-01	7.5268E-06
2.0830E-01	1.1339E-05
2.7149E-01	1.4634E-05
4.0399E-01	2.1308E-05
5.3267E-01	2.7750E-05
6.6629E-01	3.4656E-05
7.9888E-01	4.1469E-05
9.3678E-01	4.7496E-05
1.0012E+00	4.9924E-05

Adsorption Isotherm Data for PPAN

CO adsorption @ RT

P(atm)	moles ads (n/g)
1.3555E-03	8.0753E-07
3.8793E-03	2.5163E-06
6.5270E-03	4.3098E-06
9.2488E-03	6.3576E-06
1.2039E-02	8.1333E-06
1.4761E-02	1.0177E-05
1.7278E-02	1.1640E-05
2.1089E-02	1.4228E-05
2.3879E-02	1.5655E-05
2.6328E-02	1.7400E-05
2.9118E-02	1.9176E-05
3.2929E-02	2.1759E-05
4.5721E-02	3.0352E-05
6.5523E-02	4.2732E-05
9.8049E-02	6.3282E-05
1.3119E-01	8.3885E-05
1.9576E-01	1.2166E-04
2.6224E-01	1.5882E-04
3.9187E-01	2.2659E-04
5.2477E-01	2.9184E-04
6.5698E-01	3.5211E-04
7.8844E-01	4.0843E-04
9.2005E-01	4.6213E-04
9.9340E-01	4.9043E-04

CO adsorption @ -42C

P(atm)	moles ads (n/g)
1.3195E-03	1.0195E-05
3.9501E-03	3.0534E-05
6.6420E-03	5.0241E-05
9.8401E-03	7.2531E-05
1.1882E-02	8.5522E-05
1.4263E-02	1.0102E-04
1.7597E-02	1.2231E-04
2.0728E-02	1.4077E-04
2.3449E-02	1.5704E-04
2.6103E-02	1.7193E-04
2.8621E-02	1.8573E-04
3.3248E-02	2.1114E-04
4.6177E-02	2.7610E-04
6.6114E-02	3.6429E-04
9.8776E-02	4.9040E-04
1.3164E-01	5.9991E-04
1.9758E-01	7.8506E-04
2.5828E-01	9.2732E-04
3.9444E-01	1.1893E-03
5.2590E-01	1.3922E-03
6.5240E-01	1.5572E-03
7.8863E-01	1.7130E-03
9.2084E-01	1.8466E-03
9.9249E-01	1.9127E-03

CO adsorption @ -93C

P(atm)	moles ads (n/g)
1.2997E-03	1.9083E-04
3.8787E-03	4.1426E-04
6.4834E-03	5.7177E-04
9.2053E-03	7.0008E-04
1.1791E-02	8.0459E-04
1.4309E-02	8.9285E-04
1.6894E-02	9.7277E-04
2.0841E-02	1.0829E-03
2.3767E-02	1.1553E-03
2.6285E-02	1.2121E-03
2.8462E-02	1.2587E-03
3.3021E-02	1.3487E-03
4.6563E-02	1.5716E-03
6.6228E-02	1.8228E-03
9.7937E-02	2.1280E-03
1.3006E-01	2.3651E-03
1.9592E-01	2.7289E-03
2.6125E-01	2.9988E-03
3.9196E-01	3.3965E-03
5.2363E-01	3.6898E-03
6.5966E-01	3.9278E-03
7.8765E-01	4.1115E-03
9.2021E-01	4.2723E-03
9.9186E-01	4.3498E-03

CH4 adsorption @ RT

P(atm)	moles ads (n/g)
4.4678E-03	1.1520E-05
1.8134E-02	4.4740E-05
3.7963E-02	9.1070E-05
8.2589E-02	1.8240E-04
1.7201E-01	3.3430E-04
3.2037E-01	5.4160E-04
5.8265E-01	8.2010E-04

CO2 adsorption @ RT

P(atm)	moles ads (n/g)
6.9684E-04	1.5646E-05
8.4641E-03	1.1995E-04
1.6048E-02	2.1368E-04
3.4712E-02	4.0392E-04
6.7797E-02	6.5267E-04
1.3254E-01	1.0002E-03
2.0332E-01	1.2810E-03
2.6291E-01	1.4745E-03
3.9691E-01	1.8334E-03
5.3179E-01	2.1270E-03
6.6078E-01	2.3630E-03
7.9054E-01	2.5700E-03
9.1899E-01	2.7569E-03
9.9237E-01	2.8599E-03

Adsorption Isotherm Data for Ambersorb 572 (lot#2125)

N2 adsorption @ RT

P(atm)	moles ads (n/g)
6.9539E-04	2.7215E-07
6.8162E-03	3.6272E-06
1.3144E-02	7.4061E-06
3.1993E-02	1.7257E-05
6.4383E-02	3.4782E-05
1.2869E-01	6.7663E-05
1.9544E-01	1.0046E-04
2.6151E-01	1.3227E-04
3.8876E-01	1.9069E-04
5.2261E-01	2.4867E-04
6.5461E-01	3.0357E-04
7.8642E-01	3.5554E-04
9.1788E-01	4.0650E-04
9.9342E-01	4.3570E-04

N2 adsorption @ 0C

P(atm)	moles ads (n/g)
6.6692E-03	6.1301E-06
3.1506E-02	2.8812E-05
6.4236E-02	5.7553E-05
1.2704E-01	1.1048E-04
1.9475E-01	1.6449E-04
2.6137E-01	2.1485E-04
3.9487E-01	3.1036E-04
5.2280E-01	3.9553E-04
6.5481E-01	4.7765E-04
7.8627E-01	5.5481E-04
9.1808E-01	6.2803E-04
9.9313E-01	6.6855E-04

N2 adsorption @ -42C

P(atm)	moles ads (n/g)
6.5405E-03	2.6564E-05
3.2874E-02	1.2248E-04
6.6625E-02	2.2958E-04
1.3195E-01	4.0504E-04
1.9687E-01	5.5408E-04
2.5886E-01	6.7924E-04
3.9474E-01	9.1756E-04
5.2648E-01	1.1139E-03
6.5148E-01	1.2778E-03
7.8859E-01	1.4404E-03
9.2094E-01	1.5825E-03
9.9232E-01	1.6538E-03

CH4 adsorption @ RT

P(atm)	moles ads (n/g)
8.5277E-03	2.3942E-05
3.1356E-02	8.4482E-05
6.7286E-02	1.7313E-04
1.3021E-01	3.1565E-04
1.9995E-01	4.4072E-04
2.6638E-01	5.2380E-04
3.9146E-01	7.3104E-04
5.2247E-01	9.1391E-04
6.5718E-01	1.0634E-03
7.9004E-01	1.1700E-03
9.2158E-01	1.2503E-03
9.9104E-01	1.2808E-03

N2 adsorption @ -93C
-low pressure data

P(atm)	moles ads (n/g)
1.2678E-03	7.7519E-05
3.7826E-03	1.9525E-04
6.3221E-03	2.9066E-04
9.0447E-03	3.7824E-04
1.1630E-02	4.5325E-04
1.4556E-02	5.2728E-04
1.6258E-02	5.6778E-04
2.1225E-02	6.7515E-04
2.3198E-02	7.1536E-04
2.5716E-02	7.6339E-04
2.7893E-02	8.0289E-04
3.2725E-02	8.8485E-04

N2 adsorption @ -93C

P(atm)	moles ads (n/g)
6.3371E-03	2.8399E-04
3.1718E-02	8.4942E-04
6.2951E-02	1.2648E-03
1.2705E-01	1.8251E-03
1.9319E-01	2.2311E-03
2.6239E-01	2.5648E-03
3.9229E-01	3.0478E-03
5.2274E-01	3.4238E-03
6.5346E-01	3.7316E-03
7.8703E-01	3.9981E-03
9.1965E-01	4.2277E-03
9.9096E-01	4.3385E-03

Adsorption Isotherm Data for Ambersorb 572 (lot#2125)

H2 adsorption @ RT

P(atm)	moles ads (n/g)
7.5329E-04	0.0000E+00
6.9288E-03	2.0523E-07
1.5208E-02	5.3092E-07
2.7162E-02	1.0038E-06
5.9906E-02	2.3200E-06
1.2699E-01	5.1396E-06
1.9865E-01	8.3876E-06
2.6386E-01	1.1430E-05
3.9297E-01	1.7436E-05
5.2603E-01	2.3927E-05
6.5841E-01	3.0619E-05
7.8899E-01	3.7254E-05
9.1823E-01	4.4294E-05
9.9374E-01	4.8844E-05

O2 adsorption @ RT

P(atm)	moles ads (n/g)
6.9816E-04	2.4092E-07
7.3101E-03	3.3506E-06
2.4413E-02	1.1363E-05
4.8831E-02	2.2749E-05
9.3652E-02	4.3393E-05
1.3989E-01	6.4277E-05
1.9836E-01	9.0278E-05
2.7427E-01	1.2357E-04
3.9795E-01	1.7626E-04
5.2840E-01	2.2981E-04
6.5751E-01	2.8053E-04
7.8835E-01	3.2987E-04
9.1827E-01	3.7850E-04
9.9385E-01	4.0702E-04

CO2 adsorption @ RT

P(atm)	moles ads (n/g)
7.2132E-04	6.7904E-06
6.3079E-03	6.0288E-05
1.3929E-02	1.2600E-04
3.2506E-02	2.6253E-04
6.5848E-02	4.6874E-04
1.3267E-01	7.9651E-04
1.9500E-01	1.0512E-03
2.5828E-01	1.2736E-03
3.9560E-01	1.6745E-03
5.2373E-01	1.9944E-03
6.5485E-01	2.2863E-03
7.9102E-01	2.5411E-03
9.1670E-01	2.7389E-03
9.8951E-01	2.8497E-03

CO2 adsorption @ 0C

P(atm)	moles ads (n/g)
1.3099E-03	3.0642E-05
3.8984E-03	8.5067E-05
6.5664E-03	1.3516E-04
9.1522E-03	1.7912E-04
1.1806E-02	2.2202E-04
1.4596E-02	2.6479E-04
1.7454E-02	3.0606E-04
2.1128E-02	3.5656E-04
2.3578E-02	3.8890E-04
2.6028E-02	4.1948E-04
2.9090E-02	4.5691E-04
3.3173E-02	5.0593E-04
4.6782E-02	6.5289E-04
6.6311E-02	8.3829E-04
9.8633E-02	1.1018E-03
1.3123E-01	1.3310E-03
1.9730E-01	1.7250E-03
2.6262E-01	2.0535E-03
3.9368E-01	2.6030E-03
5.2481E-01	3.0588E-03
6.5457E-01	3.4476E-03
7.8794E-01	3.7994E-03
9.1988E-01	4.1112E-03
9.9072E-01	4.2657E-03

CO2 adsorption @ 40C

P(atm)	moles ads (n/g)
7.2947E-04	3.8012E-06
7.2591E-03	3.3055E-05
1.4965E-02	6.7034E-05
3.5380E-02	1.5435E-04
6.9767E-02	2.8809E-04
1.3345E-01	4.9955E-04
1.9375E-01	6.7249E-04
2.6023E-01	8.4178E-04
3.9875E-01	1.1451E-03
5.2853E-01	1.3875E-03
6.5503E-01	1.5974E-03
7.9060E-01	1.8041E-03
9.2384E-01	1.9925E-03
9.9225E-01	2.0857E-03

CO2 adsorption @ 75C

P(atm)	moles ads (n/g)
6.3296E-03	1.1792E-05
3.3344E-02	6.0534E-05
6.3693E-02	1.1130E-04
1.3262E-01	2.1477E-04
1.9366E-01	3.0049E-04
2.5953E-01	3.8836E-04
3.9651E-01	5.5206E-04
5.3192E-01	7.0058E-04
6.5447E-01	8.2128E-04
7.9560E-01	9.5845E-04
9.1801E-01	1.0644E-03
9.9170E-01	1.1265E-03

Adsorption Isotherm Data for Ambersorb 572 (lot#2125)

CO adsorption @ RT		CO adsorption @ -42C		CO adsorption @ -93C	
P(atm)	moles ads (n/g)	P(atm)	moles ads (n/g)	P(atm)	moles ads (n/g)
1.3296E-03	9.1461E-07	1.3289E-03	9.8867E-06	1.2942E-03	1.6066E-04
4.0120E-03	2.8911E-06	3.9304E-03	2.9165E-05	3.8841E-03	3.6690E-04
6.5154E-03	4.7381E-06	6.6433E-03	4.8345E-05	6.4671E-03	5.1764E-04
9.3733E-03	6.6075E-06	9.8414E-03	6.9889E-05	9.1209E-03	6.4041E-04
1.1891E-02	8.3921E-06	1.1815E-02	8.2792E-05	1.1707E-02	7.4710E-04
1.4749E-02	1.0480E-05	1.4264E-02	9.8969E-05	1.4497E-02	8.4669E-04
1.7335E-02	1.2104E-05	1.7463E-02	1.1852E-04	1.7014E-02	9.2869E-04
2.1009E-02	1.5138E-05	2.1409E-02	1.4190E-04	2.1097E-02	1.0474E-03
2.3935E-02	1.7070E-05	2.3791E-02	1.5605E-04	2.3479E-02	1.1105E-03
2.6521E-02	1.8694E-05	2.6309E-02	1.7026E-04	2.6200E-02	1.1794E-03
2.9107E-02	2.0541E-05	2.8554E-02	1.8260E-04	2.9058E-02	1.2455E-03
3.2985E-02	2.3088E-05	3.3113E-02	2.0753E-04	3.2869E-02	1.3268E-03
4.5506E-02	3.1949E-05	4.5634E-02	2.7083E-04	4.5526E-02	1.5614E-03
6.5171E-02	4.5811E-05	6.6048E-02	3.6424E-04	6.6824E-02	1.8749E-03
9.7697E-02	6.7949E-05	9.8574E-02	4.9688E-04	9.7989E-02	2.2279E-03
1.3084E-01	9.0662E-05	1.3178E-01	6.1520E-04	1.2936E-01	2.5104E-03
1.9507E-01	1.3221E-04	1.9738E-01	8.1629E-04	1.9604E-01	2.9753E-03
2.6189E-01	1.7383E-04	2.6297E-01	9.8781E-04	2.6076E-01	3.3239E-03
3.9064E-01	2.5031E-04	3.9471E-01	1.2756E-03	3.9140E-01	3.8572E-03
5.2414E-01	3.2539E-04	5.2549E-01	1.5127E-03	5.2239E-01	4.2592E-03
6.5636E-01	3.9473E-04	6.6111E-01	1.7239E-03	6.5672E-01	4.5890E-03
7.8823E-01	4.6002E-04	7.8815E-01	1.8982E-03	7.8648E-01	4.8536E-03
9.1949E-01	5.2409E-04	9.2030E-01	2.0612E-03	9.1917E-01	5.0848E-03
9.9366E-01	5.5869E-04	9.9195E-01	2.1433E-03	9.9041E-01	5.1958E-03

Adsorption Isotherm Data for Ambersorb 563 (lot#91/3298)

N2 adsorption @ RT		H2 adsorption @ RT		CH4 adsorption @ RT	
P(atm)	moles ads (n/g)	P(atm)	moles ads (n/g)	P(atm)	moles ads (n/g)
6.7849E-03	2.0523E-06	7.4987E-04	0.0000E+00	6.2882E-03	1.2086E-05
3.2438E-02	9.7038E-06	7.9096E-03	1.6954E-07	3.3234E-02	6.1283E-05
6.4692E-02	1.9733E-05	1.8720E-02	4.4169E-07	6.3107E-02	1.1107E-04
1.2872E-01	3.8681E-05	3.3533E-02	8.1645E-07	1.3211E-01	2.1297E-04
1.9554E-01	5.8133E-05	6.2745E-02	1.5660E-06	1.9437E-01	2.9271E-04
2.6141E-01	7.6867E-05	1.3523E-01	3.4844E-06	2.6024E-01	3.6885E-04
3.8846E-01	1.1219E-04	1.9783E-01	5.1753E-06	3.9572E-01	5.0415E-04
5.2257E-01	1.4776E-04	2.6140E-01	6.8841E-06	5.2133E-01	6.1060E-04
6.5431E-01	1.8179E-04	3.9586E-01	1.0471E-05	6.5375E-01	7.0806E-04
7.8618E-01	2.1407E-04	5.2517E-01	1.3795E-05	7.8453E-01	7.9595E-04
9.1765E-01	2.4593E-04	6.6224E-01	1.7315E-05	9.1668E-01	8.7562E-04
9.9338E-01	2.6414E-04	7.8814E-01	2.0371E-05	9.9282E-01	9.1824E-04
		9.1506E-01	2.3829E-05		
		9.9360E-01	2.6582E-05		

Adsorption Isotherm Data for NORIT 211

N2 adsorption @ RT		CO2 adsorption @ RT		CH4 adsorption @ RT	
P(atm)	moles ads (n/g)	P(atm)	moles ads (n/g)	P(atm)	moles ads (n/g)
6.8182E-03	3.2167E-06	6.3201E-03	6.5303E-05	6.3405E-03	1.4826E-05
3.3084E-02	1.5191E-05	3.2585E-02	2.6140E-04	3.3627E-02	7.3860E-05
6.5134E-02	2.9722E-05	6.3546E-02	4.3459E-04	6.3771E-02	1.3278E-04
1.2957E-01	5.7201E-05	1.2873E-01	7.1243E-04	1.3223E-01	2.5026E-04
1.9565E-01	8.4536E-05	1.9147E-01	9.1986E-04	1.9490E-01	3.4240E-04
2.6220E-01	1.1130E-04	2.5877E-01	1.1076E-03	2.6070E-01	4.3081E-04
3.9080E-01	1.6107E-04	3.9493E-01	1.4197E-03	3.9631E-01	5.8622E-04
5.2431E-01	2.0992E-04	5.2524E-01	1.6640E-03	5.2295E-01	7.0929E-04
6.5618E-01	2.5444E-04	6.5398E-01	1.8679E-03	6.5475E-01	8.2542E-04
7.8771E-01	2.9835E-04	7.8368E-01	2.0517E-03	7.8581E-01	9.2868E-04
9.1959E-01	3.3897E-04	9.1576E-01	2.2145E-03	9.1836E-01	1.0186E-03
9.9308E-01	3.6257E-04	9.9088E-01	2.3053E-03	9.9178E-01	1.0697E-03

Adsorption Isotherm Data for Calgon BPL 4x10

N2 adsorption @ RT		CH4 adsorption @ RT	
P(atm)	moles ads (n/g)	P(atm)	moles ads (n/g)
6.8420E-03	2.3958E-06	6.4038E-03	9.8644E-06
3.3040E-02	1.1970E-05	3.3758E-02	4.9161E-05
6.5566E-02	2.3222E-05	6.3699E-02	8.8721E-05
1.3028E-01	4.4909E-05	1.3188E-01	1.7070E-04
1.9676E-01	6.7186E-05	1.9462E-01	2.3845E-04
2.6249E-01	8.7999E-05	2.6062E-01	3.0336E-04
3.9157E-01	1.2848E-04	3.9481E-01	4.2303E-04
5.2460E-01	1.6822E-04	5.2158E-01	5.2464E-04
6.5614E-01	2.0685E-04	6.5379E-01	6.2136E-04
7.8808E-01	2.4382E-04	7.8505E-01	7.1036E-04
9.1975E-01	2.7900E-04	9.1666E-01	7.9615E-04
9.9317E-01	2.9972E-04	9.9328E-01	8.4474E-04

Adsorption Isotherm Data for Calgon F300 8x30

N2 adsorption @ RT		O2 adsorption @ RT	
P(atm)	moles ads (n/g)	P(atm)	moles ads (n/g)
6.728E-03	2.592E-06	6.871E-03	2.454E-06
3.163E-02	1.201E-05	3.450E-02	1.189E-05
6.423E-02	2.465E-05	6.600E-02	2.150E-05
1.272E-01	4.760E-05	1.315E-01	4.183E-05
1.946E-01	7.172E-05	1.975E-01	6.206E-05
2.608E-01	9.436E-05	2.635E-01	8.173E-05
3.949E-01	1.394E-04	3.946E-01	1.207E-04
5.220E-01	1.796E-04	5.252E-01	1.587E-04
6.523E-01	2.190E-04	6.581E-01	1.954E-04
7.844E-01	2.579E-04	7.896E-01	2.313E-04
9.161E-01	2.958E-04	9.215E-01	2.641E-04
9.934E-01	3.178E-04	1.000E+00	2.826E-04

Adsorption Isotherm Data for Kureha BAC-SP

N2 adsorption @ RT		CH4 adsorption @ RT	
P(atm)	moles ads (n/g)	P(atm)	moles ads (n/g)
6.7475E-03	2.4627E-06	6.3549E-03	1.0453E-05
3.1856E-02	1.1921E-05	3.3437E-02	5.3743E-05
6.4450E-02	2.3829E-05	6.6439E-02	1.0350E-04
1.2773E-01	4.6011E-05	1.3224E-01	1.9468E-04
1.9483E-01	6.9367E-05	1.9389E-01	2.7283E-04
2.6097E-01	9.2063E-05	2.5983E-01	3.5079E-04
3.9529E-01	1.3609E-04	3.9544E-01	4.9734E-04
5.2220E-01	1.7589E-04	5.2133E-01	6.2028E-04
6.5359E-01	2.1628E-04	6.5286E-01	7.3874E-04
7.8492E-01	2.5587E-04	7.8419E-01	8.4950E-04
9.1673E-01	2.9362E-04	9.1661E-01	9.5238E-04
9.9341E-01	3.1557E-04	9.9268E-01	1.0081E-03

Adsorption Isotherm Data for DOW XUS-43493.01

N2 adsorption @ RT		O2 adsorption @ RT		CH4 adsorption @ RT	
P(atm)	moles ads (n/g)	P(atm)	moles ads (n/g)	P(atm)	moles ads (n/g)
6.9224E-03	8.9230E-07	6.8937E-03	1.0574E-06	8.6991E-03	4.1838E-06
3.5298E-02	4.7961E-06	3.4929E-02	5.3583E-06	3.2405E-02	1.5501E-05
6.9933E-02	9.3290E-06	6.6026E-02	9.8242E-06	6.5204E-02	3.0677E-05
1.3914E-01	1.8533E-05	1.3176E-01	1.9323E-05	1.2857E-01	5.7300E-05
2.0507E-01	2.7063E-05	1.9756E-01	2.9040E-05	1.9461E-01	8.2280E-05
2.7080E-01	3.5656E-05	2.6343E-01	3.8364E-05	2.5900E-01	1.2429E-04
4.0309E-01	5.3534E-05	3.9462E-01	5.7134E-05	3.8292E-01	1.8975E-04
5.3476E-01	7.0407E-05	5.2649E-01	7.5564E-05	5.1984E-01	2.5426E-04
6.6615E-01	8.7784E-05	6.5789E-01	9.4289E-05	6.5414E-01	3.1822E-04
7.9769E-01	1.0476E-04	7.8956E-01	1.1301E-04	7.8791E-01	3.8371E-04
9.2929E-01	1.2149E-04	9.2116E-01	1.3103E-04	9.2733E-01	4.4507E-04
1.0009E+00	1.3107E-04	9.9349E-01	1.4135E-04	9.9185E-01	4.9485E-04

Adsorption Isotherm Data for Anderson AX21

N2 adsorption @ RT		O2 adsorption @ RT		CH4 adsorption @ RT	
P(atm)	moles ads (n/g)	P(atm)	moles ads (n/g)	P(atm)	moles ads (n/g)
6.8814E-03	2.7929E-06	6.7461E-03	8.3073E-06	1.2679E-02	1.9151E-05
3.4168E-02	1.3978E-05	3.4033E-02	1.8975E-05	3.0903E-02	4.6766E-05
6.5809E-02	2.7371E-05	6.8396E-02	3.2426E-05	7.5311E-02	1.1270E-04
1.3093E-01	5.4096E-05	1.3107E-01	5.6505E-05	1.2445E-01	1.8192E-04
1.9727E-01	8.1293E-05	1.9721E-01	8.1226E-05	1.9143E-01	2.7184E-04
2.6294E-01	1.0771E-04	2.6280E-01	1.0585E-04	2.5620E-01	3.6287E-04
3.9338E-01	1.5983E-04	3.9318E-01	1.5344E-04	3.9072E-01	5.2859E-04
5.2560E-01	2.1244E-04	5.2546E-01	2.0112E-04	5.2222E-01	6.7173E-04
6.5727E-01	2.6348E-04	6.5713E-01	2.4821E-04	6.5871E-01	8.3288E-04
7.8887E-01	3.1445E-04	7.8866E-01	2.9494E-04	7.9677E-01	9.7472E-04
9.1958E-01	3.6377E-04	9.2026E-01	3.4147E-04	9.1111E-01	1.0917E-03
9.9341E-01	3.9149E-04	9.9355E-01	3.6837E-04	9.8702E-01	1.1675E-03

APPENDIX C
FORTRAN PROGRAM FOR SIMPLEX DATA ANALYSIS

```
      CHARACTER*60 INFILE, OUTFILE
   DIMENSION B(10,250),H(250),P(18),D(18),DIF(250),IFIX(250)
   DIMENSION HH(250),SD(18), BB(6)
   AVGC=0.00
   AVGE=0.00
   WRITE (6,1)
 1 FORMAT (5X,'Name of Data File? ')
   READ (5,'(A)') INFILE
   OPEN (8,FILE=INFILE,STATUS='OLD')
   READ (8,*) NC,GC
   DO 6 I=1,NC
   READ (8,*) B(1,I),H(I)
 6 CONTINUE
   READ (8,*) NE,GE
      N=NC+NE
   DO 7 I=NC+1,N
   READ (8,*) B(1,I),H(I)
 7 CONTINUE
   READ (8,*) NS, EP, KX
   READ (8,*) (P(I),IFIX(I),I=1,3*NS)
   CLOSE(8)
   DO 5 I=NC+1,N
   AVGE=AVGE+H(I)/NE
 5 CONTINUE
   DO 10 I=1,NC
   AVGC=AVGC+H(I)/NC
   HH(I)=H(I)/GC
10 CONTINUE
   IF (AVGE.EQ.0) AVGE=1.00
   B(10,250)=AVGC/AVGE
   IF (AVGE.EQ.0.OR.AVGC.EQ.0) B(10,250)=1.00
   DO 15 I=NC+1,N
   HH(I)=H(I)*B(10,250)/GE
15 CONTINUE
   DO 20 I=1,3*NS
   SD(I)=0.000
   D(I)=P(I)*0.1
   IF (IFIX(I).EQ.1) D(I)=0.000
20 CONTINUE
   WRITE (6,224)
224 FORMAT(//5X,'WORKING')
```

```
      CALL SIMPLEX(EP,3*NS,NC,N,KX,P,D,HH,B,NS)
      DEVN=0.00
      DO 30 I=1,N
      G=GC
      IF (I.GT.NC) G=GE
      DIF(I)=H(I)-G*CAL(I,P,B,NC,NS)
   30 CONTINUE
      DO 40 I=1,N
      DEVN=DIF(I)**2
      DO 40 IS=1,NS
      L1=3*IS-2
      L2=3*IS-1
      L3=3*IS
      B1=P(L2)*B(1,I)
      IF (I.GT.NC) GO TO 50
      SD(L1)=SD(L1)+(((1.0+B1)/(P(L3)*B1))**2)*DEVN
      SD(L2)=SD(L2)+((((1.0+B1)**2)/(P(L1)*P(L3)*B(1,I)))**2)*DEVN
      SD(L3)=SD(L3)+(((1.0+B1)/(P(L1)*B1))**2)*DEVN
      GO TO 40
   50 SD(L1)=SD(L1)+(((1.0+B1)/B1)**2)*DEVN
      SD(L2)=SD(L2)+((((1.0+B1)**2)/(P(L1)*B(1,I)))**2)*DEVN
   40 CONTINUE
      DO 60 IS=1,NS
      SD(3*IS-2) = SQRT(SD(3*IS-2)/N)
      SD(3*IS-1) = SQRT(SD(3*IS-1)/N)
      IF (NC.GT.0) SD(3*IS) = SQRT(SD(3*IS)/NC)
   60 CONTINUE
      DO 65 I=1,3*NS
      IF (IFIX(I).EQ.1) SD(I)=-1.00
   65 CONTINUE
      WRITE (6,201)
  201 FORMAT (/5X,'Fitting Routinue Completed',
     */5X,'Name of Output File? ')
      READ (5,'(A)') OUTFILE
      OPEN (7,FILE=OUTFILE)
      IF (NC.GT.0) WRITE (7,200)
  200 FORMAT (//3X,'#',6X,'BSOL',11X,'HEXP',11X,'HCAL',11X,
     *'ERR',11X,'PER',/)
      DO 70 I=1,NC
      HCAL1=GC*CAL(I,P,B,NC,NS)
      PER1=ABS(100.0*DIF(I)/H(I))
      WRITE (7,210) I,B(1,I),H(I),HCAL1,DIF(I),PER1
  210 FORMAT (2X,I3,3X,E12.6,3(3X,E12.6),3X,F5.2)
   70 CONTINUE
      IF (NE.GT.0) WRITE (7,202)
  202 FORMAT (//3X,'#',6X,'BSOL',11X,'BPDO',11X,'BCAL',11X,'ERR',11X,
     *'PER',/)
      DO 71 I=NC+1,N
      HCAL2=GE*CAL(I,P,B,NC,NS)
      PER2=ABS(100.0*DIF(I)/H(I))
```

```
      WRITE (7,211) I-NC,B(1,I),H(I),HCAL2,DIF(I),PER2
  211 FORMAT (2X,I3,3X,E12.6,3(3X,E12.6),3X,F5.2)
   71 CONTINUE
      DO 72 IS=1,NS
      WRITE (7,220) (IS,P(I+(IS-1)*3),SD(I+(IS-1)*3),I=1,3)
  220 FORMAT (//3X,'n',I1,' is ',E11.5,' with a stand. dev. of ',
     *E11.5,' in mole/g',/3X,'K',I1,' is ',E11.5,
     *' with a stand. dev. of ',E11.5,/3X,'H',I1,' is ',E11.5,
     *' with a stand. dev. of ',E11.5,' in cal/mole')
   72 CONTINUE
      IF (NC.GT.0) WRITE (7,222) GC
      IF (NE.GT.0) WRITE (7,223) GE
  222 FORMAT(//3X,'Grams of Solid for calorimetry data is ',E11.5)
  223 FORMAT(/3X,'Grams of Solid for equilibrium data is ',E11.5)
      CLOSE (7)
      STOP
      END
CCCCCCCCCCCCCCCCCCCCCCCCCCCCCCCCCCCCCCCCCCCCCCCCCCCCC
CCCCCCCCC
C
C
CCCCCCCCCCCCCCCCCCCCCCCCCCCCCCCCCCCCCCCCCCCCCCCCCCCCC
CCCCCCCCC
      FUNCTION FUNK(H,P,B,NC,N,NS)
      DIMENSION H(250),P(18),B(10,250)
      FUNK=0.0
      DO 10 I=1,N
      FUNCTION=0.0
      DO 15 IS=1,NS
      B1=P(3*IS-2)*P(3*IS-1)*B(1,I)/(1.0+P(3*IS-1)*B(1,I))
      IF (I.LE.NC) FUNCTION=FUNCTION + B1*P(3*IS)
      IF (I.GT.NC) FUNCTION=FUNCTION + B1*B(10,250)
   15 CONTINUE
      FUNK=FUNK+(H(I)-FUNCTION)**2
   10 CONTINUE
      FUNK=SQRT(FUNK/(N-1))
      RETURN
      END
CCCCCCCCCCCCCCCCCCCCCCCCCCCCCCCCCCCCCCCCCCCCCCCCCCCCC
CCCCCCC
C
C
CCCCCCCCCCCCCCCCCCCCCCCCCCCCCCCCCCCCCCCCCCCCCCCCCCCCC
CCCCCCCCC
      FUNCTION CAL(I,P,B,N,NS)
      DIMENSION P(18),B(10,250)
      CAL=0.0
      DO 10 IS=1,NS
      B1=P(3*IS-2)*P(3*IS-1)*B(1,I)/(1.0+P(3*IS-1)*B(1,I))
      IF (I.LE.N) B1=B1*P(3*IS)
```

```
      CAL=CAL+B1
   10 CONTINUE
      RETURN
      END
CCCCCCCCCCCCCCCCCCCCCCCCCCCCCCCCCCCCCCCCCCCCCCCCC
CCC
C
C  This subroutine is used to fit non-linear equations,
C  the subroutine uses a Simplex Routine to solve the
C  the equation.
C
C  The program the number of parameters, NP, the
C  convergence factor, EP, the variables, B, the number
C  of points, N, the maximum number of loops, KX, the
C  measured value, H, initial guesses for parameter, T,
C  and the interval for varying the parameters, D.
C  Set D equal to zero to fix parameter.
C
C  This is a sample of what the function FUNK looks like
C
C       FUNCTION FUNK(H,P,B,N)
C       DIMENSION H(250),P(10),B(10,250)
C       FUNK=0.0
C       DO 10 I=1,N
C       FUNCTION=function you wish to solve parameters for
C       FUNK=FUNK+(H(I)-FUNCTION)**2
C    10 CONTINUE
C       FUNK=SQRT(FUNK/(N-1))
C       RETURN
C       END
C
C   This function is where the function that you wish to
C   solve the parameters for will go in.
C
C   Attach this function to the main part of the program
C   that you write for input and output of your data
C
CCCCCCCCCCCCCCCCCCCCCCCCCCCCCCCCCCCCCCCCCCCCCCCCC
CCC
C
C
      SUBROUTINE SIMPLEX(EP,NP,NC,N,KX,T,D,H,B,NS)
      DIMENSION RI(18),T(18),TT(18),S(18,19)
      DIMENSION H(250),B(10,250),D(18)
      CALL PARMAT(NP,S,T,RI,D,B,H,NC,N,NS)
      NV=NP+1
      IF ((N.EQ.0).OR.(RI(1).EQ.0.0)) GO TO 110
      KI=0
   10 IF ((BR.EQ.0.0).OR.(BR.GE.EP)) GO TO 20
      EP=EP/10
```

```
   GO TO 10
20 WR=RI(1)
   BR=WR
   JW=1
   JB=1
   DO 30 I=2,NV
   IF (RI(I).GE.WR)  WR=RI(I)
   IF (RI(I).GE.WR)  JW=I
   IF (RI(I).LT.BR)  BR=RI(I)
   IF (RI(I).LT.BR)  JB=I
30 CONTINUE
   IF ((KI.GE.KX).OR.(BR.LT.EP))  GO TO 110
   IF (((WR-BR)/BR).LT.EP)  GO TO 110
   KI=KI+1
   IF (BR.NE.PR)  PR=BR
   F=1.0
   CALL VERTIX(S,T,JW,NP,F,H,B,R,NC,N,NS)
   IF (R.GT.BR)  GO TO 40
   RT=R
   DO 50 I=1,NP
   TT(I)=T(I)
50 CONTINUE
   F=2.0
   CALL VERTIX(S,T,JW,NP,F,H,B,R,NC,N,NS)
   IF (R.GT.RT) GO TO 60
90 DO 70 I=1,NP
   S(I,JW)=T(I)
70 CONTINUE
   RI(JW)=R
   GO TO 20
60 R=RT
   DO 80 I=1,NP
   T(I)=TT(I)
80 CONTINUE
   GO TO 90
40 IF (R.LE.WR)  GO TO 90
   F=-0.5
   CALL VERTIX(S,T,JW,NP,F,H,B,R,NC,N,NS)
   IF (R.LE.WR)  GO TO 90
   DO 100 I=1,NP
   DO 100 J=1,NV
   IF (J.NE.JB)  S(I,J)=(S(I,JB)+S(I,J))/2
100 CONTINUE
   GO TO 20
110 IF (KI.GE.KX) WRITE (6,120)
   IF (KI.LT.KX) WRITE (6,130)
120 FORMAT (/5X,'MAXIMUM NUMBER OF LOOPS EXCEEDED',/)
130 FORMAT (/5X,'CONVERGENCE CRITERIA REACHED',/)
   RETURN
   END
```

```
CCCCCCCCCCCCCCCCCCCCCCCCCCCCCCCCCCCCCCCCCCCCCCCCCCCC
CCC
C
C   Set up of parameter matrix
C
CCCCCCCCCCCCCCCCCCCCCCCCCCCCCCCCCCCCCCCCCCCCCCCCCCCC
CCC
      SUBROUTINE PARMAT(NP,S,T,RI,D,B,H,NC,N,NS)
      DIMENSION T(18),S(18,19),RI(18),D(18),B(10,250),H(250)
      NV=NP+1
      DO 30 I=1,NP
      DO 30 J=1,NV
      AI=0.0
      IF (I.GE.J) AI=-1.0
      S(I,J)=T(I)-D(I)*AI-D(I)/2
   30 CONTINUE
      DO 40 I=1,NV
      DO 50 J=1,NP
      T(J)=S(J,I)
   50 CONTINUE
      R=FUNK(H,T,B,NC,N,NS)
      RI(I)=R
   40 CONTINUE
      RETURN
      END
CCCCCCCCCCCCCCCCCCCCCCCCCCCCCCCCCCCCCCCCCCCCCCCCCCCC
CCCCCCCC
C
C   Find a new vertrix
C
CCCCCCCCCCCCCCCCCCCCCCCCCCCCCCCCCCCCCCCCCCCCCCCCCCCC
CCCCCCCC
      SUBROUTINE VERTIX(S,T,JW,NP,F,H,B,R,NC,N,NS)
      DIMENSION S(18,11),T(18),C(18),B(10,250),H(250)
      NV=NP+1
      DO 10 I=1,NP
      SU=0.0
      IF (F.NE.1.0) GO TO 30
      DO 20 J=1,NV
      IF (J.NE.JW) SU=SU+S(I,J)
   20 CONTINUE
      C(I)=SU/NP
   30 T(I)=C(I)*(1.0+F)-F*S(I,JW)
   10 CONTINUE
      R=FUNK(H,T,B,NC,N,NS)
      RETURN
      END
```

APPENDIX D

SAMPLE OF SIMPLEX DATA FITTING ROUTINE FOR A-572: CO ADSORPTION ISOTHERM DATA

Step (1): Employing the data reported in Appendix B, the CO adsorption data on A-572 at -42°C is fit to two processes. Initial guesses for n_i's and $K_{i,ads}$'s are made based on empirical observations and best estimates. The output from the resultant fit follows:

#	Experimental P_{equil} (atm)	Experimental moles ads. (n/g)	Theoretical moles ads. (n/g)	Error (Expt. - Theor.)	% Error
1	0.132895E-02	0.988668E-05	0.969299E-05	0.193687E-06	1.96
2	0.393039E-02	0.291648E-04	0.282594E-04	0.905398E-06	3.10
3	0.664329E-02	0.483448E-04	0.470762E-04	0.126860E-05	2.62
4	0.984145E-02	0.698894E-04	0.685903E-04	0.129909E-05	1.86
5	0.118149E-01	0.827920E-04	0.815261E-04	0.126586E-05	1.53
6	0.142645E-01	0.989694E-04	0.972427E-04	0.172674E-05	1.74
7	0.174626E-01	0.118520E-03	0.117225E-03	0.129523E-05	1.09
8	0.214093E-01	0.141898E-03	0.141102E-03	0.796281E-06	0.56
9	0.237909E-01	0.156054E-03	0.155119E-03	0.935266E-06	0.60
10	0.263087E-01	0.170264E-03	0.169636E-03	0.628192E-06	0.37
11	0.285542E-01	0.182600E-03	0.182334E-03	0.266446E-06	0.15
12	0.331133E-01	0.207527E-03	0.207433E-03	0.937289E-07	0.05
13	0.456337E-01	0.270826E-03	0.272194E-03	-0.136771E-05	0.51
14	0.660475E-01	0.364237E-03	0.367175E-03	-0.293803E-05	0.81
15	0.985736E-01	0.496881E-03	0.498917E-03	-0.203605E-05	0.41
16	0.131780E+00	0.615205E-03	0.616238E-03	-0.103324E-05	0.17
17	0.197376E+00	0.816293E-03	0.815188E-03	0.110513E-05	0.14
18	0.262973E+00	0.987807E-03	0.985574E-03	0.223354E-05	0.23
19	0.394710E+00	0.127557E-02	0.127399E-02	0.158476E-05	0.12
20	0.525494E+00	0.151272E-02	0.151290E-02	-0.177068E-06	0.01
21	0.661110E+00	0.172392E-02	0.172565E-02	-0.172562E-05	0.10
22	0.788152E+00	0.189816E-02	0.190016E-02	-0.200479E-05	0.11
23	0.920298E+00	0.206121E-02	0.206131E-02	-0.991859E-07	0.00
24	0.991950E+00	0.214329E-02	0.214132E-02	0.197301E-05	0.09

n_1 is 0.53940E-03 with a stand. dev. of 0.10483E-04
K_1 is 0.86051E+01 with a stand. dev. of 0.21325E+00

n_2 is 0.43378E-02 with a stand. dev. of 0.13437E-03
K_2 is 0.62401E+00 with a stand. dev. of 0.19439E-01

NOTE: The large number of significant figures in the above table are not meant to imply increased accuracy, but are solely an artifact of the simplex data-fitting routine. No rounding to the correct number of significant figures is done until all data fits are completed.

For this first fit, it was found that two processes were sufficient for initial solution of Eqn. III-1. In determining whether a good data fit had been obtained, the percentage error in comparing the experimental number of moles of gas adsorbed per gram of carbonaceous adsorbent versus that calculated by the simplex fit routine was compared to the experimental error of the measured values. It is not meaningful to fit the data any more precisely than this. If a poor fit, and therefore large error, arose from the initial guesses for n_i and K_i, the data set was refit using the newest calculated values of n_i and K_i. This process was repeated until an acceptable fit of the data was obtained.

Step (2): Using the value for n_1 obtained in Step 1, the -93°C data is now fit to three processes while not allowing the value of n_1 to vary:

#	Experimental P_{equil} (atm)	Experimental moles ads. (n/g)	Theoretical moles ads. (n/g)	Error (Expt. - Theor.)	% Error
1	0.129421E-02	0.160659E-03	0.154947E-03	0.571218E-05	3.56
2	0.388408E-02	0.366900E-03	0.367655E-03	-0.754895E-06	0.21
3	0.646711E-02	0.517636E-03	0.519540E-03	-0.190368E-05	0.37
4	0.912092E-02	0.640412E-03	0.644700E-03	-0.428775E-05	0.67
5	0.117066E-01	0.747104E-03	0.748683E-03	-0.157900E-05	0.21
6	0.144966E-01	0.846685E-03	0.847585E-03	-0.899658E-06	0.11
7	0.170142E-01	0.928687E-03	0.928162E-03	0.525324E-06	0.06
8	0.210970E-01	0.104743E-02	0.104579E-02	0.163831E-05	0.16
9	0.234786E-01	0.111048E-02	0.110851E-02	0.197417E-05	0.18
10	0.262004E-01	0.117943E-02	0.117583E-02	0.359712E-05	0.30
11	0.290584E-01	0.124548E-02	0.124224E-02	0.324205E-05	0.26
12	0.328689E-01	0.132679E-02	0.132493E-02	0.185554E-05	0.14
13	0.455255E-01	0.156141E-02	0.156291E-02	-0.150420E-05	0.10
14	0.668239E-01	0.187489E-02	0.187907E-02	-0.417745E-05	0.22
15	0.979891E-01	0.222787E-02	0.223226E-02	-0.439212E-05	0.20
16	0.129358E+00	0.251043E-02	0.251255E-02	-0.211573E-05	0.08
17	0.196043E+00	0.297529E-02	0.297270E-02	0.258745E-05	0.09
18	0.260755E+00	0.332390E-02	0.331875E-02	0.515440E-05	0.16
19	0.391404E+00	0.385724E-02	0.385437E-02	0.286801E-05	0.07
20	0.522392E+00	0.425921E-02	0.426115E-02	-0.194181E-05	0.05
21	0.656715E+00	0.458903E-02	0.459334E-02	-0.431016E-05	0.09
22	0.786479E+00	0.485356E-02	0.485720E-02	-0.364007E-05	0.07
23	0.919169E+00	0.508483E-02	0.508413E-02	0.695232E-06	0.01
24	0.990413E+00	0.519577E-02	0.519172E-02	0.404892E-05	0.08

n_1 is 0.53900E-03 with a stand. dev. of -.10000E+01
K_1 is 0.19361E+03 with a stand. dev. of 0.88283E+02

n_2 is 0.19449E-02 with a stand. dev. of 0.58949E-04
K_2 is 0.15838E+02 with a stand. dev. of 0.52932E+00

n_3 is 0.53119E-02 with a stand. dev. of 0.79411E-03
K_3 is 0.11488E+01 with a stand. dev. of 0.17205E+00

From this data series, the values for n_1, n_2 and n_3 are now known. These are then fixed, and all the data then reanalyzed to determine the values for $K_{i,ads}$ at the various temperatures. These data fitting routines resulted in the values reported in Table III-2. Although the above data does not agree exactly with the values reported in Table III-2, it should be kept in mind that these fits were not solved as rigorously (less iterations in fit routine and larger tolerances to meet fit criteria) as those reported in Chapter III, but were simply shown here to exemplify the method. However, it is still found that these values agree with those reported in Table III-2 within the errors shown.

LIST OF REFERENCES

[1] Murell, L.L. Advanced Materials in Catalysis. Burton, J.J.; Garten, R.L., Eds.; Academic Press: New York, 1977, pp 235-64.

[2] Vayenas, C.G.; Ioannides, A.; Bebelis, S. *J. Catal.* **1991**, *129*, 67.

[3] Murray, C.G.; Nowak, R.J.; Rolison, D.R. *J. Electroanal. Chem.* **1984**, *164*, 205.

[4] Tateishi, N.; Yahikozawa, K.; Nishimura, K.; Suzuki, M.; Iwanaga, Y.; Watanabe, M.; Enami, E.; Matsuda, Y.; Takasu, Y. *Electrochimica Acta*, **1991**, *36*, 1235.

[5] Drago, R.S. Physical Methods for Chemists, 2nd ed.; Saunders College Publishing: New York, 1992.

[6] Kritzenberger, J.; Gaede, H.C.; Shore, J.S.; Pines, A.; Bell, A.T. *J. Phys. Chem.*. **1994**, *98*, 10173.

[7] a.) Raftery, D.; Reven, L.; Long, H.; Pines, A.; Tang, P.; Reimer, J.A. *J. Phys. Chem.* **1993**, *97*, 1649.
b.) Ito, T.; Bohordet, J.L.; Fraissard, J.; Nagy, J.B.; Andre, C.; Gabelica, Z.; Derouane, E.G. *Appl. Catal.* **1988**, *43*, L5.
c.) Demarquay, J.; Fraissard, J. *Chem. Phys. Lett.* **1987**, *136*, 314.
d.) Derouane, E.G.; Nagy, J.B. *Chem. Phys. Lett.* **1987**, *137*, 341

[8] Lim, Y.Y.; Drago, R.S.; Babich, M.W.; Wong, N.; Doan, P.E. *J. Am. Chem. Soc.* **1987**, *109*, 169.

[9] Chronister, C.W.; Drago, R.S. *J. Am. Chem. Soc.* **1993**, *115*, 4793.

[10] Gregg, S.J.; Sing, K.S.W. Adsorption, Surface Area and Porosity, 2nd ed.; Academic Press: London, 1982.

[11] Adamson, A.W. Physical Chemistry of Surfaces, 5th ed.; John Wiley & Sons: New York, 1990.

[12] Jenkins, G.M.; Kawamura, K. Polymeric Carbons - Carbon Fibre, Glass and Char; Cambridge University Press: New York, 1976.

[13] Dollimore, D.; Heal, G.R. *Carbon*, **1967**, *5*, 65.

[14] Fitzer, E. *Angew. Chem. Int. Ed. Engl.* **1980**, *19*, 375.

[15] Koresh, J.; Soffer, A. *J. Chem. Soc. Faraday Trans. 1*, **1980**, *76*, 2507.

[16] Neely, J.W. U.S. Patent 4 040 990, 1977.

[17] Daer, K.M.; Levendis, Y.A. *J. Appl. Polym. Sci.* **1992**, *45*, 2061.

[18] Neely, J.W.; Isacoff, E.G. Carbonaceous Adsorbents for the Treatment of Ground and Surface Waters; Marcel Dekker: New York, 1982.

[19] Maroldo, S.G.; Betz, W. R.; Borenstein, N. U.S. Patent 4 839 331, 1989.

[20] Rafalko, J.J. *J. Polym. Sci. Polym. Phys. Ed.*, **1984**, *22*, 1211.

[21] Teoh, H.; Metz, P.D.; Wilhelm, W.G. *Mol. Cryst. Liq. Cryst.*, **1982**, *83*, 297.

[22] Manassen, J.; Khalif, S. *J. Am. Chem. Soc.*, **1966**, *88*, 1943.

[23] Wennerberg, A.; O'Grady, T. U.S. Patent 4 082 694, 1978.

[24] O'Grady, T.M.; Wennerberg, A.N. "High Surface Area Active Carbon: Petroleum-Derived Carbons," *A.C.S. Symp. Ser.*, **1986**, *303*, 302.

[25] a.) Cooney, D.O. *Clin. Toxic.*, **1980**, *16*, 123.
b.) Cooney, D.O. *Clin. Toxic.*, **1979**, *15*, 287.

[26] Grunewald, G.C. Ph.D. Dissertation, University of Florida, 1989.

[27] Brunauer, S.; Emmett, P.H.; Teller, E. *J. Am. Chem. Soc.*, **1938**, *60*, 309.

[28] Harkins, W.D.; Jura, G. *J. Chem. Phys.*, **1943**, *11*, 431.

[29] Gregg, S.J.; Sing, K.S.W. Adsorption, Surface Area and Porosity, 2nd ed.; Academic Press: London, 1982, pp 94-105.

[30] Barrett, E.P.; Joyner, L.G.; Halenda, P.P. *J. Am. Chem. Soc.*, **1951**, *73*, 373.

[31] *Micromeritics® ASAP 2000 System - Operators Manual V2.05*, Micromeritics® Instrument Corp.: Norcross, GA, **1992**; Appendix C.

[32] Sing, K.W.; Everett, D.H.; Haul, R.A.W.; Moscou, L.; Pierotti, R.A.; Rouquérol, J.; Siemieniewska, T. *Pure Appl. Chem.* **1985**, *57*, 603.

[33] Rouquérol, J.; Avnir, D.; Fairbridge, C.W.; Everett, D.H.; Haynes, J.H.; Pernicone, N.; Ramsay, J.D.F.; Sing, K.S.W.; Unger, K.K. *Pure Appl. Chem.* **1994**, *66*, 1739.

[34] *Micromeritics® ASAP 2000 Chemi System - Operators Manual V2.04*, Micromeritics® Instrument Corp.: Norcross, GA, **1992**; Appendix C.

[35] Grunewald, G.C.; Drago, R.S. *J. Am. Chem. Soc.* **1991**, *113*, 1636.

[36] Neely, J.W.; Isacoff, E.G. Carbonaceous Adsorbents for the Treatment of Ground and Surface Waters; Marcel Dekker: New York, 1982, p 61.

[37] Lowell, S.; Shields, J.E. Powder Surface Area and Porosity, 2nd ed.; Chapman and Hall: New York, 1984.

[38] Gregg, S.J.; Sing, K.S.W. Adsorption, Surface Area and Porosity, 2nd ed.; Academic Press: London, 1982.

[39] Adamson, A.W. Physical Chemistry of Surfaces, 5th ed.; John Wiley & Sons: New York, 1990.

[40] McClellan, A.L.; Harnsberger, H.F. *J. Colloid Interface Sci.* **1967**, *23*, 577.

[41] a.) Kodera, K.; Onishi, Y. *Bull. Chem. Soc. Japan.* **1960**, *33*, 338.
b.) Kodera, K.; Onishi, Y. *Bull. Chem. Soc. Japan.* **1959**, *32*, 356.

[42] Gregg, S.J.; Sing, K.S.W. Adsorption, Surface Area and Porosity, 2nd ed.; Academic Press: London, 1982, pp 42-54.

[43] Gregg, S.J.; Langford, J.F. *Trans. Faraday Soc.* **1969**, *65*, 1394.

[44] Brunauer, S.; Deming, L.S.; Deming, W.E.; Teller, E. *J. Am. Chem. Soc.*, **1940**, *62*, 1723.

[45] Gregg, S.J.; Sing, K.S.W. Adsorption, Surface Area and Porosity, 2nd ed.; Academic Press: London, 1982, p 103.

[46] Kritzenberger, J.; Gaede, H.C.; Shore, J.S.; Pines, A.; Bell, A.T. *J. Phys. Chem.*. **1994**, *98*, 10173.

[47] Ahmed, S.N.; Baldwin, R.; Derbyshire, F.; McEnaney, B.; Stencel, J. *Fuel*, **1993**, *72*, 287.

[48] Bansal, C.; Donnet, B.J.; Stoeckli, F. Active Carbon, Dekker: New York, 1988.

[49] Boehm, H.P. *Adv. Catal.* **1966**, *16*, 179.

[50] a.) Orcel, G. Ph.D. Dissertation, University of Florida, 1987.
b.) Boer. J.H.; Lippens, B.C. *J. Catal.*, **1964**, *3*, 38.

[51] Harkins, W.D.; Jura, G. *J. Am. Chem. Soc.*, **1944**, *66*, 919.

[52] Brunauer, S.; Emmett, P.H.; Teller, E. *J. Am. Chem. Soc.*, **1938**, *60*, 309.

[53] Sing, K.W.; Everett, D.H.; Haul, R.A.W.; Moscou, L.; Pierotti, R.A.; Rouquérol, J.; Siemieniewska, T. *Pure Appl. Chem.* **1985**, *57*, 603.

[54] Everett, D.H.; Powl, J.C. *J. Chem. Soc., Faraday Trans. 1*, **1976**, *72*, 619.

[55] Gregg, S.J.; Sing, K.S.W. Adsorption, Surface Area and Porosity, 2nd ed.; Academic Press: London, 1982.

[56] Adamson, A.W. Physical Chemistry of Surfaces, 5th ed.; John Wiley & Sons: New York, 1990.

[57] a.) Lange's Handbook of Chemistry, 13th ed.; Dean, J.A., Ed.; McGraw-Hill: New York, 1985.
b.) CRC Handbook of Chemistry and Physics, 72nd ed.; Lide, D.R., Ed.; CRC Press: Boca Raton, 1991.
c.) Hildebrand, J.H.; Prausnitz, J.M.; Scott, R.L. Regular and Related Solutions; Van Nostrand Reinhold Company: New York, 1970, p217.

[58] Lim, Y.Y.; Drago, R.S.; Babich, M.W.; Wong, N.; Doan, P.E. *J. Am. Chem. Soc.* **1987**, *109*, 169.

[59] a.) Massart, D.L.; Vandeginste, B.; Deming, S.; Michotte, Y.; Kaufman, L. Chemometrics: A Textbook; Elsevier: Amsterdam, 1988.
b.) Deming, S.N.; Morgan, S.L. *Anal. Chim. Acta,* **1983**, *150*, 183.
c.) Routh, M.W.; Swartz, P.A.; Denton, M.B. *Anal. Chem.* **1977**, *49*, 1422.

[60] Chronister, C.W. Ph.D. Dissertation, University of Florida, 1994.

[61] Drago, R.S.; Rose, N.J. *J. Am. Chem. Soc.* **1959**, *81*, 6141.

[62] Taylor, H.S. *Proc. Royal Soc.* **1925**, *105*, A108.

[63] Everett, D.H.; Whitton, W.I. *Proc. Royal Soc.* **1955**, *91*, A230.

[64] Farell, J.; Reinhard, M. *Environ. Sci. Tech.* **1994**, *28*, 53.

[65] Drago, R.S.; Ferris, D.C.; Burns, D.S. Submitted for publication.

[66] McClellan, A. L.; Harnsberger, H. F. *J. Colloid Interface Sci.* **1967**, *23*, 577.

[67] *Micromeritics® ASAP 2000 System - Operators Manual V2.05,* Micromeritics® Instrument Corp.: Norcross, GA, **1992**; Appendix C.

[68] Henry, Patrick M. Palladium Catalyzed Oxidation of Hydrocarbons; D. Reidel Publishing: London, 1980.

[69] Heck, Richard F. Palladium Reagents in Organic Synthesis; Academic Press: New York, 1985.

[70] a.) Smidt, J.; Hafner, W.; Jira, R.; Sedlmeier, J.; Seiber, R.; Ruttinger, R.; Kojer, H. *Angew. Chem.* **1959**, *71*, 176.
b.) Smidt, J.; Hafner, W.; Jira, R.; Seiber, R.; Sedlmeier, J.; Sable, A. *Angew. Chem.* **1962**, *74*, 93.

[71] Bäckvall, J.E.; Åkermark, B.; Ljunggren, S.O. *J. Am. Chem. Soc.* **1979**, *101*, 2411.

[72] Cotton, F.A.; Wilkinson, G. Advanced Inorganic Chemistry, 5th ed.; John Wiley & Sons: New York, 1988, p1276.

[73] Encyclopedia of Chemical Technology, 3rd ed.; John Wiley & Sons: New York, 1978, vol. 1.

[74] Winstein, S.; McCaskie, J.; Lee, Hing-Biu; Henry, P.H. *J. Am. Chem. Soc.* **1976**, *98*, 6913.

[75] Henry, P.M. *J. Org. Chem.* **1973**, *38*, 1681.

[76] Parshall, G.W. Homogeneous Catalysis: The Applications and Chemistry of Catalysis by Soluble Transition Metal Complexes; John Wiley & Sons: New York, 1980, pp 101-108.

[77] Evnin, A.B.; Rabo, J.A.; Kasai, P.H. *J. Catal.* **1973**, *30*,109.

[78] Matveev, K.I. *Kinetika i Kataliz*, **1977**, *18*, 862.

[79] Grennberg, H.; Simon, V; Bäckvall, J.E. *J. Chem. Soc., Chem. Commun.* **1994**, 265.

[80] Fujimoto, K.; Negami, Y.; Takahashi, T.; Kunugi, T. *Ind. Eng. Chem. Prod. Res. Develop.* **1972**, *11*, 303.

[81] Petrosius, S.; Drago, R.S. *J. Chem. Soc., Chem. Commun.* **1992**, *4*, 344.

[82] Grunewald, G.C.; Drago, R.S. *J. Am. Chem. Soc.* **1991**, *113*, 1636.

[83] Drago, R.S.; Jurczyk, K. *Appl. Cat. A*, **1994**, *112*, 117.

[84] Neely, J.W.; Isacoff, E.G. Carbonaceous Adsorbents for the Treatment of Ground and Surface Waters; Marcel Dekker: New York, 1982.

[85] Woolcock, J.; Zafar, A. *J. Chem. Ed.* **1992**, *69*, A176.

[86] Drago, R.S. Physical Methods for Chemists, 2nd ed.; Saunders College Publishing: New York, 1992, pp 360-400.

[87] a.) Arai, H.; Yamashiro, T.; Kubo, T.; Tominaga, H. *Bull. Jap. Pet. Inst.* **1976**, *18*, 39.

b.) Katz, G.; Pismen, L.M. *Chem. Eng. Journal.* **1979**, *18*, 203.

c.) Espeel, P.H.; Tielen, M.C.; Jacobs, P.A. *J. Chem. Soc., Chem. Commun.* **1991**, *10*, 669.

BIOGRAPHICAL SKETCH

Todd James Lafrenz was born in Mesa, Arizona, on July 25, 1966, to James and Joan Lafrenz. He graduated from West High School in Waterloo, Iowa, in May 1984. During this time, he was actively involved in advanced courses in math, science and English, as well as the honor society, band and swimming. After high school he moved to Panama City, Florida, and attended Gulf Coast Community College. His tenure here included several semesters as an officer of a local community service fraternity. Todd graduated from Gulf Coast in April 1987 with an Associate of Arts, majoring in biology.

Todd then attended the University of West Florida in Pensacola on a chemistry scholarship, and graduated with a Bachelor of Science in chemistry in May 1989. He went on to the University of Florida in Gainesville, where he was a graduate student under Dr. Russell S. Drago. While at the University of Florida, Todd was active in research involving heterogeneous catalysis and carbonaceous adsorbents, as well as being a regular attendee to the Florida Environmental Chemistry and the Florida Catalysis Conferences. Apart from the chemistry department, he actively pursued his interests in writing poetry and playing rugby.

After receiving his Doctor of Philosophy in inorganic chemistry, Todd plans to pursue his interests in environmental chemistry and chemical education. After finishing his dissertation work, Todd will be continuing his chemistry career with a new, small company called C.I.N.C., in Newbury Park, California.

I certify that I have read this study and that in my opinion it conforms to acceptable standards of scholarly presentation and is fully adequate, in scope and quality, as a dissertation for the degree of Doctor of Philosophy.

Russell S. Drago, Chair
Graduate Research Professor of Chemistry

I certify that I have read this study and that in my opinion it conforms to acceptable standards of scholarly presentation and is fully adequate, in scope and quality, as a dissertation for the degree of Doctor of Philosophy.

R. Carl Stoufer
Associate Professor of Chemistry

I certify that I have read this study and that in my opinion it conforms to acceptable standards of scholarly presentation and is fully adequate, in scope and quality, as a dissertation for the degree of Doctor of Philosophy.

Daniel R. Talham
Assistant Professor of Chemistry

I certify that I have read this study and that in my opinion it conforms to acceptable standards of scholarly presentation and is fully adequate, in scope and quality, as a dissertation for the degree of Doctor of Philosophy.

William Jones
Distinguished Service Professor of Chemistry

I certify that I have read this study and that in my opinion it conforms to acceptable standards of scholarly presentation and is fully adequate, in scope and quality, as a dissertation for the degree of Doctor of Philosophy.

H. Anson Moye
Professor of Food Science and Human Nutrition

This dissertation was submitted to the Graduate Faculty of the Department of Chemistry in the College of Liberal Arts and Sciences and to the Graduate School and was accepted as partial fulfillment of the requirements for the degree of Doctor of Philosophy.

December 1995

Dean, Graduate School